

AD A108427

LEVEL II



AFWAL-TR-81-3081

FLOW VELOCITY AND ANGULARITY MEASUREMENTS IN THE FDL
TRANSONIC GASDYNAMIC FACILITY AND SELF-ADAPTIVE
WALL WIND TUNNELS WITH A LASER TRANSIT ANEMOMETER

Spectron Development Laboratories
3303 Harbor Blvd., Suite G-3
Costa Mesa, California 92626

12 143

August 1981

Final Report for period April 1980 through November 1980

Approved for public release; distribution unlimited.

FILE COPY

DTIC
ELECTE
S DEC 10 1981 D

FLIGHT DYNAMICS LABORATORY
AIR FORCE WRIGHT AERONAUTICAL LABORATORIES
AIR FORCE SYSTEMS COMMAND
WRIGHT-PATTERSON AIR FORCE BASE, OHIO 45433

392057 Jm


81 12 09 023


NOTICE

When Government drawings, specifications, or other data are used for any purpose other than in connection with a definitely related Government procurement operation, the United States Government thereby incurs no responsibility nor any obligation whatsoever; and the fact that the government may have formulated, furnished, or in any way supplied the said drawings, specifications, or other data, is not to be regarded by implication or otherwise as in any manner licensing the holder or any other person or corporation, or conveying any rights or permission to manufacture use, or sell any patented invention that may in any way be related thereto.


The report has been reviewed by the office of Public Affairs (ASD/PA) and is releasable to the National Technical Information Service (NTIS). At NTIS, it will be available to the general public, including foreign nations.

The technical report has been reviewed and is approved for publication.


DANIEL M. PAROBK, Technical Manager
Mechanical Instrumentation Group
Experimental Engineering Branch


JOSEPH M. HAMBLE, Chief
Experimental Engineering Branch
Aeromechanics Division

FOR THE COMMANDER


JOHN R. CHEVALIER, Colonel, USAF
Chief, Aeromechanics Division
Flight Dynamics Laboratory

"If your address has changed, if you wish to be removed from our mailing list, or if the addressee is no longer employed by your organization please notify AFWAL/FIMN, Wright-Patterson AFB, OH 45433 to help us maintain a current mailing list."

Copies of this report should not be returned unless return is required by security consideration, contractual obligations, or notice on a specific document.

UNCLASSIFIED

SECURITY CLASSIFICATION OF THIS PAGE (When Data Entered)

REPORT DOCUMENTATION PAGE		READ INSTRUCTIONS BEFORE COMPLETING FORM
1. REPORT NUMBER AFWAL-TR-81-3081	2. GOVT ACCESSION NO. AD A308 4127	3. RECIPIENT'S CATALOG NUMBER
4. TITLE (and Subtitle) FLOW VELOCITY AND ANGULARITY MEASUREMENTS IN THE FDL TRISONIC GASDYNAMIC FACILITY AND SELF ADAP- TIVE WALL WIND TUNNELS WITH A LASER TRANSIT ANEMOMETER	5. TYPE OF REPORT & PERIOD COVERED Final Apr 80 - Nov 80	
7. AUTHOR(s) W. T. Mayo, Jr., A. E. Smart, R. J. Hermes and J. D. Trolinger	6. PERFORMING ORG. REPORT NUMBER SDL No 81-2162-05FR	
9. PERFORMING ORGANIZATION NAME AND ADDRESS SPECTRON DEVELOPMENT LABORATORIES 3303 Harbor Blvd., Suite G-3 Costa Mesa, California 92626	8. CONTRACT OR GRANT NUMBER(s) F33615-79-C-3030	
11. CONTROLLING OFFICE NAME AND ADDRESS Flight Dynamics Laboratory (AFWAL/FIMN) Wright-Patterson AFB, OH 45433	10. PROGRAM ELEMENT, PROJECT, TASK AREA & WORK UNIT NUMBERS Project Element 62201F Project 2404, Task 240413 Work Unit 24041307	
14. MONITORING AGENCY NAME & ADDRESS (if different from Controlling Office)	12. REPORT DATE August 1981	
	13. NUMBER OF PAGES 141	
	15. SECURITY CLASS. (of this report) Unclassified	
	16. DECLASSIFICATION/DOWNGRADING SCHEDULE	
16. DISTRIBUTION STATEMENT (of this Report) Approved for Public Release; distribution unlimited.		
17. DISTRIBUTION STATEMENT (of the abstract entered in Block 20, if different from Report)		
18. SUPPLEMENTARY NOTES		
19. KEY WORDS (Continue on reverse side if necessary and identify by block number) Laser Velocimetry, Wind Tunnel Measurements, Anemometry, Transonic Flow Analysis		
20. ABSTRACT (Continue on reverse side if necessary and identify by block number) The measurement capability of a backscatter laser transit anemometer was tested in the FDL Trisonic Gasdynamics Facility (TGF) and the nine-inch Self Adapting Wall (SAW) wind tunnel. The tests included flow analysis in the two foot by two foot subsonic, transonic and supersonic test sections as well as the fifteen-inch transonic test section insert all in the TGF. The magnitude and flow angle precisions were as good as 0.3% and 0.3°, respec- tively, as limited by the statistical fluctuation of the data. Calculations indicate that the minimum natural particle size observed in the TGF was		

DD FORM 1 JAN 73 1473

EDITION OF 1 NOV 68 IS OBSOLETE

UNCLASSIFIED

SECURITY CLASSIFICATION OF THIS PAGE (When Data Entered)

20.

approximately 0.2 μ m in diameter. Flow speed and angle were mapped about a microfighter flow field in the TGF fifteen-inch transonic test section at Mach number 0.7 and 0.9 to develop a data base for evaluation of the Self Adaptive Wall wind tunnel concept. Measurements were then made to the same model in the FDL nine-inch Self Adaptive Wall wind tunnel. These indicated that the precision of the instrument exceeded the current precision to establish and repeat flow conditions in the tunnel. The SAW results indicated non-uniform particle content of the flow which adversely affected the available angle precision; however, velocity measurements were good. Presentation of the equipment and measurement results of the present project are included.

Accession For	
NTIS GRA&I	<input checked="" type="checkbox"/>
DTIC TAB	<input type="checkbox"/>
Unannounced	<input type="checkbox"/>
Justification	
By	
Distribution/	
Availability Codes	
Dist	Avail and/or Special
A	

PREFACE

This report was prepared as part of a contract effort conducted under a visiting scientist arrangement through the University of Dayton under Task 80-13 of Air Force Contract F33615-79-C-3030. Drs. James D. Trolinger, William T. Mayo, Jr., and Anthony E. Smart of Spectron Development Laboratories, Inc., Costa Mesa California, were the principal scientists. The performance period was April through November 1980. The tests were carried out at the aerodynamic test facilities of the Aeromechanics Division of the Flight Dynamics Laboratory, Air Force Wright Aeronautical Laboratories, at Wright-Patterson AFB, Ohio. The tests were an element of in-house work unit 24041307, "Development of Testing Techniques and Aero-Optical Diagnostics to Advance Aerodynamic Ground Simulation" of Task 240413, "Aerodynamic Ground Test Technology".

Mr. Daniel M. Parobek of the Experimental Engineering Branch (AFWAL/FIMN) was contract monitor and principal investigator of the in-house work unit. Mr. Clifford Weissman and Mr. Charles O'Heren of AFWAL/FIMN were the optical and electronic engineers supporting the tests.

The authors wish to acknowledge the assistance of Messrs Joseph Martin, Thomas Norris, Howard White and Maurice Cain of the Aeromechanics Division for their facility support of these tests, and Messrs David Boyer and Ronald Tinsley of Technology Scientific Services, Inc. for their instrumentation support of the program.

The authors also wish to acknowledge the loan of Malvern Digital Correlator from Dr. Harold Wright of the Air Force Institute of Technology and an Apple microcomputer from the Experimental Engineering Branch.

TABLE OF CONTENTS

<u>Section</u>	<u>Page</u>
I INTRODUCTION	1
1. Objectives	1
2. Background	2
3. Scope	3
II LASER TRANSIT ANEMOMETER USED FOR MEASUREMENTS	5
1. System Description	5
2. Background	10
3. Optical System Parameters	12
III LASER TRANSIT ANEMOMETER PRECISION AND SMALL PARTICLE SENSITIVITY	17
1. Introduction	17
2. Bias Errors	17
3. Statistical Errors of Velocity Magnitude Measurements	19
4. Statistical Errors of the Flow Angle Estimate	20
5. Particle Size Sensitivity	21
6. Data Rate and Particle Number Density	24
IV EXPERIMENTAL CHARACTERIZATION	27
1. Overview	27
2. TGF Characterization	27
a. Experiment 1	30
b. Experiment 2	30
c. Experiment 3	33

TABLE OF CONTENTS (Continued)

<u>Section</u>	<u>Page</u>
d. Experiment 4	35
e. Experiment 5	37
f. Experiment 6	41
g. Experiment 7	44
g. Experiment 8	49
V AERODYNAMIC MEASUREMENTS IN THE TRISONIC GAS DYNAMICS FACILITY	53
1. Overview	53
2. Measurements at Mach 0.7 and 0.9	57
3. Discussion of Results in the TGF	57
VI MICROFIGHTER MEASUREMENTS IN THE SELF ADAPTIVE WALL TUNNEL	57
1. Tunnel Characteristics	65
2. Measurements Near the Microfighter Model	71
VII CONCLUSIONS AND RECOMMENDATIONS	73
REFERENCES	76
APPENDIX A	79
Papers Describing LTA Theory and Systems ICIASF '79 Record	
APPENDIX B	97
Papers Describing LTA Theory and Systems A Tutorial: Laser Transit Anemometer	

LIST OF ILLUSTRATIONS

<u>No.</u>		<u>Page</u>
1	LTA SYSTEM	6
2	SIGNIFICANT OPTICAL COMPONENTS	7
3	SDL MODEL 105 LTA OPTICAL HEAD MOUNTED ON TRAVERSE AT TRISONIC GASDYNAMICS FACILITY	8
4	LTA ELECTRONIC DATA ACQUISITION SUBSYSTEM	9
5	EXAMPLE DATA PRINTOUT	11
6	INSTALLATION FOR TGF TRANSONIC MICROFIGHTER MEASUREMENTS	28
7	INSTALLATION FOR SAW MICROFIGHTER MEASUREMENTS	29
8	TYPICAL CORRELOGRAMS FOR MACH 0.4, $P_o = 2208$ PSF WITHOUT SEEDING	32
9	MACH 0.4 RESULTS WITH DROPLET SEEDING	34
10	CORRELOGRAMS FROM MACH 0.4, $P_o = 860$ PSF, ILLUSTRATING THRESHOLD EFFECTS	36
11	EXAMPLES OF MACH 0.7 CORRELOGRAMS WITH INCREASED RELATIVE THRESHOLD	38
12	MACH 2.3 DATA WITH SEEDING	40
13	MEASUREMENTS WITHOUT SEEDING AT MACH 2.3 (661 M/S)	43
14	REPEATABILITY TEST	47
15	VERY LOW DATA AND BACKGROUND CORRELOGRAMS FROM TRANSONIC FLOWS	48
16	THREE-FOURTHS SCALE DRAWING OF THE MICROFIGHTER MODEL SHOWING THE COORDINATE SYSTEM USED IN THE TGF WIND TUNNEL	54
17	EXAMPLE OF DATA FROM TGF MICROFIGHTER TEST	56
18	VELOCITY MEASUREMENTS AT MACH 0.7 AND 0.9	58

LIST OF ILLUSTRATIONS (Continued)

<u>No.</u>		<u>Page</u>
19	FLOW ANGLE AT MACH 0.7 AND 0.9	60
20	VELOCITY PROFILE ACROSS THE WIND TUNNEL AT MACH 0.7	61
21	FLOW VELOCITY AT MACH 0.9	62
22	SCHLIEREN PHOTO OF THE MICROFIGHTER MODEL IN THE SAW TUNNEL	66
23	TYPICAL 5 SECOND DATA RUN FROM SAW TUNNEL	68
24	EXAMPLE OF AN ANGLE SEARCH IN THE SAW TUNNEL: DATA VERSUS ANGLE WITH 5 SECONDS/ANGLE	70
25	MEAN VELOCITY ALONG THE LINE $z = 0$, $y = +4$	72

LIST OF TABLES

<u>No.</u>		<u>Page</u>
1	OPTICAL SYSTEM PARAMETERS.	13
2	FACTORS OF RECEIVER TRANSMISSION EFFICIENCY.	14
3	ESTIMATED LTA SYSTEMATIC ERROR LEVELS.	18
4	PHOTON DETECTION NUMBER VS. DIAMETER FOR TABLE 1 CONDITIONS	23
5	DATA FROM MACH 0.4	31
6	MACH 0.7 $P_0 = 1319$ PSF DATA SUMMARY	39
7	RESULTS AT MACH 2.3	42
8	SUMMARY OF COMPUTED DATA	46
9	MEASUREMENTS NEAR THE MICROFIGHTER AT Z = 0, x = -1.5	51

SECTION I
INTRODUCTION

1. Objective

The objectives of this study were several: for Task I, a Laser Transit Anemometer (LTA) system was to be used for backscatter measurements in a continuous closed circuit tunnel, the Trisonic Gasdynamics Facility (TGF). These LTA measurements were to be for characterization of observable naturally existing particles existing in the facility to determine particle size and measurement precision. Under Task II, velocity profiles were mapped around a 3-dimensional microfighter model in the TGF and the Nine-Inch Self-Adaptive Wall (SAW) wind tunnels. The purpose of the flow field mapping program about the common test model in both facilities was for support of a program at Flight Dynamics Laboratory to develop an adaptive wall concept to reduce wall interference effects in transonic wind tunnels. The 9" SAW tunnel features 2D computer contoured top and bottom tunnel walls to correct for wall interference. The TGF portion of the LTA mapping tests initiated development of a data base for the case of minimal wall interference. The LTA mapping in the SAW was intended to start evaluating the wall interference correction when compared with the TGF data. A third Task (Task III) was devoted to measurements with a thermal emission velocimeter (TEV) of the particle velocities in the RENT accelerator. The activity under Task III, is reported in reference 1 and is not discussed further here. Task IV of this program was the analysis and discussion of the results of Task I and II including recommendations for future laser velocimeter systems applications to the TGF and SAW facilities and the requisite data acquisition hardware and software.

2. Background

Previous attempts^(2,4) have been made to make fringe laser velocimeter (LDV) measurements in the TGF with naturally existing particulates. Observation of oscilloscope traces of the photomultiplier output revealed the absence of particles sufficiently large for classical burst counter detection after a period of 20 minutes⁽³⁾. Attempts to use photon correlation^(3,4) have also failed to produce usable data after the first 20 minutes of tunnel run time. The indications have been that the larger particles (say greater than .5 microns) are removed by the tunnel operation apparently whether or not the facility drying and filtering systems were in the circuit. After the beginning of tunnel operation the focussed beams are usually faintly visible as scatter from a large number of very small particles which have been estimated to be less or equal to 0.1 to 0.2 μm diameter because of the visual similarity of scatter brightness in the forward and backwards directions. The logical ways to proceed in such cases are to either a) try to develop a reference beam velocimeter which could utilize nonresolved signals from many small particles at once, or b) use a system such as an LTA system with smaller probe volume and greater sensitivity to very small particles. No relevant success is known for a) above.

Spectron Development Laboratories (SDL) has been developing LTA systems for 3 years. Following Schodl⁽⁵⁾ at the DFVLR in Germany and Smart⁽⁶⁾ at Rolls-Royce, Smart and Mayo^(7,8) have conceived and implemented at SDL many detailed improvements of technique and directed the production of several LTA systems of increasing sensitivity, precision of measurement, and data processing sophistication. A description of one

of the prototype systems fielded in the summer of 1979 is provided in the Appendixes, which also include a recent (August 1980) tutorial discussion of LTA principles and technology with an extensive bibliography. In addition to two versions of LTA Optical System development for the U.S. Air Force Arnold Engineering Development Center, SDL has fielded measurements at NASA Ames Research Center, the General Electric Company, the AEDC, and the Naval Postgraduate School, and has delivered several commercial systems. These activities are described in Appendix A and in the references provided there.

3. Scope

The following sections present the experimental arrangements, the resulting data, analysis and discussions of the data, and recommendations for using the LTA system for the laser velocimeter system and subsystems for the TGF and SAW tunnels. A summary is provided which refers to the figures and other key results.

SECTION II

LASER TRANSIT ANEMOMETER USED FOR MEASUREMENTS

1. System Description

As illustrated schematically in Figure 1, the LTA system employed several standard Spectron LTA subsystems and the recently introduced Model 105 optical head with 150 mm diameter transceiver optics. Figure 2 shows the optical schematic of the system. Figures 3 and 4 are photographs of the optical head and electronics taken during the tunnel characterization measurements. A Malvern K7023 digital correlator (50 ns resolution) was used as the data processor in lieu of the new SDL Correlex processor (5 ns resolution) which was not yet available at the time of the measurements. The unavailability of the Correlex was unfortunate because not only did the 50 ns correlator have inadequate time resolution for meaningful turbulence measurements, but also the Malvern computer output circuitry apparently malfunctioned producing scrambled data about one time in every five measurements. The software of the LTA experiment control computer (VGU-101) was modified to ignore occasions when the Malvern unit malfunctioned and to repeat the last measurement.

In Figure 1 the MC-101 controller and VGU-101 videographics unit include almost identical subsystems and functional behavior as the "Data Management System" described in the 1979 ICIASF paper (see Appendix A). The units used are simply a newer version of the former "Data Management System". It is noted, however, that the angle search computation utilized a plot of data rate versus angle rather than the data to data + background

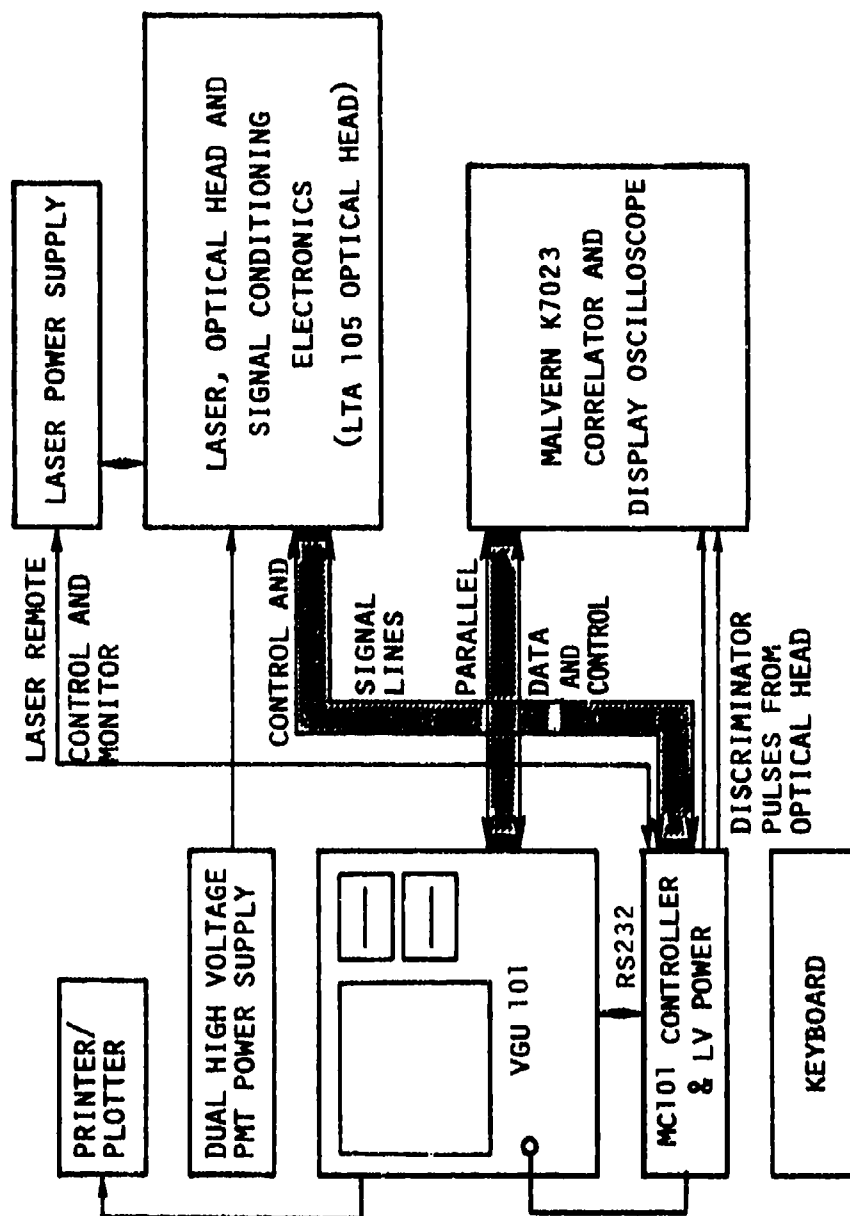


Figure 1. LTA System

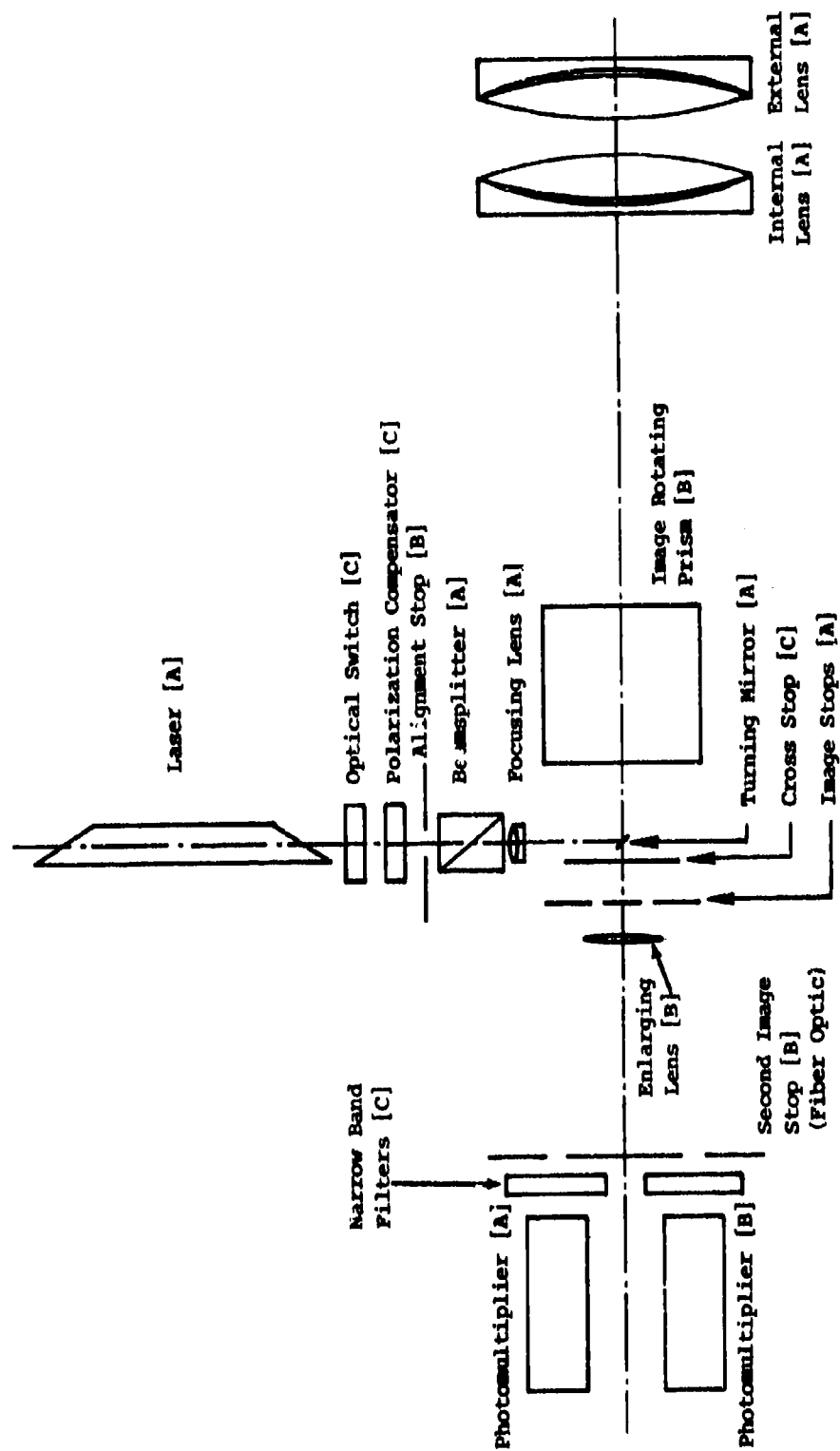


Figure 2. Significant Optical Components

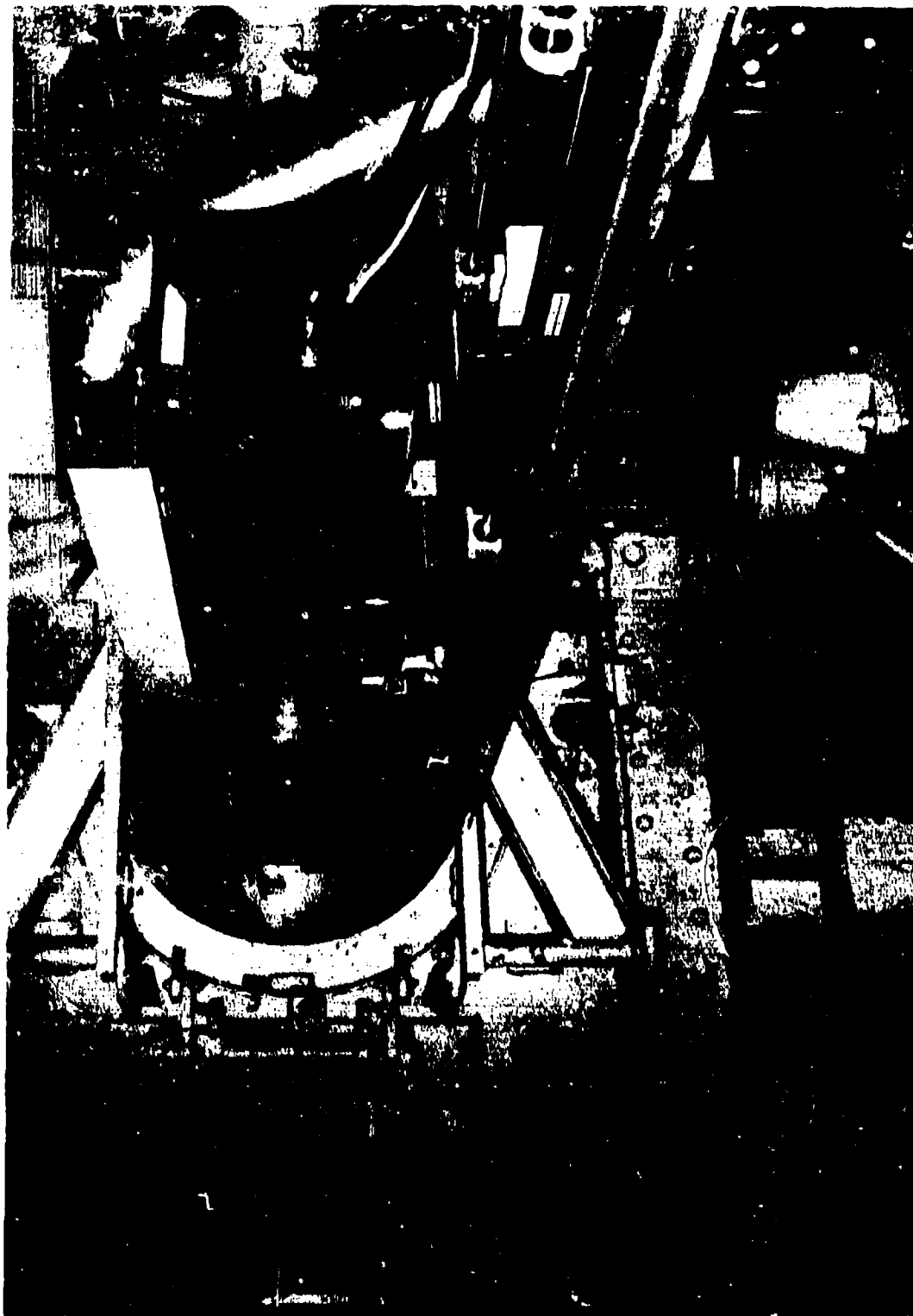


Figure 3. SDL Model 105 LTA Optical Head Mounted on Traverse at Trisonic Gasdynamics Facility.

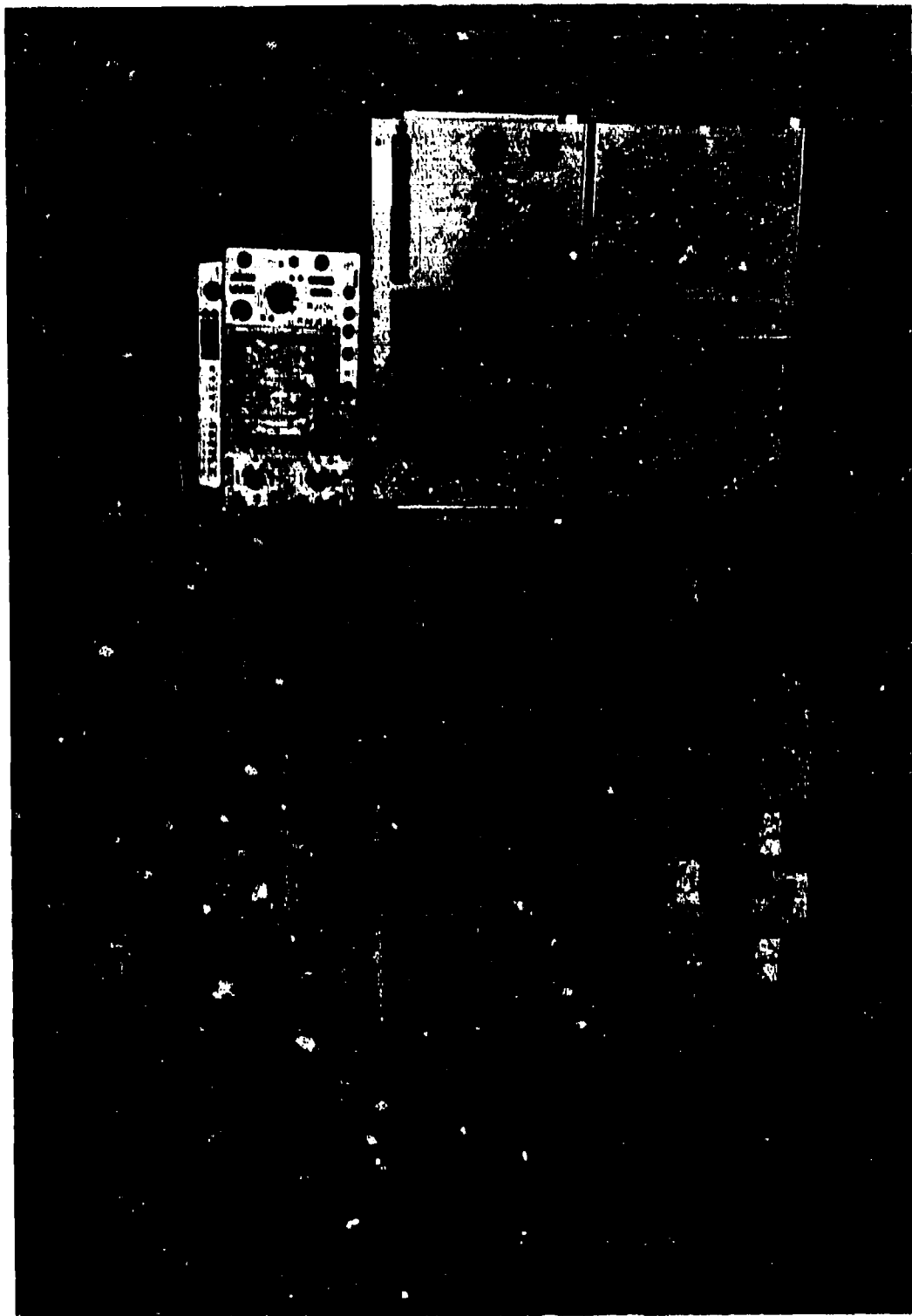


Figure 4. LTA Electronic Data Acquisition Subsystem.

figure of merit described in the 1979 ICIASF paper. The output formats have also been improved as described below.

The new SDL Model LTA 105 optical head was utilized in this test. The first customer for a Model 105 head is NASA Ames Research Center, and the experiments described here allowed a demonstration, prior to delivery, of several extensions of previously developed technology. These included the use of a more efficient turning mirror assembly, more versatile fiber optic mounts, the new 6" diameter, larger throw optics, the Lexel Model 85 - 1.0 laser, improved photomultiplier tube assemblies, and the improved RS-232 controlled versions of the discriminator cards. These new subsystems all performed well. The use of the larger optical system proved to be advantageous because the TGF mechanical constraints required a throw of 30 inches. This much range would have significantly reduced the small particle sensitivity of the previously developed smaller (4" diameter) optical systems.

2. Data Acquisition

The data collection method for the experiments consisted of printing standard formats 1 and 2 of the experiment control software of the VGU-101 (BASIC version used with Malvern K7023 correlator). Notebook logs were also kept of position, time, laser power, and high voltage settings for the photomultiplier tube high voltage power supplies (HVA and HVB).

An example data printout is given in Figure 5. The top graph is a reproduction, with a peak normalized scale, of the correlogram taken with the angle of rotation of the spots set near the correct mean

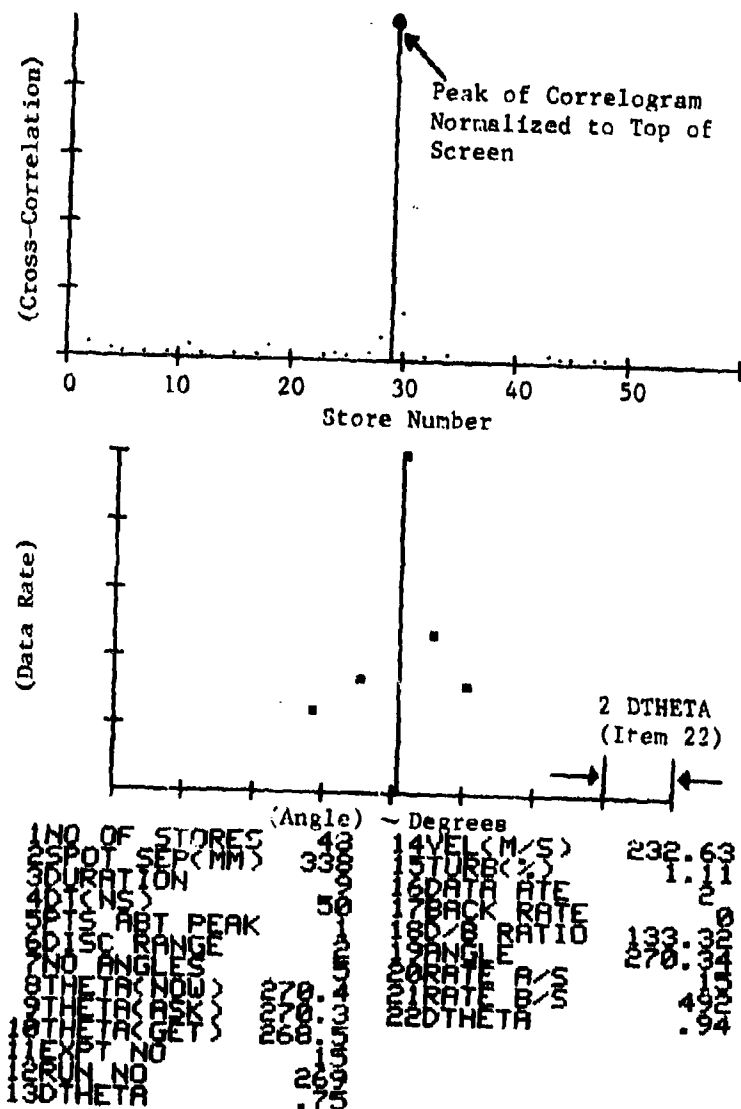


Figure 5. Example Data Printout.

flow direction. The bottom graph (on runs that included the angle search sequence) was the plot of data rate vs. angle. A parabolic fit of the peak and one point either side of the peak is used to estimate the flow angle in situations where a valid peak is found (peak not at one end), the printed data lists the experimental input parameters given by the operator (left hand column) and the resulting output values calculated by the VGU computer from the input parameters and measured data appear in the right hand column.

3. Optical System Parameters

The critical optical system parameters are listed in Table 1. Most of these are obvious in intent. A few require further definition as provided here. The f/number is simply the standard range/output-diameter without consideration of the receiver blockage due to the turning mirror (see Figure 2). The receiver efficiency is given by the product of the (estimated) efficiency factors itemized in Table 2. The standard formula for focal spot diameter would give

$$D = \frac{4R\lambda}{\pi D_t} \quad (1)$$

This would predict a focal spot diameter of $\approx 12.2 \mu\text{m}$ for a 40 mm diameter transmitted beam diameter. The measured value of 16 μm diameter (with microscope projection technique) reflects inaccuracies in visual estimates of D_t and D_f as well as any imperfections of the lenses which might tend to produce larger than diffraction limited spots. The laser power varied somewhat until it was discovered that an error in the wavelength selector prism installation had been made. After correction, the laser produced 300 mw reliably.

TABLE 1

OPTICAL SYSTEM PARAMETERS

<u>Description</u>	<u>Symbol</u>	<u>Value</u>
Wave/Length	λ	0.5145 μm
Laser Power	P_L	100 - 300 mW
Output Lens Diameter	D_o	150 mm
Output Lens Focal Range	R	745 mm
Collection F/D ratio	F/No.	30/6 = F/5
Transmission Efficiency	η_t	0.7
Receiver Efficiency*	η_r	0.4
Tunnel Window Efficiency per Window <u>per pass</u>	η_w	0.9
PMT Quantum Efficiency	η_d	0.2
Output Beam Diameter (1/e ² intensity)	D_t	\approx 40 mm
Focal Beam Diameter	D_f	16 μm
Probe Volume Length	L	0.4 mm
Spot Separation	S	338 μm
Separation to Diameter Ratio	SSR	21
Detection Filter Impulse Response	T_d	25 ns

*See factors listed in Table 2.

TABLE 2

FACTORS OF RECEIVER TRANSMISSION EFFICIENCY

1. Output lens	0.98
2. Collimating lens	0.99
3. Rotator prism	0.86
4. Turning mirror and cross-stop	0.65
5. Pinholes	1.00
6. Fiber optic (diameter loss)	0.80
7. Fiber ends reflection loss	0.92

$$\text{Total} = (0.98)(0.99)(0.86)(0.65)(1.0)(0.8)(0.92) = 0.40$$

The optical system parameters are sufficient to determine the number of photoelectrons detectable for a particle transit in terms of the Mie scattering coefficient of spherical homogeneous particles with the assumed typical index of $n = 1.50$. This is done in the next section for the TGF tunnel characterization. The estimate considers that 3-5 photoelectron pulses were being used as the threshold setting. This calculation only requires the detection filter time constants and not the absolute system gain for calibration.

2437-19

SECTION III

LASER TRANSIT ANEMOMETER PRECISION AND SMALL PARTICLE SENSITIVITY

1. Introduction

A major limitation of any laser velocimeter working with naturally seeded (unseeded) air, is the statistical variability error which results from inadequate measurement precision and small number statistics. As an example consider the following which was typical for the TGF measurements: a single particle transit produced, for example, a contribution of one unit in the correlator bin number 25 of the 48 bins which represent the correlation function. Since this is distinguished from bin number 24 or 26, the single-particle precision in this example was 4% of the actual mean flow (2 parts in 48). An experiment with zero background light produced fluctuations of 50 seconds in duration with a mean data pulse rate of 0.5/s. In this example 25 transit measurements produce 10 units in store number 25 and 15 of store number 26. The estimate of delay is then 25.4 DT, where $DT = 50$ ns is the delay time, and the measurement precision is 0.4% as discussed below. This section examines briefly both bias (or systematic) errors and statistical (or variability) errors and relates these to particle size and data rate through system detection sensitivity and probe volume dimensions.

2. Bias Errors

Systematic or bias errors are those that cannot be removed by taking more data and averaging long, but they can be removed by better calibration or fixed compensation. Table 3 lists the investigators'

TABLE 3

ESTIMATED LTA SYSTEMATIC ERROR LEVELS

(Correctable by Additional Calibration)

Velocity Magnitude

1. Spot Separation	0.5%
2. System Differential Delay	
Mach 2.3 5 ns/700 ns	0.7%
Mach 0.9 5 ns/1260 ns	0.4%
3. Correlator Clock Frequency	≤0.001%
4. Bias Errors due to Calculation Algorithm (at 1% flow turbulence or less)	negligible
<hr/>	
Total Accuracy Without Further Calibration (Root mean square sum)	1%

Flow Angle

Linear Potentiometer	0.3°
Leveling of Optical Head	0.2°
Parabolic Curve Fit	≤0.1°
<hr/>	
Total accuracy without filter calibration (root mean square sum)	0.37°

educated estimates of the absolute accuracy of the LTA system at the level of calibration used in the tests. These could all be improved by more careful calibration procedures.

3. Statistical Errors of Velocity Magnitude Measurements

In the recent ISL paper,⁽⁷⁾ a formula was derived for the statistical error in the mean flow magnitude for the limiting case of high detection threshold where the flat "background" portion of the correlogram is zero:

$$\frac{\sigma_v}{v_o} \approx \frac{\sigma_\tau}{\tau_o} = \frac{1}{k_o} \sqrt{\frac{\Delta k (1 - \Delta k)}{N}} \leq \frac{1}{2k_o} \sqrt{\frac{1}{N}} \quad (2)$$

where $k_o = DT/\tau_o$ = mean (non-integer) correlator bin no.

σ_v/v_o = Fractional rms velocity deviation.

σ_τ/τ_o = Fractional rms transit delay deviation.

Δk = Fraction of bin no. that k_o differs from integer.

N = Total number of transit data pulses crossing both spots.

The formula thus gives for the example of section 3.1 with $k_o = 25.4$, the fractional rms error due to small number statistics if

$$\frac{\sigma_v}{v_o} \approx \frac{1}{(2)(25.4)} \sqrt{\frac{1}{25}} = 0.004 \quad (3)$$

This is a result of 0.4% which would be acceptable in many applications.

The significance of a faster correlator is especially apparent here. Not only is the mean delay more accurately calculable with less interpolation, but the percentage variability error is reduced for low

turbulence flow. With $DT = 5$ ns instead of 50 ns, then for the same transit delay, $k_0 = 254$ instead of 25.4. If the actual turbulence were 0.4% or less, then the mean could be measured to a fraction of this with only a few particle transits.

Previous work had indicated that setting the detection threshold to produce correlogram data peak to background ratios of 5 to 10 seemed to optimize available data rate without introducing excessive additional variability error due to the statistical fluctuations of the background. The experimental results reported in section IV quickly revealed that under conditions of very little data, the background-contributed variability is quite significant at peak to background levels of 5 and, in fact, this is not a useful measure for setting thresholds. All experimental measurements after the initial test runs were made at low values of background so that the existing formula for error estimation based on zero background could be used.

4. Statistical Errors of the Flow Angle Estimate

In previous measurements with low turbulence flows, the particle concentration has been statistically steady and at least 100 data pulse pairs per second were obtained when the spot pair was aligned near the true flow angle. Under these conditions, 0.1° angle repeatability was obtained in the past.⁽⁹⁾ No detailed theory for the angular error has yet been developed; however, any such theory would have proved useless in the case of the SAW tunnel results due to particle rate fluctuation. We, therefore, can only report experimentally observed variability in the angle estimates, which varied from 0.1° to several tenths of a

degree in the TGF to more than one degree in the unstationary particle conditions of the SAW tunnel.

5. Particle Size Sensitivity

This section presents a derivation of the minimum detectable particle size for the LTA system which is used later with the experimental results. The mathematical model used here is very simplified. The statistically expected number of detected photoelectrons released by the photocathode during a detection integration interval by a scattering particle is $\langle N_d \rangle$ given by

$$\langle N_d \rangle = \lambda_d T_d \quad (4)$$

here T_d is the transit time of one spot (D_f/V) or the detection filter impulse response width, whichever is smaller, and λ_d is the rate of emission of photoelectrons from the photocathode. If $\langle N_d \rangle$ is greater than 3, then the pulse is presumed to be detected by a discriminator with the detection level set at about 3 times the mean photoelectron impulse response pulse height. Now λ_d is calculated as

$$\lambda_d = - \frac{\eta_d \eta_r \eta_w^2 \Omega I_o}{h\nu} \left(\frac{i_p}{k^2} \right) \quad (5)$$

where the efficiency factors denoted by η are listed in Table 1, i_p is the differential Mie scattering coefficient at 180° backscatter (presumed constant over the collecting solid angle Ω for submicron particles as an approximation), and k is the wave number $2\pi/\lambda$.

$$I_o \approx \frac{P_\ell}{2} \eta_t \eta_w^2 / (\pi D_f^2 / 4) \quad (6)$$

and the collecting solid angle Ω is approximated as

$$\Omega \approx \frac{\pi}{4(F/no)^2} \quad (7)$$

combining all these factors we obtain:

$$\langle N_d \rangle = \frac{T_d d r t w^4 P_\ell}{2D_f^2 (F/no)^2 h\nu} \left(\frac{1}{k^2} \right) \quad (8)$$

where $k = 2\pi/\lambda = 12.21 \times 10^{+6} \text{ m}^{-1}$ for the laser radiation wavelengths $\lambda = 514.5 \text{ nm}$.

The results of Equation 8 can be condensed to a simple result by using the actual parameter listed above in Table 1. Thus:

$$\langle N_d \rangle = \frac{(25 \times 10^9)(0.2)(0.4)(0.7)(0.9)^4}{(2)(16 \times 10^{-6} \text{ m})^2 (5)^2 (4 \times 10^{-19})(12.2 \times 10^6)^2} (P_\ell) \left(\frac{1}{k^2} \right) = 1205 \left(P_\ell \right) \left(\frac{1}{k^2} \right) \quad (9)$$

In previous work,⁽⁷⁾ we have modeled the Mie scattering coefficient for a lossless spherical scatterer of index of refraction 1.5 in air by a simple formula approximately valid in the range $0.1 \mu\text{m} \leq d \leq 1.25 \mu\text{m}$, where d is the particle diameter in meters of

$$i_p(d) = 23.7 (dx10^6)^4 \quad (10)$$

In order to determine the detected number of photoelectrons within the impulse width of the detection filter, we have tabulated the results of applying Equation (9) with an assumed laser power of 300 mW. This tabulation is given in Table 4, which indicates that particles between 0.15 and 0.2 micrometers in diameter were being observed. It is pointed out that the approximate formula for the Mie scattering coefficient is conservative by a factor of 2 in the range 0.1 to 0.2 μm diameter which

TABLE 4
 PHOTON DETECTION NUMBER VS. DIAMETER
 FOR TABLE 1 CONDITIONS

d (μm)	I_p	$N_d(300\text{mw})$	$N_d(100 \text{ mw})$
0.10	0.0024	0.86	0.29
0.15	0.012	4.32	1.44
0.20	0.038	13.7	4.6
0.25	0.093	33.5	11.2
0.30	0.19	68.4	22.8
0.35	0.61	130	43
0.40	1.5	220	73
0.50	3.1	540	180

allows room for some loss on the part of the scatterer and/or errors in estimating system efficiency factors. For a very conservative estimate, one could use the values given in Table 3 for 100 mW even when the 300 mW power was used. The results still indicate that 0.2 μ m diameter particles were detected at up to 700 m/s.

6. Data Rate and Particle Number Density

We make certain deductions concerning the number of density of small particles from the LTA system parameters. The probe volume cross section of area A_p is given by:

$$A_p = D_f L \quad (11)$$

where D_f is the diameter of each of the focused beams, and L is the effective length of the probe volume (as limited by the receiving optics). This, of course, is only the true projected pulse-pair capture area for particles traveling exactly parallel to the plane of the two focused beams. For laminar flow with perfect angular alignment, then the pulse pair data rate R_d is given approximately in terms of the number density of detectable particles as

$$R_d = N_p VA \quad (12)$$

which is easily inverted to determine number density:

$$N_p = \frac{R_d}{VA} \quad (13)$$

Example values of particle number densities may be determined from the experimental results as follows:

The Mach 0.9 data at about 270 m/s gave a rough average of 1 pulse pair/second in the TGF and 50 pp/s in the SAW. These

results correspond to number densities of $0.580 \times 10^6 \text{ m}^{-3}$ and $29 \times 10^6 \text{ m}^{-3}$ respectively, of particles greater than 0.15 to 0.2 μm diameter.

Some attempt was made to see if particle number density could be correlated with pressure, P_0 . Although data tend to indicate an increase in number density with P_0 , the amount of data collected while varying P_0 was insufficient to establish a direct relationship.

SECTION IV

EXPERIMENTAL CHARACTERIZATION

1. Overview

Measurements of three types were made. First subsonic and supersonic measurements with and without seeding were conducted through the single windows in the 2 by 2 foot test section of the TGF (TGF Characterization Measurements). The optical setup was as illustrated previously in Figure 3 with the system operating at normal incidence to the window. The second set of measurements in the TGF was mapping the mean velocity and flow angle on selected lines near a three-dimensional microfighter model inside the 15 x 15 inch transonic test section insert of the TGF. This facility configuration has two windows on each side as illustrated in Figure 6. The last set of measurements was along some of the same relative lines near the same microfighter model installed in the 9 inch SAW wind tunnel which also has two windows on each side, Figure 7. The microfighter data is reported in Sections V and VI. This section presents the results of the system characterization for subsonic, supersonic, and transonic test sections with examples of raw data.

2. TGF Characterization

The subsonic and supersonic tests were conducted through a single (laminated) Schlieren window 2.44" thick with the LTA beams at normal incidence and focused at a point approximately at the center of the test



Figure 6. Installation for TCF Tansonic Microfighter Measurements.

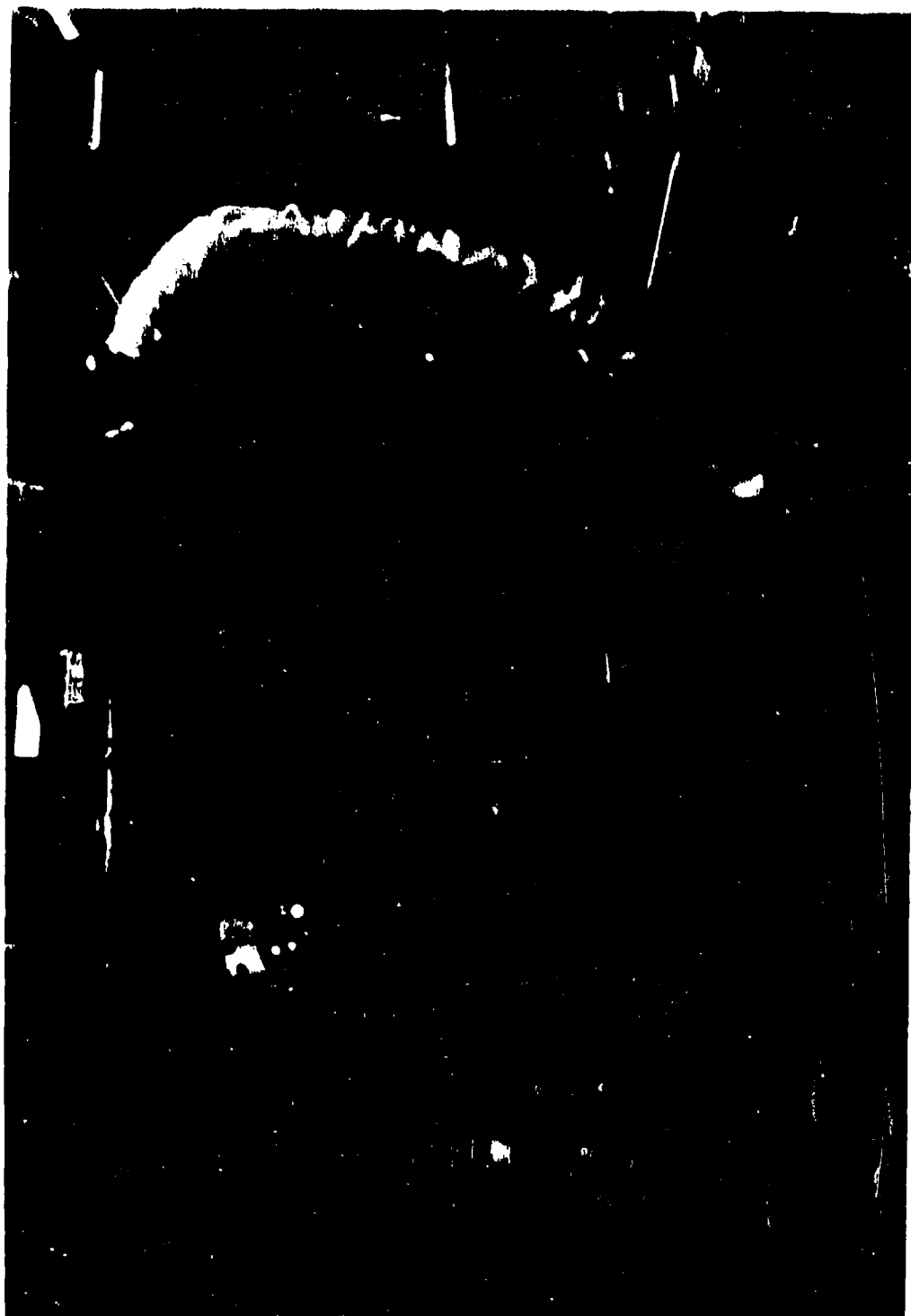


Figure 7. Installation for SAW Microfighter Measurements.

section as previously illustrated in Figure 3. The raw data consists of notebook log entries and the experiment parameters, correlograms, angle plots, and estimates of velocity, angle, data rate and background rate (rate of building of correlogram background). Each major change of tunnel condition, date, or purpose was given a new experiment number, although run numbers were incremented throughout all experiments. The results are summarized here according to experiment number subheading.

a. Experiment 1

Wednesday, October 22, 1980. Shake-down runs with no data printed out by the Video Graphics Unit (VGU).

b. Experiment 2

Mach 0.4, stagnation pressure $P_0 = 2215$ pounds per square foot (PSF). October 23, 1980, Runs 8-39. During this set of data, the correlator interface read the correlograms with a shift of one place (each correlator store number was one too low, so that the software interpreted an actual 140.7 m/s as 146.74 m/s, as for example in run 19. For this experiment, due to the low speed, the discriminator was set to range 4 (100 ns detection filter gives 4 times more photons within detection filter width than Range 2). Laser power varied between 120 and 200 mW during experiment. The data is summarized in Table 5 for 10 consecutive repetitions of runs at the best angle. Although the average of the measurements was within 0.6% of the tunnel computer mean flow estimate, the statistical scatter on the results was not very low (2%). This is much more than would be predicted by the theory for low background correlograms with typically 125 data pulse pairs per 10 second run. Figure 8

TABLE 5
DATA FROM MACH 0.4

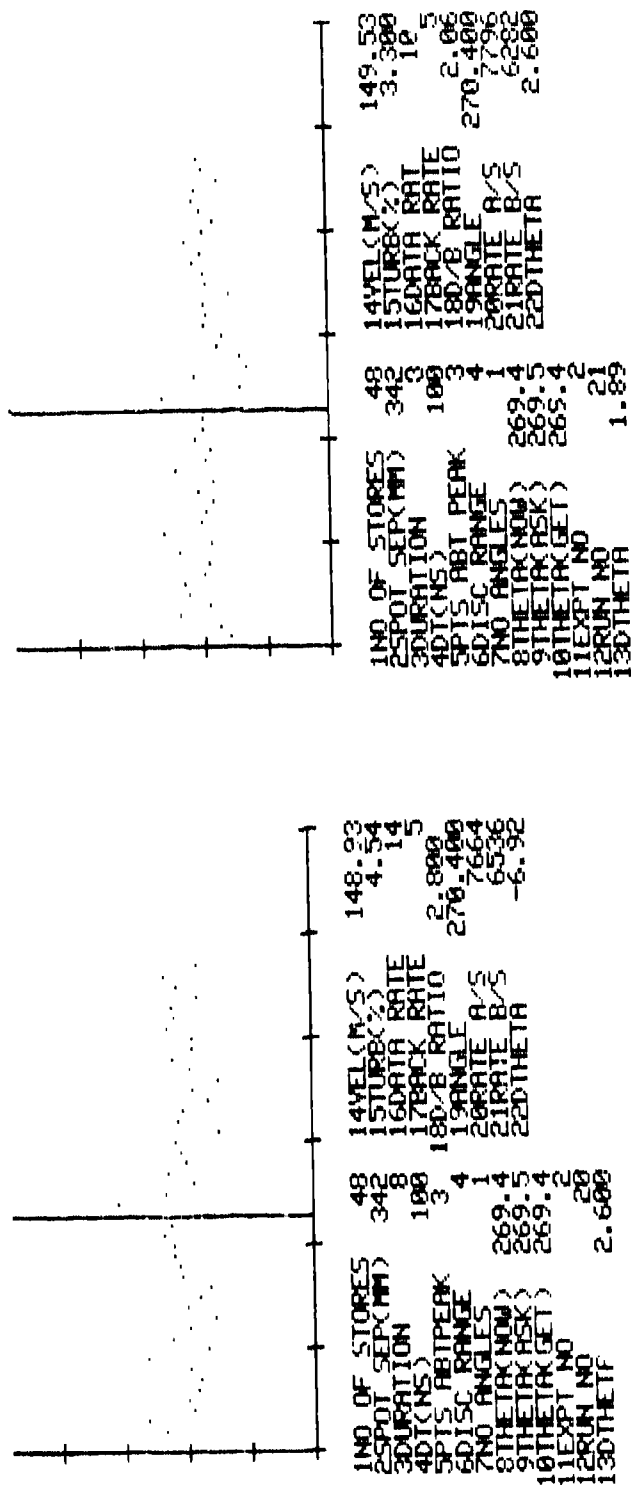
Natural Seeding

Mean data rate	12.5 pulse pairs/s
Mean speed (10 measurements, 10 s each)	140.0 m/s
RMS Dev. of mean estimates	2.73 => 1.95%
Tunnel speed	140.8 m/s
Tunnel RMS dev.	0.3 => 0.2%
P_o	2205.0 PSF

Artificial Seeding

Mean data rate		2200 pulse pairs/s
Run	Tunnel Speed m/s	LTA speed m/s
36	139.7	137.8
37	139.8	137.8
38	137.7	136.8

NOTE: ¹See Figure 5 For Detailed Explanation.
²Correlator Shift Error Correction Not Included Here.



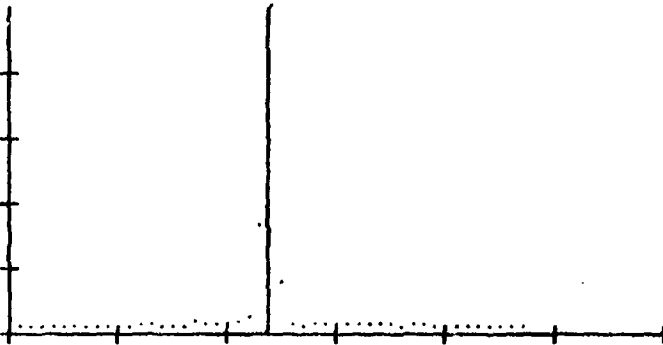
*NOTE: Correlator Shift Error Correction Not included here.

Figure 8. Typical Correlograms for Mach 0.4, Po = 2208 PSF Without Seeding.

illustrates two typical results. Note that in the run, 3 points either side of the peak were included in the mean flow calculation, and the variability thus introduced by the background fluctuations is obvious by inspection of the two correlograms. Also in these results, the computed turbulence level is erratic due to the effects of limited resolution. The 100 ns range of the correlator was used due to the fact that the upper 48 stores of the correlator could not read out at all and had to be abandoned. With only 48 stores, 50 ns would have been inappropriate. As an experiment during the Mach 0.4 tunnel condition a droplet seeder was installed by the Experimental Engineering Branch and used to inject a water-glycerine mixture of small droplets into the flow up stream of the screens and tunnel contraction section. Figure 9 is an example of a typical result, and Table 5 includes the corrected new velocity estimates and the tunnel computer estimates. It is conjecture as to whether the results with the seeder show systematic error between the computed tunnel velocity data and the LTA data, or perhaps particle lag of the droplets. It is interesting to observe, however, that the correlograms from the seeded flow indicate turbulence levels higher than one would suspect for the tunnel which could be due to particle lag dispersion. The turbulence computed by the LTA is not meaningful, in a quantitative sense, due to correlator shift error.

c. Experiment 3

Mach 0.4, $P_o = 860$ PSF. October 23, Runs 40-46. The pressure was reduced to $P_o = 860$ PSF. The mean data rate fell to 7 per second (from 12.5 at $P_o = 2205$ PSF). A better procedure for optimum data accuracy might have been to increase the detection threshold to reduce the relative amount of the



1NO OF STORES	48	14VEL(M/S)	143.57
2SPOT SEP(MM)	342	15TURB(%)	2.200
3DURATION	8	16DATA RAE	2101
4DT(NS)	100	17BACK RATE	61.34
5PTS APT PEAK	3	18O/B RATIO	269.53
6DISC RANGE	4	19ANGLE	15303
7NO ANGLES	1	20RATE A/S	10870
8THETA(NOW)	269.8	21RATE B/S	.75
9THETA(ASK)	269.6	22THETA	
10THETA(GET)	269.8		
11EXPT NO	3		
12RUN NO	3		
13DTHETA	1.26		

NOTE: Correlator shift error not included here.

Figure 9. Mach 0.4 Results with Droplet Seeding.

background to signal. The results of 3 ten second measurements yielded an average estimate of 139.8 m/s with a standard deviation of 3 m/s. The average of two 100 second measurements was 136.0 m/s with a difference between the two of 1.6 m/s. The tunnel computer indicated a mean speed of 138.7 m/s with a standard deviation of 0.75 m/s as determined from conventional pressure and temperature measurements. The agreement is actually remarkable considering the very low quality of the correlograms due to incorrect threshold setting illustrated in the right side correlogram in Figure 10.

d. Experiment 4

Mach 0.7, $P_0 = 1319$ PSF. Runs 47-59, October 23, 1980. The previous results had indicated the need for a change of threshold. This is a relative setting which can also be effected by changing the PMT high voltage (HV) settings. Decreasing the PMT HV is somewhat equivalent to increasing the detection threshold within limits. This is limited by the constant 2.2 volt overload detection threshold which rejects large signals by inhibiting the discriminator output, and on the other extreme, by drift and noise of the discriminators at the level of a few millivolts. The detection threshold range is generally maintained at 100 to 200 mv. Generally speaking, the pulse detection rates on discriminator channels A and B were kept matched by using the correlator monitor stores to check balance when adjusting the HVA and HVB settings. A fault in the Malvern computer output circuit caused incorrect readings at times to be printed in the data for Rate A and Rate B so that the apparent disparity of the printed data is not factual.

By lowering the PMT gain and thus effecting a relative increase in the detection thresholds, the typical correlograms for the Mach 0.7

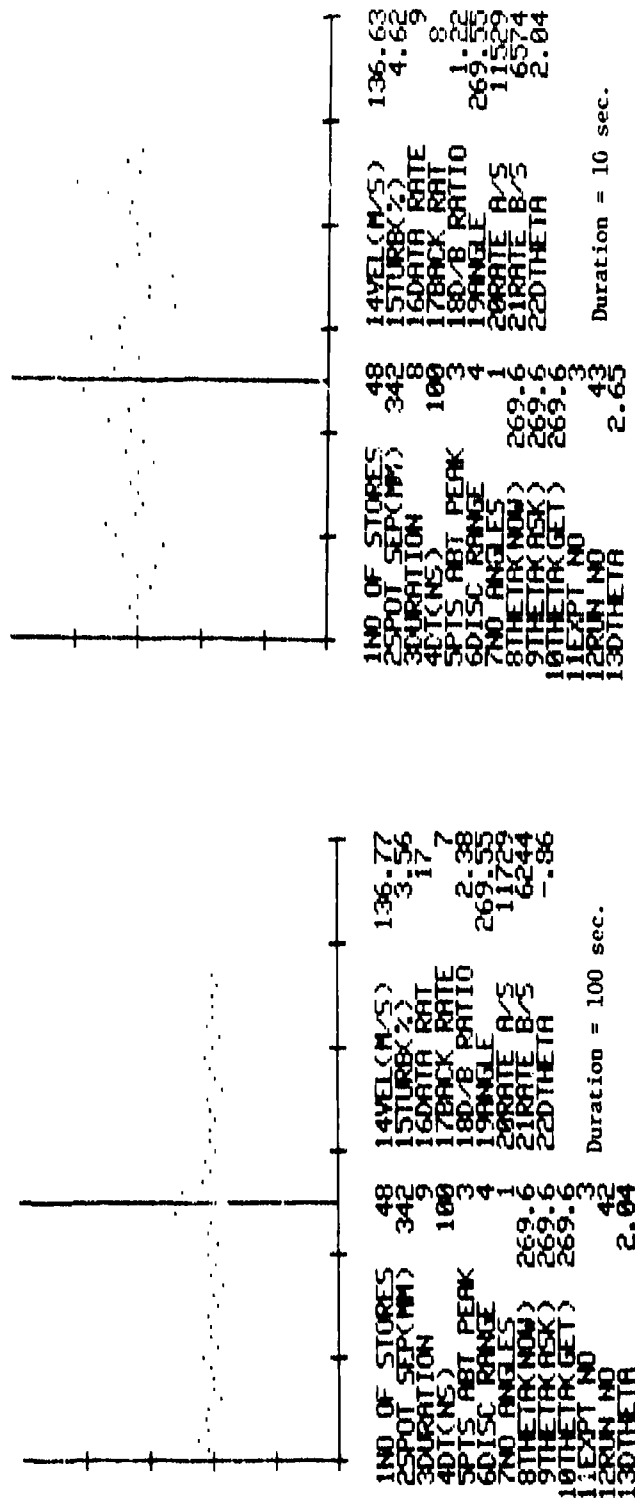


Figure 10. Correlograms from Mach 0.4, $P_0 = 860$ PSF, Illustrating Threshold Effects.

runs were made to appear as shown in Figure 11, where the right side correlogram illustrates the effects of a higher threshold setting. Table 6 summarizes the results of 5 consecutive runs of 5 seconds interval and also two runs of 50 seconds each. Even though 3 points either side of the peak of the correlogram were still used, the measurement standard deviation was reduced by the increase in the relative detection threshold. Also, it was observed that the variation in the total number of data pulse pairs per run significantly exceeded the predictions of Poisson statistics, as evidenced by the sequence of data rates given in the table.

It was observed that the average of the 5 consecutive 5 second runs agreed with the tunnel estimate average absolutely to within 0.3%. This may be a fortunate accident since the average of the two 50 second runs only agreed to within 0.8%. However, for absolute agreement without collaboration or extensive calibration, this seems quite good.

e. Experiment 5

Mach 2.3 $P_0 = 715$ PSF. Runs 60-64. October 23, 1980. This series was started with only 25 minutes until tunnel shut-down time. There were difficulties due to the Malvern readout. With limited test time remaining for the day it was decided to use the seeder to increase data rate for remaining runs. The results are shown in Figure 12. The velocities were corrected by the one store error as shown in the figure. The repeatability was to 0.12%. The tunnel computer gave 545.7 m/s, which differs by 3%. The source of the discrepancy is not known, but until shown otherwise both tunnel calibration and the LTA system are

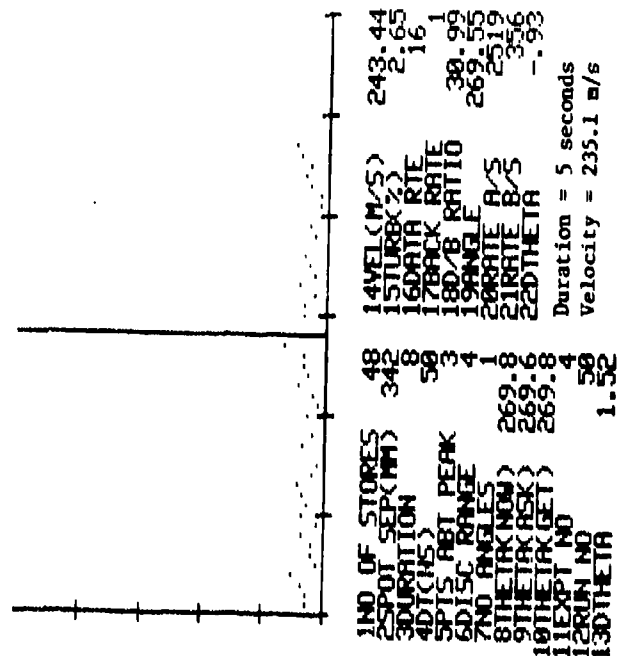
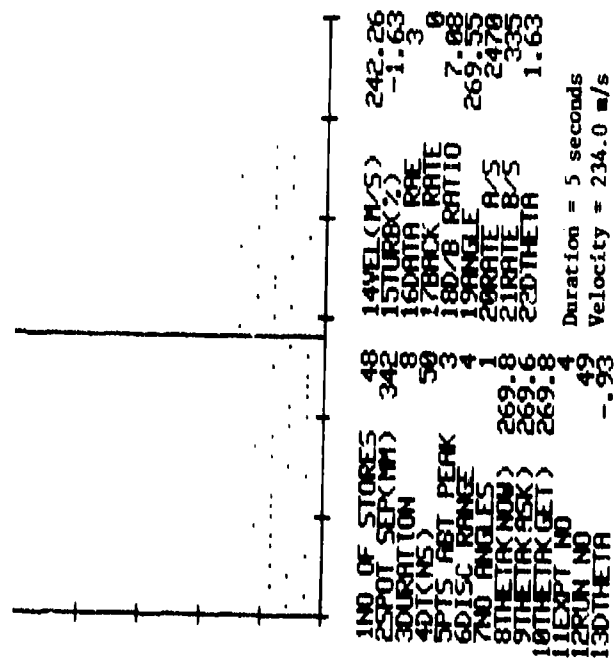
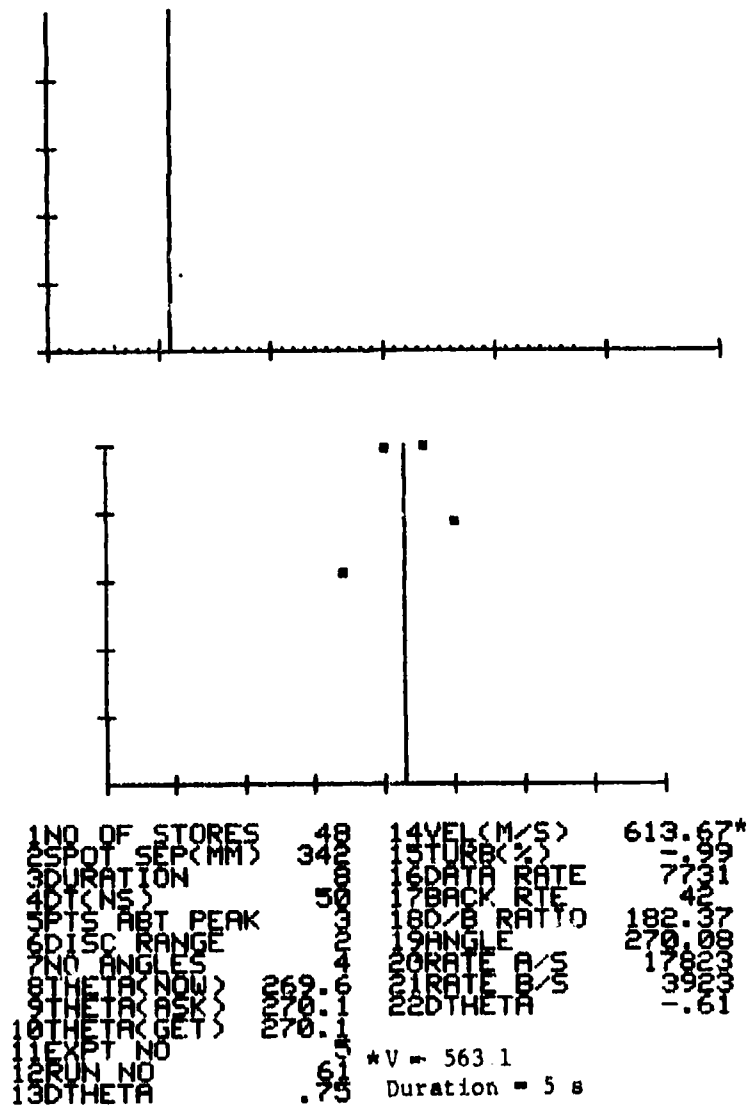


Figure 11. Examples of Mach 0.7 Correlograms with Increased Relative Threshold.

TABLE 6

MACH 0.7 P₀ = 1319 PSF DATA SUMMARY

Run	Data Rate (S ⁻¹)	Corrected Velocity m/s	Tunnel Estimate m/s	Duration
48	6	234.2	236.7	5s
49	3	234.0	236.8	5s
50	16	235.1	237.1	5s
51	6	239.5	N/A	5s
52	<u>13</u>	<u>237.2</u>	<u>236.1</u>	
Mean, Dev.	8.8, 5.4	236.0, 2.3	236.7, 0.42	
57	5	235.3		50s
58	<u>4</u>	<u>234.4</u>	236.7	50s
Mean, Diff.	4.5, 1	234.8, 0.9		



See Figure 5 For Detailed Explanation.

Figure 12. Mach 2.3 Data with Seeding.

suspect. Although there should have been no bias errors due to the somewhat coarse correlator time resolution, it would certainly have been preferable to use the 5 ns correlator for the measurements.

f. Experiment 6

Mach 2.3, $P_0 = 2846$ PSF, Friday, October 24, 1980, Runs 65-88. A series of runs was made while the tunnel was approaching condition and after reaching condition. The data rate varied widely as did the measurements, as illustrated in Table 7 and Figure 13 where the left hand side represents the low data rate case and the right hand side represents the high data rate. Reasonable agreement with the tunnel estimate of 560.1 m/s was obtained when the data rate was adequate, but, it is clear from Figure 13 and Table 6 that several things could have been improved. The threshold was still sufficiently low to allow significant background when the data rate was low. This, combined with inadequate correlator time resolution and the variation of 2 points of the correlogram either side of the peak, resulted in lack of repeatability. Near the unplanned shut-down of this series (due to a tunnel cooling system problem) another attempt at seeding was made. Runs 85 and 86 did not show the same large data rates obtained the day before, presumably because the seeding streamline missed the probe volume.

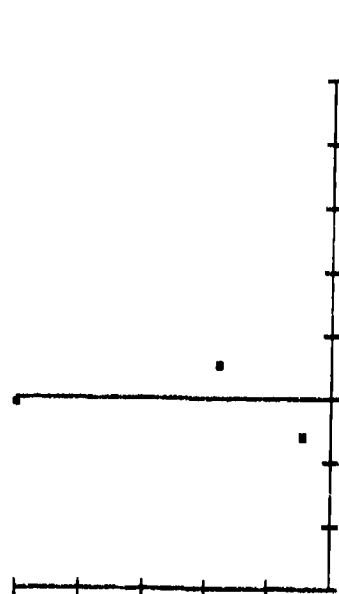
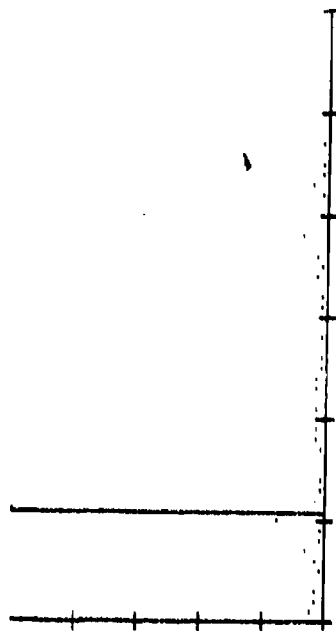
Just prior to tunnel shut-down it was observed that the tunnel contained a very fine mist, clearly visible by scattering from the laser beams, however, since there was no large data rate, these droplets were smaller than the detection size (estimated at $\leq 0.2 \mu\text{m}$ diameter).

TABLE 7

RESULTS AT MACH 2.3

Run No.	Time	Data Rates-1	Recorded Velocity-M/S	Angle Deg.	Duration	Pulse Pairs	S = 338 m	
							Tunnel Velocity M/S	Velocity Corrected-M/S
65	11:17	2	568.6	270.3	5s	10		525.0
66	11:18:10	15	620.5	269.5	5s	75		568.9
67	11:20:10	11	623.7	269.4	5s	55		571.6 Warm Up
68	11:24:30	15	582.6	270.1	5s	75		536.9
69	11:25	35	632.8	270.0	5s	175		579.2
72	11:33:20	2	584.51	270.2	50s	100		538.5
73	11:35:30	1	590.5	269.9	50s	50		543.6
75	11:39:40	2	619.6	270.3	50s	100		568.1
76	11:41:30	4	625.4	269.7	50s	200		573.0 Warm Up
77	11:43	27	629.7	269.5	50s	1350	560.9	576.6
79	11:48	1	656.1	269.6	50s	50	560.7	598.7 on condition
82	11:54	2	623.5	269.6	50s	100	560.7	571.4
84	12:00	2	629.9	269.7	50s	100	560.8	574.0
85	12:02	17	563.3	269.7	.5s	8.5	560.8	520.4
86	12:03	18	608.4	270.5	.5s	9	560.8	558.7
87	12:08:20	1	570.2	269.7	50s	50	561.1	526.3
88	12:11:30	1	631.8	269.7	50s	50		578.3

NOTE: The axial flow direction is defined to be 270 degrees with the convention that 0 degrees is vertical and above the centerline of the tunnel.



1NO OF STORES	48	14VEL (M/S)	620.500*
2SPOT SEP (MM)	338	15TURB(X%)	-1.600
3DURATION	8	16DATA RATE	15
4DT (MS)	50	17BACK RATE	0
5PTS FBI PEAK	2	18D/B RATIO	61.53
6DISC RANGE	2	19ANGLE	269.52
7NO ANGLES	2	20RATE A/S	54
8THEIR (MM)	269.3	21RATE B/S	1342
9THEIR (PS)	269.5	22DTHETA	-2.36
10THEIR (GT)	268.6		
11EXPT NO	6		
12RUN NO	66	*V = 568.8	
13DTHETA	.75	Duration 5 s	

1NO OF STORES	48	14VEL (M/S)	568.64*
2SPOT SEP (MM)	338	15TURB(X%)	-4.12
3DURATION	8	16DATA RATE	2
4DT (MS)	50	17BACK RATE	0
5PTS FBI PEAK	2	18D/B RATIO	10.97
6DISC RANGE	2	19ANGLE	271.400
7NO ANGLES	2	20RATE A/S	54
8THEIR (MM)	270.3	21RATE B/S	3156
9THEIR (PS)	269.5	22DTHETA	1.48
10THEIR (GT)	270.3		
11EXPT NO	6		
12RUN NO	65	*V = 525.0	
13DTHETA	-2.36	Duration 5 s	

Figure 13. Measurements Without Seeding at Mach 2.3 (661 M/S).

g. Experiment 7

Microfighter Transonic Mach 0.7, $P_0 = 3218$ PSF, October 27, 1980, Runs 83-102. The microfighter model was installed inverted in the TGF 15-inch transonic test section. The setup is illustrated in Figure 6. The outer window was the same, 2.44" thick, and the inner window 1.22" thick with 3.27" separation between the windows. The spot separation was remeasured by the fringe method with both windows in place. A light change is within the measurement precision of the spot separation.

The experiment control software was revised to correct for the displacement by one store which had occurred in the previous measurements. An interim review of the subsonic and supersonic data revealed the need for higher thresholds, even at the expense of lost data when data rates are low. Also, additional software changes were made to test each correlogram for consistency of numerical levels of the background with previous data and rerun any measurements for which the Malvern unit produced unusable data. This allowed successful angular measurements to be made (during the previous measurements the probability of obtaining 5 successive usable correlograms from the correlator was too small to be useful).

In order to characterize the precision obtained experimentally, a series of runs was made at a location 4" below the model on the upstream end (near free stream conditions). The mean velocity and direction were repeatedly measured from the time the tunnel began running. Due to a higher scattered or flare light levels from the two windows, the PMT high voltage had to be turned down about 100 volts with respect to earlier measurements

in order to obtain low background correlograms. This resulted in a lower overall data rate.

Table 8 is a summary of the computed results of this series. The measured velocity (bottom graph) and angle history (top graph) are also plotted in Figure 14. The mean and standard deviation of the measured magnitude as compared with the tunnel estimates were as follows:

	<u>Mean</u>	<u>S. D.</u>	<u>S. D. %</u>
LTA	233.1 m/s	2.67	1.15%
Tunnel Computer	236.45 m/s	0.83	0.35%
Angle LTA	270.40°	0.31°	

These results are actually quite amazing when one considers that at the lowest data rate about 1 per second, the correlograms for a 5 second run have about 5 correlated pulse pairs in a background level of less than one per store as illustrated by the left hand side of Figure 15. Run 119 shown on the right hand side of Figure 15 was taken with 50 seconds per angle to observe the effects of more data. The result is a measurement much closer to the average measurement than the standard deviation of the 5 second data sets. We note that the LTA measurement is a little below that of the tunnel computer. This is probably the result of a combination of both statistical fluctuations, the difference between any systematic errors of both the tunnel calibration and the LTA and, of course, any actual reduction in velocity at the measurement location due to the presence of the model.

At the end of the sequence of runs just described, the LTA probe volume was moved up near the nose of the model in an attempt to find the stream line of droplets produced by the seeder. The data rate increased

10/27 - Exp. 7

TABLE 8
SUMMARY OF COMPUTED DATA

Run No.	Time S	Data Rate s ⁻¹	Recorded Velocity M/S	Angle Deg.	Duration	Total Data Pulse Pairs	
93	11:36:37	10	403.6	270.45	5s	50	P
94	11:40:32	36	418.3	271.57	5s	180	P
95	11:44:36	6	425.3	270.9	5s	30	P
96	11:47:56	3	417.9	271.64	5s	15	P
97	11:50:56	18	260.6	270.83	5s	90	P
98	11:55:09	2	235.3	270.90	5s	10	P
99	11:58:47	7	235.3	270.90	5s	35	P
100	12:02:00	3	231.1	269.78	5s	15	P
101	12:05:31	6	235.9	270.83	5s	30	P
102	12:11:10	5	236.6	270.45	5s	25	P
103	12:15:25	4	229.0	270.16	5s	20	P
104	12:19:10	3	230.1	270.44	5s	15	P
107	12:25:00	2	231.6	270.39	5s	10	P
109	12:29:30	2	235.6	270.36	5s	10	P
110	12:31:45	3	228.9	270.54	5s	10	P
112	12:35:39	1	236.2	270.52	5s	5	P
113	12:38:23	2	232.2	270.45	5s	10	P
115	12:44:00	1	229.1	270.47	5s	5	P
116	12:49:10	1	234.7	269.89	5s	5	P
119	1:01:33	1	232.1	270.67	50s	50	P
120	1:35:05	45	228.1	283.7	5s	225	S
121	1:37:44	8	228.4	283.78	5s	40	P S
122	1:40:51	7	226.9	283.75	5s	35	P S

Warm
Up

on
condition

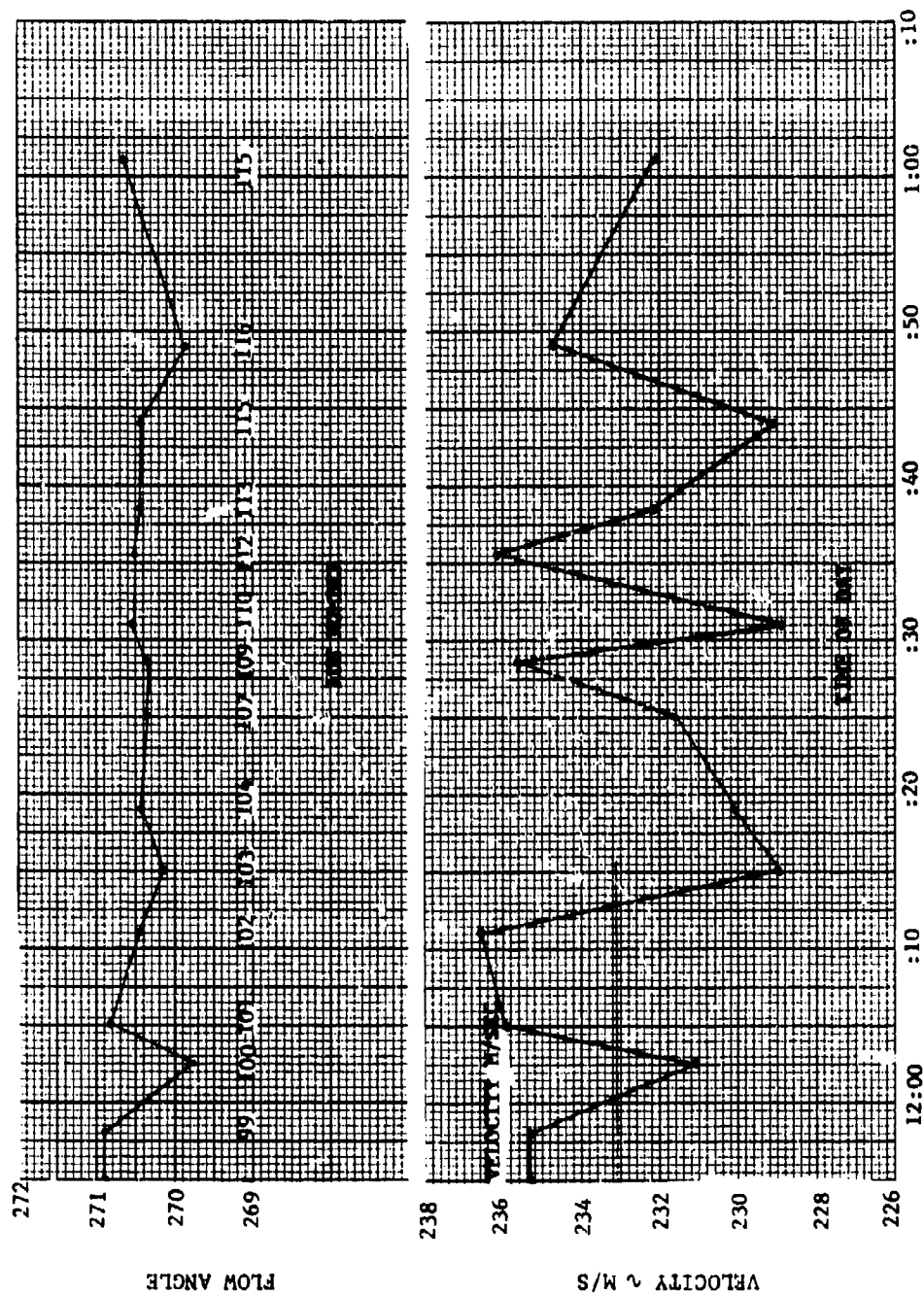
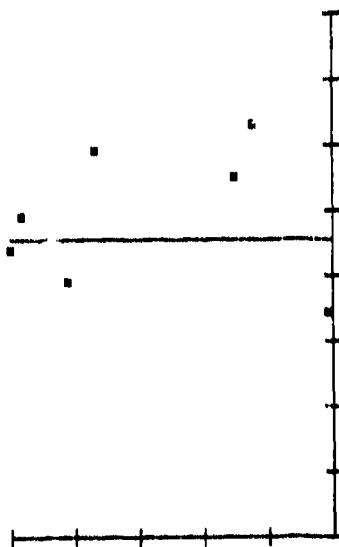
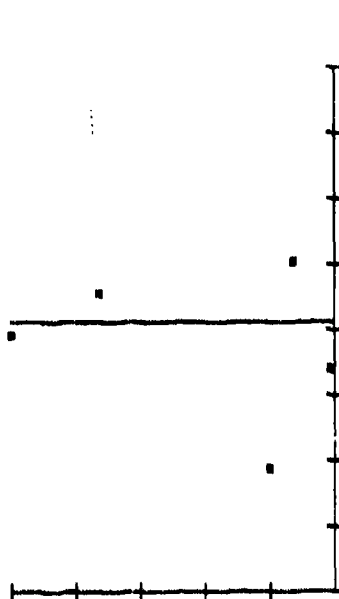
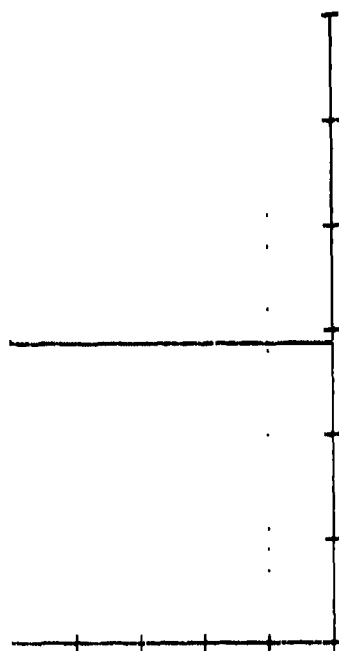
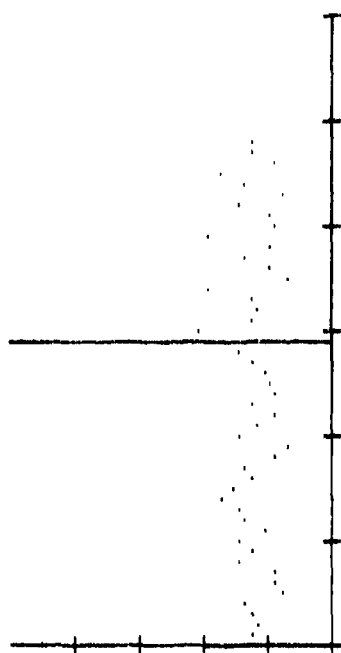


Figure i4. Repeatability Test.



1NO OF STORES	48	14VEL (M/S)	232.07
2SPOT SEP(MM)	338	15TURB(%)	1.500
3DURATION	50	16DATA RATE	1
4D(CNS)	50	17BACK RAT	0
5PTS ABT PEAK	2	18D/B RATIO	4.38
6DISC RANGE	2	19ANGLE	270.67
7NO ANGLES	2	20RATE A/S	1823
8THETA(NOM)	270.3	21RATE B/S	2623
9THETA(ASK)	270.7	22DTHETA	.75
10THETA(GET)	266.7		
11EXPT NO	119		
12RUN NO	119		
13DTHETA	.86		

1NO OF STORES	48	14VEL (M/S)	234.56
2SPOT SEP(MM)	338	15TURB(%)	-1.94
3DURATION	50	16DATA RATE	1
4D(CNS)	50	17BACK RAT	0
5PTS ABT PEAK	2	18D/B RATIO	31.85
6DISC RANGE	2	19ANGLE	269.89
7NO ANGLES	2	20RATE A/S	1983
8THETA(NOM)	270.4	21RATE B/S	1782
9THETA(ASK)	270.9	22DTHETA	.75
10THETA(GET)	268.2		
11EXPT NO	116		
12RUN NO	116		
13DTHETA	.75		

Figure 15. Very Low Data and Background Correlograms from Transonic Flows.

to 45/second, but was nowhere near that obtained in the earlier single window measurements with the seeder. This could be due to the fact that the PMT high-voltage was reduced due to increased flare light or due to poor streamline probe volume relative positioning. After some trials, it was decided that the seeding streamline could not be readily moved far enough down to reach the location 4" below the model centerline at which the primary measurements were desired.

The tunnel was shut-down and several changes were made. The seeding probe was modified in an attempt to allow seeding at 4" below the model centerline, and the LTA system was inclined at angle of 6° to the tunnel window (rotation about a vertical axis) in order to reduce window flare light. This last measure proved helpful and showed that there were multiple reflection flare effects produced by going through two sets of windows which were not sufficiently rejected in some positions. Anti-reflection coating on the inner window or a movable flare stop between the window would have been helpful. By using a 6° angle of incidence, all of the multiple window effects were eliminated except light from the inner window which was reflected and focused on the outer window. This problem occurred at only a few very specific probe volume depths and did not affect most of the succeeding measurements.

h. Experiment 8

Microfighter Transonic Mach 0.7, $P_0 = 3230$ PSF, October 28, 1980, Runs 124-149. After the modifications were made, a series of runs were conducted. Despite the improvements which allowed raising the PMT high voltage levels to even higher than was used with the single windows, the

data pulse-pair rate remained at one per second or less. This fact required the measurement duration to be set at 50 seconds. Measurements were made 5 successive times at a point 4" below the model centerline (runs 131-135), 2 times at a point 1/16" above the model centerline just above the surface of the model, and again 4 measurements 2" below the centerline of the model. The results in Table 9 may be related to the coordinates x,y,z given in the next section.

These results were the last of the characterization measurements before the microfighter flow mapping was undertaken.

A few additional modifications were made to the equipment on Wednesday, October 29. These consisted of changing the 6° off-axis angle of the instrument with respect to the window to that of pitch (down) instead of yaw to see if data rate was affected (it was not). Also, optical stop was inserted in the LTA head to eliminate one additional lens flare source. However, these changes had little effect on the system performance.

TABLE 9

MEASUREMENTS NEAR THE MICROFIGHTER AT Z=0, x=-1.5

Y	Mean V M/S	SDV%	Mean Angle Deg.	Angle SD
-4.0	251.5	0.5%	272.3	N/A
+11/16	255.5	0.3%	258.2	N/A
-2	235.0	0.9%	270.4	0.23°

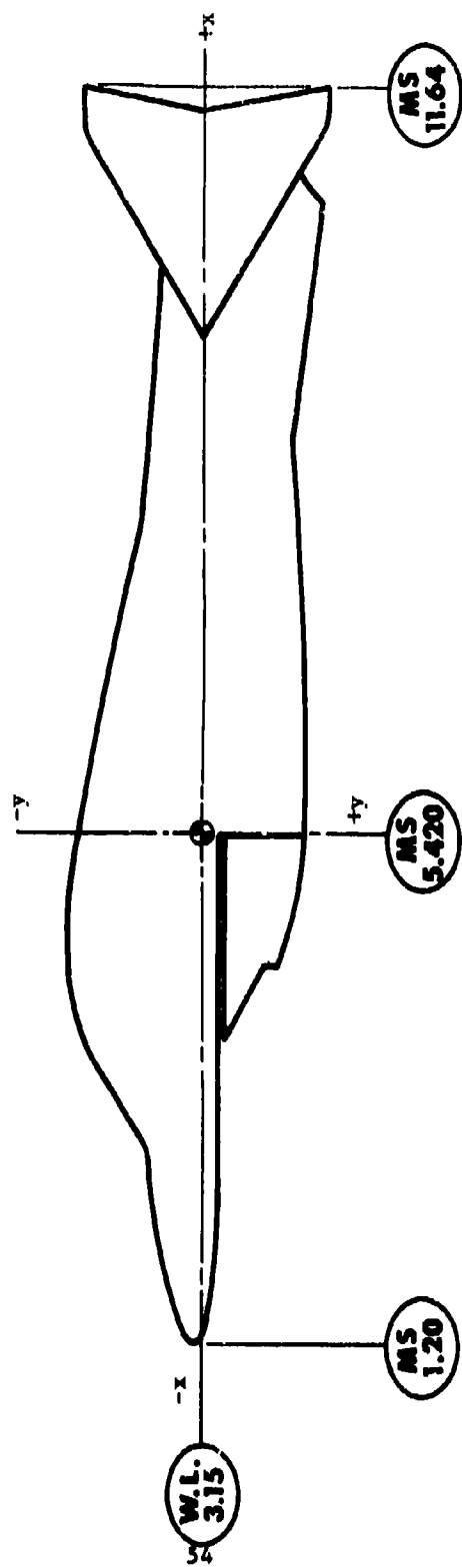
SECTION V

AERODYNAMIC MEASUREMENTS IN THE TRISONIC GASDYNAMICS FACILITY

1. Overview

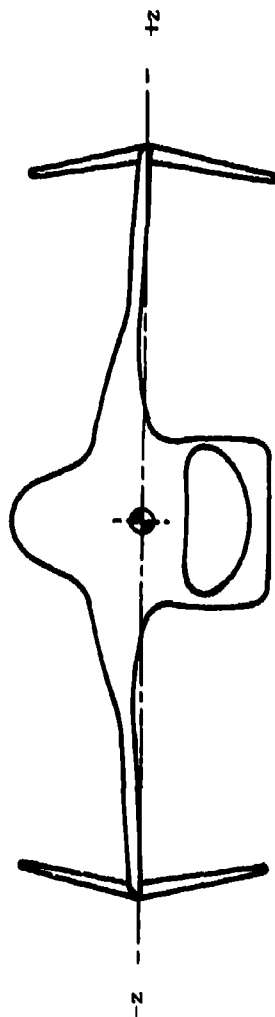
Figures 16a and b are three-fourths scale drawings of the micro-fighter model showing the model coordinate system used as a reference system for the TGF and SAW wind tunnel tests. The model was mounted at zero angle of attack for the entire test series in both tunnels. It was mounted upside down in the TGF and right side up in the SAW wind tunnel. Data were acquired on 0.5" increments along lines located above and below the model centerline at $y = \pm 4.0$ ". The precise location of the chosen origins and axes is presented in subsequent figures with representative data.

To check consistency, some of the data points were repeated on different days, as illustrated on data plots. The data rates obtained were generally from about 0.5 to 1 per second. For these low data rates, 50 seconds per spot pair angle were used to assure good quality correlograms. The experimental run numbers were 150-270 which comprise experiment numbers 9-15. Figure 17 illustrates typical results after the laser power was adjusted to 300 mW. The angle plot shown in Figure 17 is typical. In some cases the statistical fluctuations of data rate with time are clearly limiting the angle estimate precision. When the data output format software was written, it was not envisioned that rounding the data and background rates to whole units would pose any limitations. The data to background ratio does retain additional decimal places which provide a more accurate measure of the background rate.



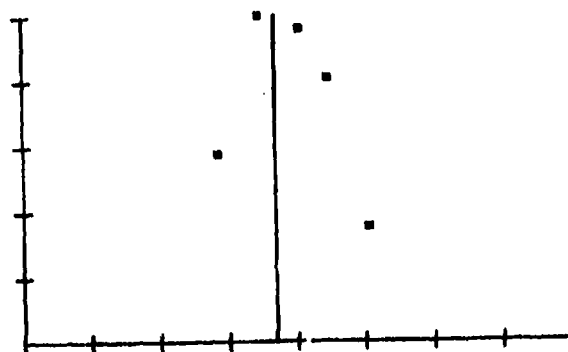
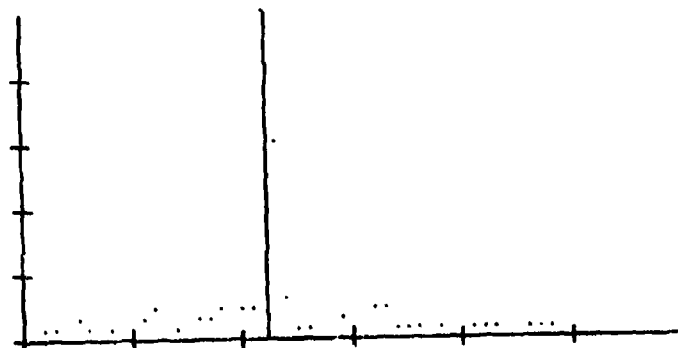
(a) Side View

Figure 16. Three-Fourths Scale Drawing of the Microfighter Model Showing the Coordinate System Used in the TCF Wind Tunnel.



(b) Front View

Figure 16. Three-Forths Scale Drawing of the Microfighter Model Showing the Coordinate System Used in the TGF Wind Tunnel. (Continued).



4NO OF STORES	400	14VEL (M/S)	302.84
5DPT SEP (MM)	3300	15STUF (%)	1.21
6DURATION	500	16DATA RATE	1
7ADT (NS)	500	17BACK RATE	0
8PTS ABT PEAK	100	18D/B RATIO	49.500
9DISC RANGE	100	19ANGLE	270.47
10NO ANGLES	100	20RATE B/S	41
11THETA (NOW)	271.	21RATE B/S	630
12THETA (ASK)	270.	22THETA	.75
13THETA (GET)	270.		
14EXPT NO	200		
15RUN NO	200		
16THETA	.75		

NOTE: See Figure 5 for detailed explanation.

Figure 17. Example of Data from TGF Microfighter Test.

2. Measurements at Mach 0.7 and 0.9

Figure 18 shows plots of mean velocity versus position along lines at 4 inches above and below the model at two Mach numbers. Figure 20 contains the corresponding plots of flow angle. Scans across the tunnel at $y = -4$, $x = 0$ were also made. Results of these scans are presented in Figures 21 and 22.

It was observed that the tunnel computer printout of velocities during these Mach 0.7 runs had a mean value of 237.57 m/s and a standard deviation of 0.62 m/s over the 35 runs of Experiment 9. These tunnel values are indicated on Figure 18 at the left hand side of the figure.

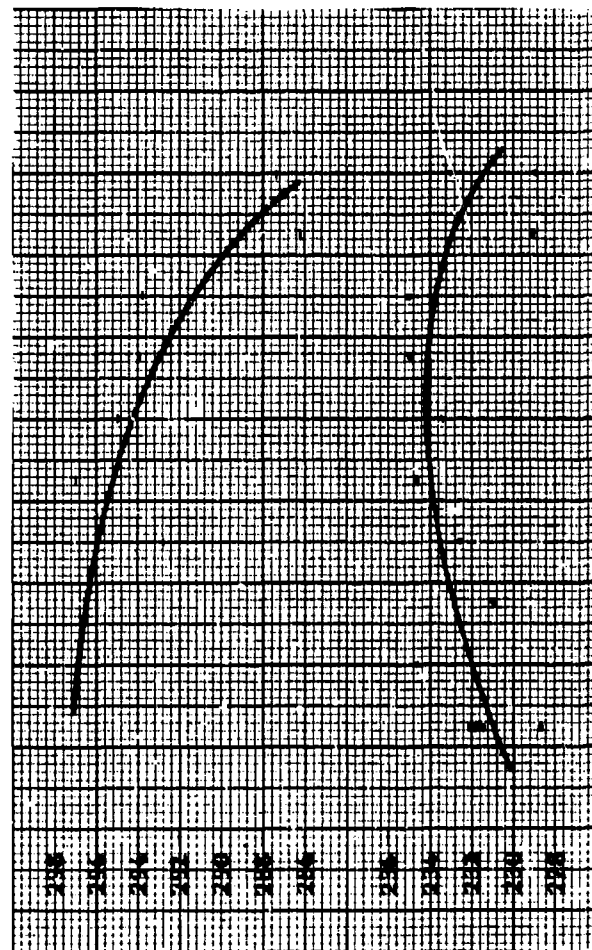
In order to experimentally observe the repeatability of the measurements, portions of the centerline scan at $y = -4$ were repeated on different days as indicated in the figures. The small group of 5 measurements at $x = 0$ were taken near the beginning of tunnel operations when the data rate was higher than average; hence the smaller statistical scatter in these points. The mean and standard deviation of the tunnel computer printouts for the free stream velocity are shown on Figure 18 for comparison.

3. Discussion of Results in the TGF

The mean velocity measurements in the TGF generally had statistical scatter of 1% or less. These results were obtained typically with 10-50 data pulse pairs obtained in a 50 second data collection interval. The results indicate that a faster correlator would have been helpful as would the availability of even a small amount of additional scattering particles.

- Mach 0.9; $P_0 = 3100$ PSF; Mean
Velocity at $y = +4$ ", $z=0$

- Exp. 11



- Mach 0.7; Mean Velocity
Along $y = +4$ ", $z=0$
 $P_0 = 3200$ PSF

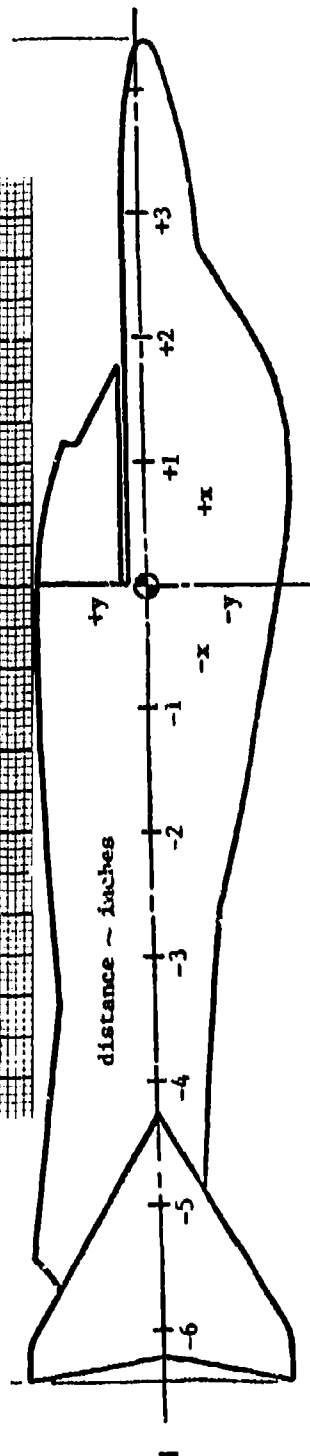
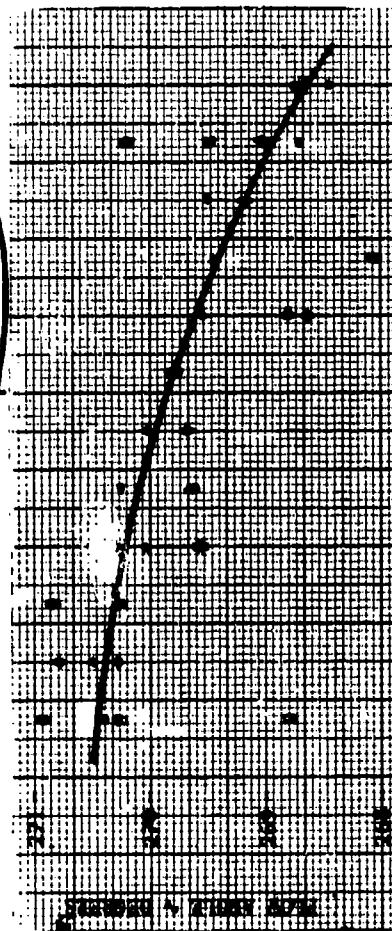
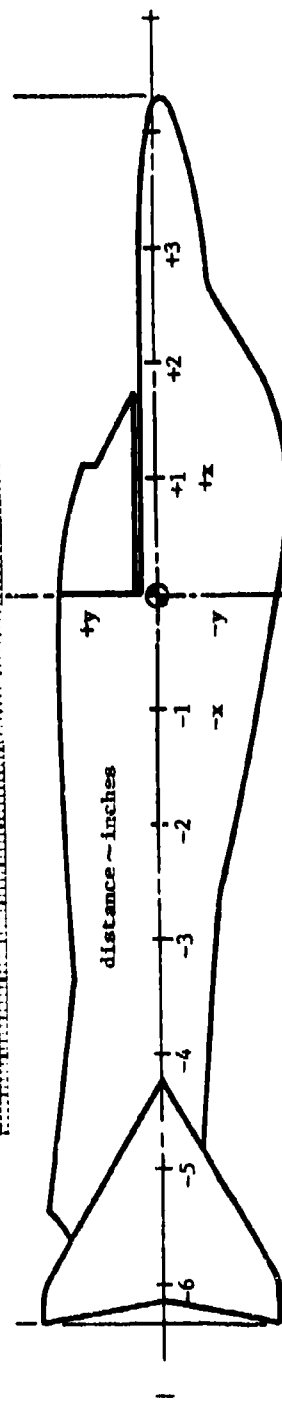
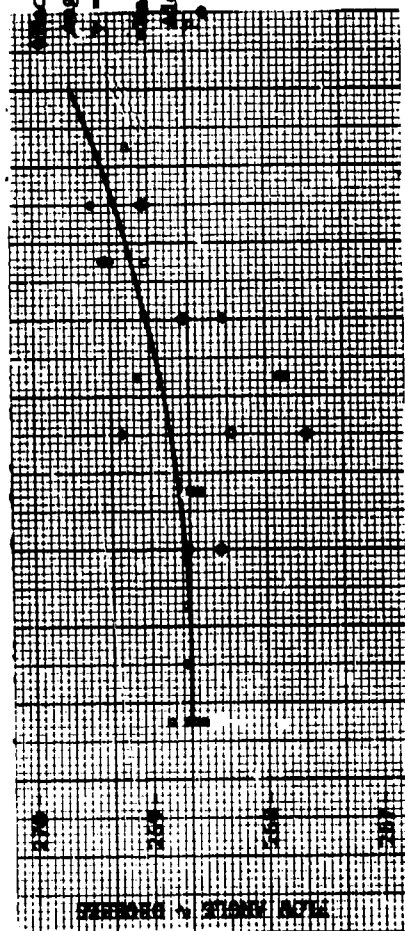


Figure 18. Velocity Measurements at Mach 0.7 and 0.9.

Mach 0.9, $P_0 = 3100$ PSF; Flow
Angle Along the Line
 $y = +4"$, $z=0$

Mach 0.7; Flow Angle
Along Line $y = +4$, $z=0$
 $P_0 = 3200$ PSF



• Mach 0.9 $P_0 = 3100$ PSF
Flow Angle at
 $z = 0$, $y = -4"$

• Mach 0.7; Flow Angle
Along $y = -4$, $z=0$
 $P_0 = 3200$ PSF

• 10/29 Experiment 9
• 10/29 Experiment 10
• 10/30 Experiment 11

Figure 19. Flow Angle at Mach 0.7 and 0.9.

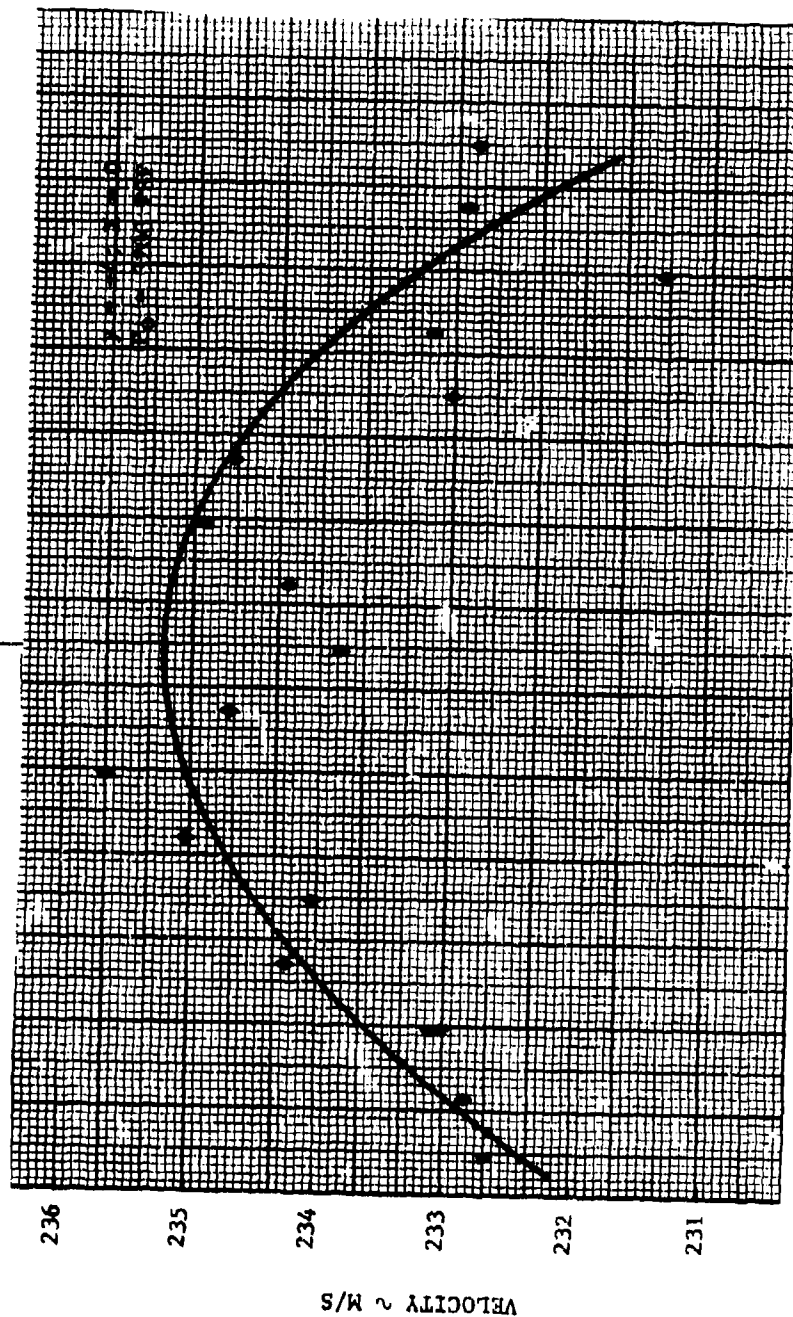
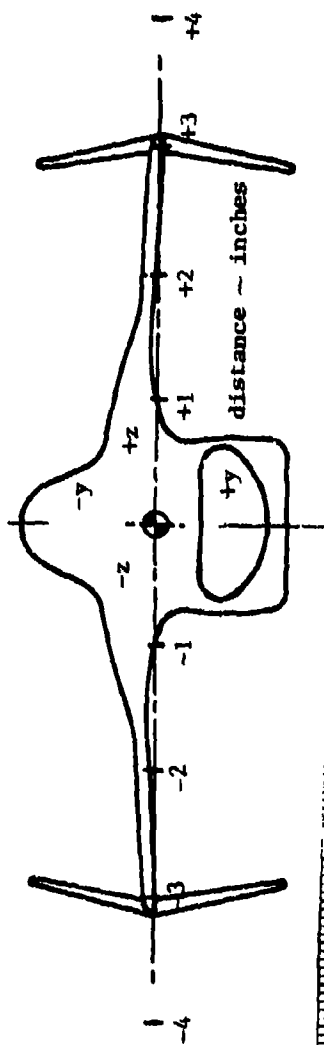


Figure 20. Velocity Profile Across the Wind at Mach 0.7.

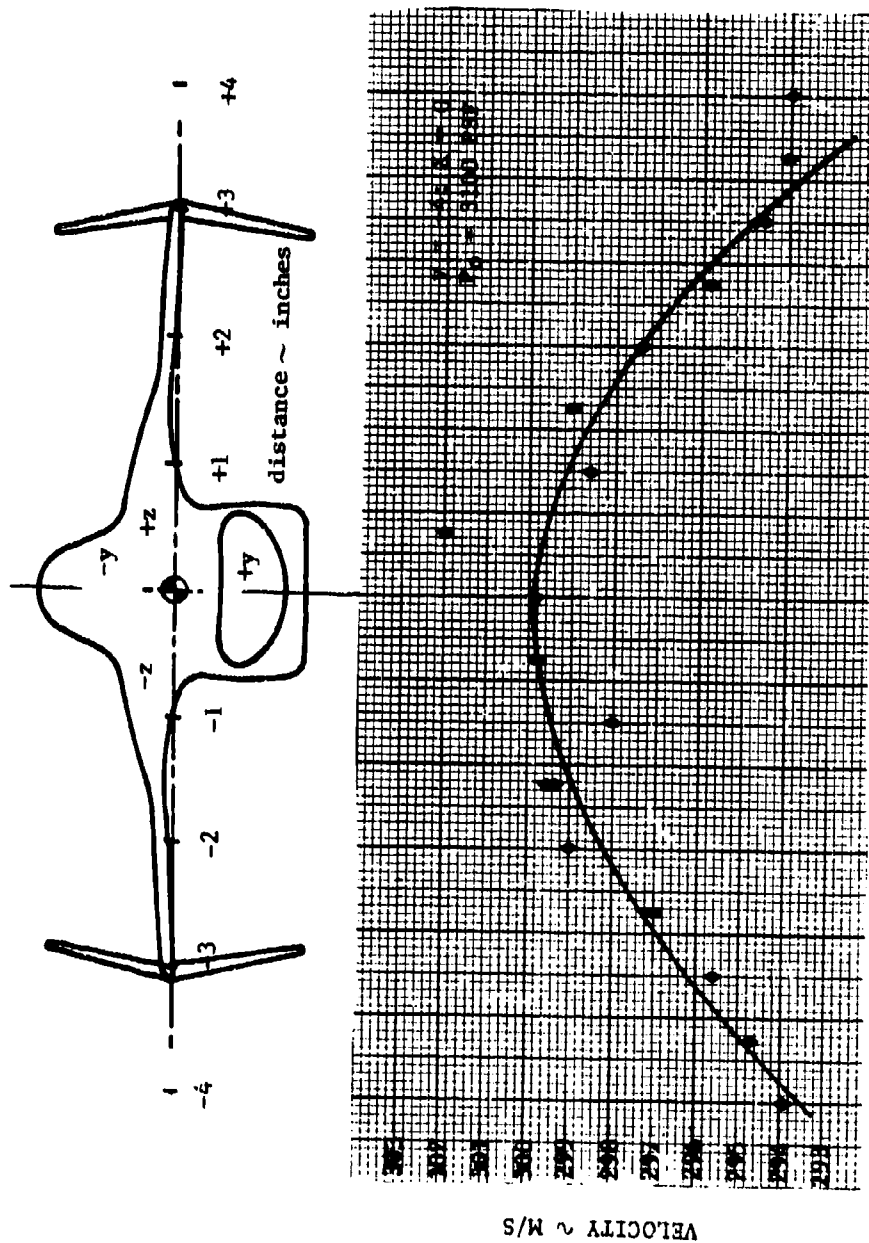


Figure 21. Flow Velocity at Mach 0.9.

The turbulence estimation algorithms which are included in the LTA software package were not useful in this exercise due to the coarse correlator resolution and the very small amounts of data. A faster correlator would presumably have allowed such measurements.

SECTION VI

MICROFIGHTER MEASUREMENTS IN THE SELF-ADAPTIVE WALL TUNNEL

1. Tunnel Characterization

After the completion of the TGF measurements, the LTA system was moved to the Self-Adaptive Wall (SAW) wind tunnel which has a 9 inch square test section and operates in a blowdown mode. It was desired that the same array of data points be measured in the SAW as had been measured in the TGF for the purpose indicated in the introduction (page 1). However, it should be noted that the stagnation pressure was 35 PSIA for both Mach numbers 0.7 and 0.9. This was substantially higher than in the TGF. In the SAW wind tunnel the model was to be oriented in the more usual fashion (i.e., cockpit up), so the supports for the LTA system were changed from 6° to 4° to avoid incidence of the laser beams on the translucent white silicone rubber rods which comprise the top walls^{*}; the prime region of interest of the measurements was $y = -4$ and $z = 0$. Figure 22 is a schlieren photograph of the microfighter taken in the nine inch SAW wind tunnel.

Prior to commencing a series of runs to duplicate the TGF points, a few runs were made to check out the system and the SAW tunnel characteristics. No internal changes or alignments were required of the LTA optical head after the move from the TGF.

^{*}At the limits of sensitivity light colored walls which partially diffuse and retransmit light have been found to be detrimental to sensitivity due to the increased background photon level. Opaque low reflectance surfaces are preferable.

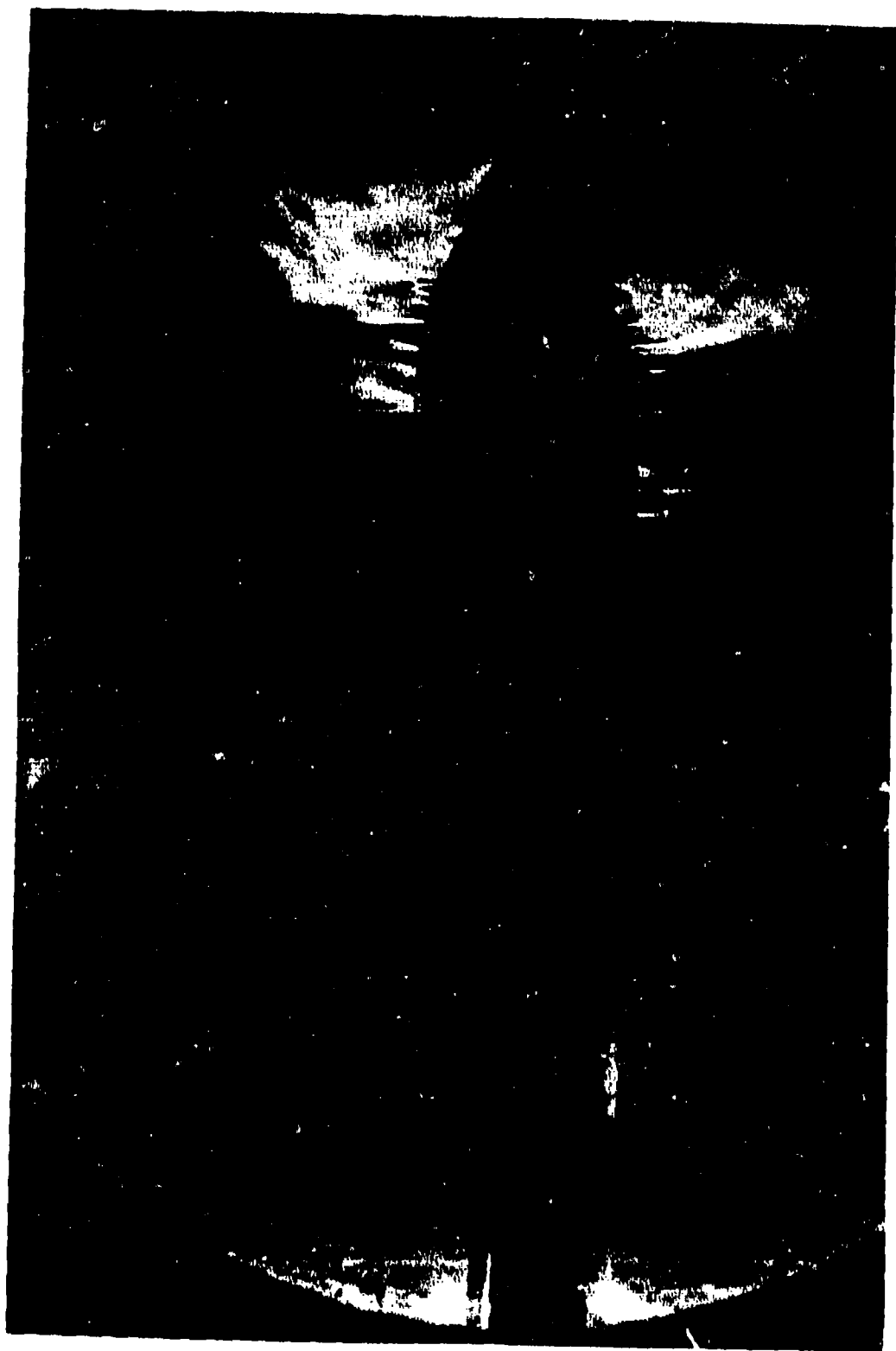


Figure 22. Schlieren Photo of the Microfighter Model in the SAW Tunnel.

These first checkout SAW runs produced some interesting results. The data rate was as high as 50 per second on some 5 second runs. An example of a typical printout is shown in Figure 23. This was excellent because it meant that 100 to 250 data pairs could be obtained in a 5 second run. As illustrated earlier in Section III, 100 data pulse pairs would typically give rms deviation of less than 0.3%. The results in the TGF measurements typically exhibited scatter of less than 1% with fewer than 25 data pulse pairs. This is further evidence that repeatability of measurements with no more than 0.5% rms deviation would be expected in the SAW.

The next interesting observation concerned flare light. It was observed that when a reflection from the inner window of the transmitted beam comes to focus on one of the less than perfectly clean surfaces of the outer window, light scattered by the outer window surface will reflect back (by way of the inner window surface) on to the LTA photo detectors. There is no way to shield or protect the photo detectors from this flare light source from inside the LTA head. The problem can be minimized externally as follows:

- a) Clean all surfaces of outer windows carefully to reduce scatter.
- b) If feasible, antireflection coat the inner windows.
- c) If possible, direct the input beam at an angle to the window and use a reflection stop not located at the focus of the reflected transmitted beams, or
- d) Simply avoid the isolated locations for which the reflection focus occurs.

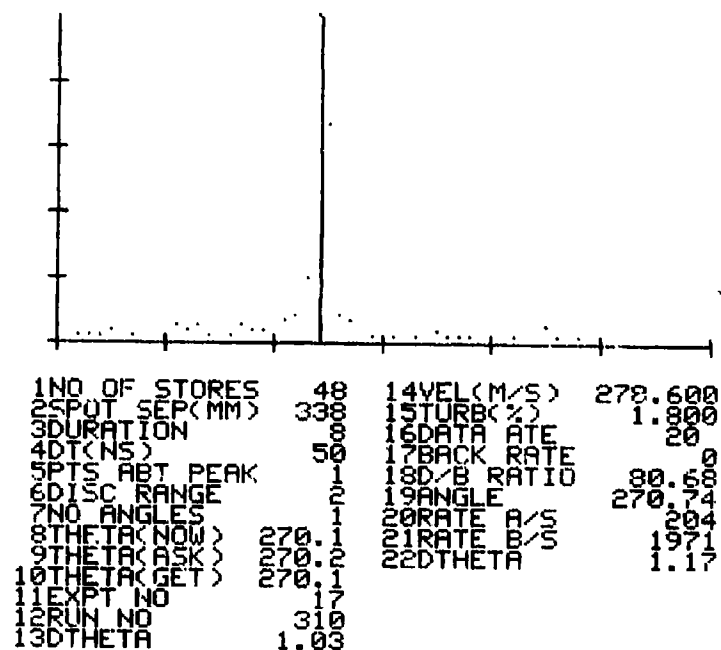


Figure 23. Typical 5 Second Data Run From SAW Tunnel.

The third item of interest observed on the checkout runs was the highly time variable scattering particle concentration. The oscilloscope traces of the raw signal pulses showed visually changing pulse pair data rates which varied noticeably at random intervals from a fraction of a second to several seconds. Next, visual observation of the laser beams during some of these checkout runs showed that the light scattered from the beams as a whole varied greatly, sometimes in "puffs" and sometimes more slowly (seconds' duration). These observations were made during several runs, each of from 1.5 to 1.75 minutes duration, in which 5 to 7 different measurements of 5 seconds each were made in an angle search sequence. Because the angle estimation algorithm in its present form is based on the assumption of stationary particle concentration statistics, these findings ruled out the use of the instrument for flow angle measurements without modifications of the angle algorithm.* No records were obtained of the worst examples of the effects of particle rate fluctuation due to the fact that the "peak" was found at the extreme end of the angle sequence, which the software considers as "no peak found" and did not record. However, Figure 24 is one example of the results of an angle search.

* The most sensitive way to use the LTA system is to set the detection thresholds low enough to detect many single photo-electron pulses in the presence of only a few correlated pulse pairs and even when the threshold was "high", several times as many background photon pulses as signal pulse pairs were detected. When data rate and small particle size are not a problem, then by turning the detection threshold sufficiently high, only particle produced pulses will be detected. Under such conditions, the number of data versus angle can be normalized by the number of pulses on channel A to obtain the conditional probability that a particle is detected by channel B if it is detected by channel A. This is nothing new. It has been used by both Smart at Rolls Royce and Schodl at DFVLR in the past. But it does not allow the full sensitivity of the instrument to be utilized, and this approach has not been used recently.

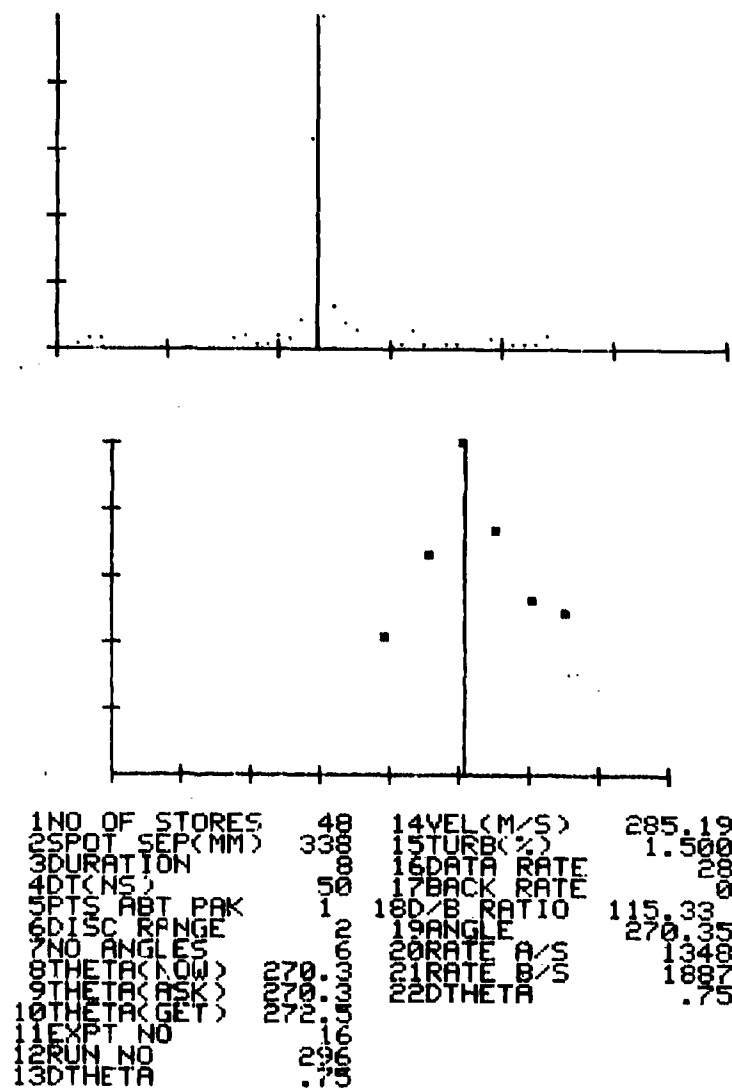
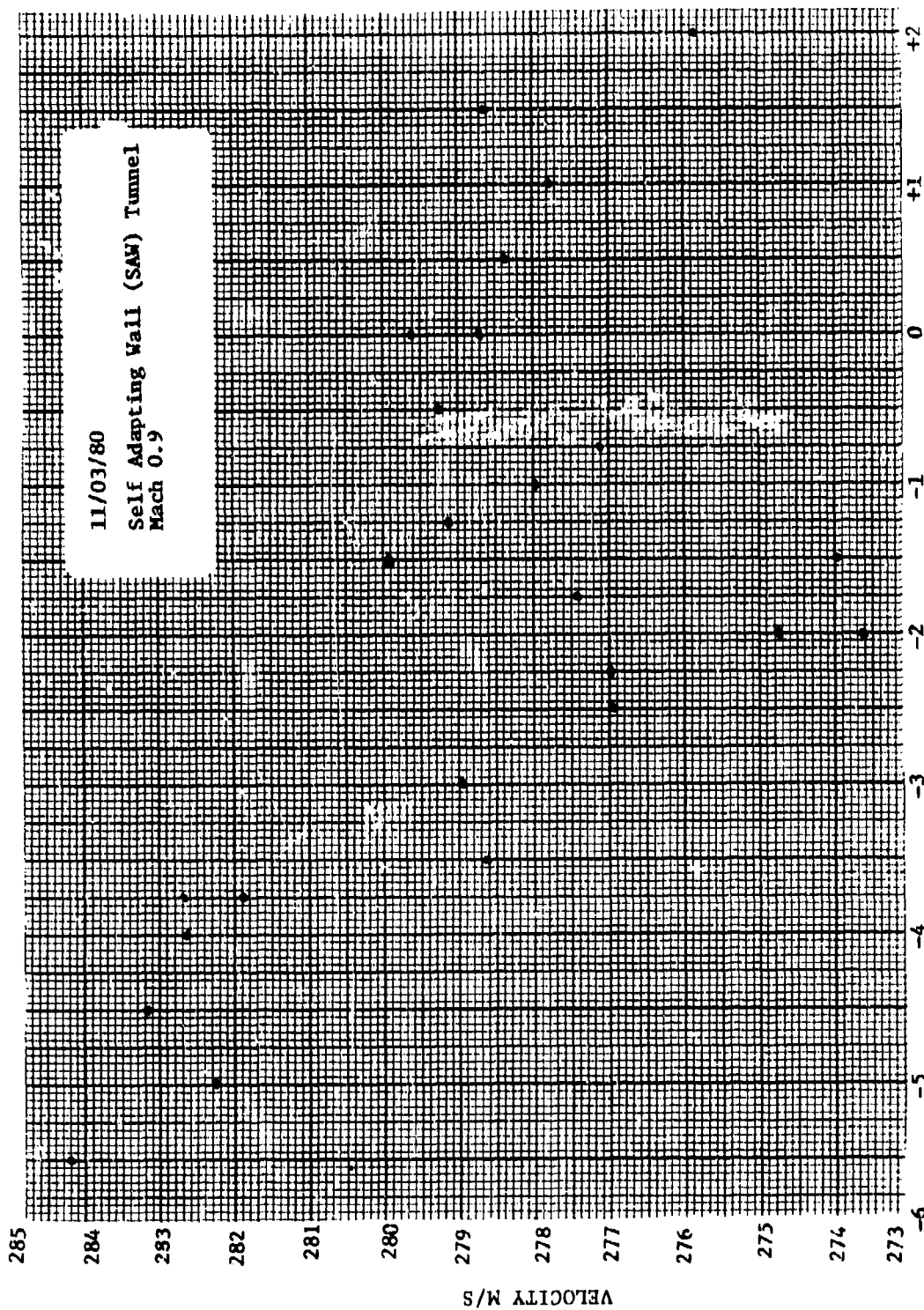


Figure 24. Example of an Angle Search in the SAW Tunnel:
Data Versus Angle with 5 Seconds/Angle.

2. Measurements Near the Microfighter Model

After the checkout runs additional testing was devoted to making a series of measurements along two lines above the microfighter model at Mach 0.9 for velocity only. Flow angle measurements could not be made for reasons described on the previous page. The same spot orientation angle was used throughout (270 degrees is parallel to the tunnel center-line). This is of little consequence to the mean flow velocity magnitude measured in this manner because there is high probability the maximum flow angle deviation is no more than 2° from horizontal and the cosine of 2° is 0.9994.

Some results of the SAW measurements are plotted in Figure 25. Several repeat and fill-in points were taken in an attempt to determine the repeatability (statistical fluctuation level) of these measurements. It became apparent that the tunnel velocity conditions were difficult to maintain and repeat to the precision already established for the LTA.



x inches (See Figure 18)

Figure 25. Mean Velocity Along the Line $z = 0$, $y = +4$.

SECTION VII

CONCLUSIONS AND RECOMMENDATIONS

After running the TGF for 20 to 30 minutes, the flow contains on the average less than 0.5 particle per cc greater than $0.2\text{ }\mu\text{m}$ in diameter. These tests still have not defined the number which exist below $0.2\text{ }\mu\text{m}$ in diameter in question. This produces 1 or less data pulse pairs per second at transonic speeds with the SDL LTA system. Previous experience shows that fringe LV systems with larger probe volumes, which would intercept more particles per second, have not had adequate sensitivity to be usable. One conclusion is that there are too few of the larger particles (nearer to $1\text{ }\mu\text{m}$ in diameter) that would be needed for a fringe system to operate after initial start up.

The LTA system was demonstrated to be capable of making accurate backscatter mean flow speed and angle measurements in a 2 foot test section of the TGF without seeding at all Mach numbers. In a transonic test section measurements were made through 2 windows without artificial seeding at a rate of 1 measurement per 6 minutes and at an error level of less than 1%. The results indicate that a faster (5 ns) correlator and faster data storage (without printing each run) could have obtained error levels of a small fraction of one percent in mean flow in less than two minutes per point (by reducing the data collection time from 50 seconds/angle to about 10 to 15 seconds).

Since a minimally designed LTA system can respond to at least 0.5 micron particles, it should be a simple matter to obtain 0.1% statistical repeatability levels with 1 to 5 seconds per angle increment with only a

small mass density of added seeding scatterers of this size along the measurement path. It should be borne in mind that the practical limits of flow angle precision and turbulence intensity measurements may be set by data rates which are marginal in the TGF without a very small amount of seeding. The achievement of optimal seeding will require further analysis, design and experimentation.

Measurements in the Self-Adaptive Wall Tunnel indicate that there are an adequate number of detectable particles in the facility for rapid LTA measurements (20-50/second) at Mach 0.9. However, due to the instability of the particle concentration, higher thresholds (with lower data rates) and conditional statistics must be used to reliably measure flow angle with the LTA. This can probably be accomplished without seeding. However, since time constraints are more severe in the SAW, it would be time efficient to seed and get the measurements down to one second per angle. This would allow an entire angle scan to be conducted in less than 10 seconds. If this capability were coupled with a fast computer driven traverse mechanism, it should be possible to obtain very precise mean flow angle, and turbulence intensity at 5 per run minute. Key points to consider is that these measurements could be made with 0.5 μm diameter particles or smaller which are responsive to flow behind shocks.

The overall conclusion from this series of measurements is that the LTA system is capable of making useful aerodynamic measurements in the TGF and SAW wind tunnels without seeding. These

capabilities can be enhanced by seeding with very minute mass quantities of seeding material. Furthermore, a useful data base was produced in the TGF with the microfighter for use in characterization of the effectiveness of the adaptive wall concept.

REFERENCES

1. Trolinger, J. D., M. Houser, "Development and Laboratory Testing of a Thermal Emission Velocimeter for Application to an Erosion Nose Tip Test Facility," AFWAL-TR-81-3080.
2. Cline, V. A., "Application of the Laser Velocimeter in the AFFDL Transonic Gasdynamic Facility," ASD Reserve Program Project Report 76-108-B5, April 1978.
3. Trolinger, J. D., A. E. Smart and V. A. Cline, "Feasibility of Utilizing Laser Doppler Velocimeter Techniques in Very Clean Wind Tunnels," AFFDL-TR-79-3084, August, 1979.
4. Parobek, D., private communication concerning unpublished efforts by others.
5. Schodl, R., "A Laser Dual Beam Method for Flow Measurement in Turbomachines," ASME Paper No. 74-GT-157, 1974.
6. Smart, A. E. "Measurement of Velocity Fields Within Rotating Blades With a Photon Correlator," Proc. Conf. on Photon Correlation Techniques and Fluid Mechanics, Cambridge, England, April, 1977.
7. Mayo, W. T., A. E. Smart, "Limitations of LTA Technology at Mach 8: Theory and Practice," submitted to the German-French Research Institute, ISL, Symposium on Long Range and Short Range Optical Velocity Measurements, Saint-Louis, France, September 15-18, 1980.

REFERENCES Continued

8. Smart, A. E., W. T. Mayo, "Experimental and Analytical Development of the Application of a Transit Laser Velocimeter," AEDC-RT-80-28, November, 1980.
9. Mayo, W. T., Jr., "A Two Component LDV System With Photon Counting for the NASA, Langley, V/STOL Tunnel Preliminary Design Study." Final Report on Contract NAS 1-13737, October, 1976.

APPENDIX A

PAPERS DESCRIBING LTA THEORY AND SYSTEMS

ICIASF '79 RECORD

W. T. Mayo, Jr., A. E. Smart and T. E. Hunt, "Laser Transit Anemometer with Microcomputer and Special Digital Electronics: Measurements in Supersonic Flows," presented at the 8th International Congress on Instrumentation in Aerospace Simulation Facilities, reprinted from ICIASF '79 Record, held at the Naval Postgraduate School, Monterey, CA, 24-26 September 1979.

REPRINTED FROM

ICIASF '79 RECORD

International Congress on Instrumentation in
Aerospace Simulation Facilities

Held at the
Naval Postgraduate School
Monterey, California
September 24-26, 1979



IEEE Publication 79 CH 1500-6 AES

LASER TRANSIT ANEMOMETER WITH MICROCOMPUTER
AND SPECIAL DIGITAL ELECTRONICS:
MEASUREMENTS IN SUPERSONIC FLOWS

by W. T. Mayo, Jr., A. E. Smart and T. E. Hunt

Spectron Development Laboratories, Inc.
3303 Harbor Boulevard, Suite G-3
Costa Mesa, California 92626

Summary

An advanced laser transit anemometer system has been developed for difficult optical flow measurement applications. This co-axial backscatter system measures mean velocity, flow angle, and turbulence intensity. The use of highly focused spots, special pulse detection circuitry, a fast single bit digital correlator, and a microcomputer data management system allow unseeded subsonic measurements to ranges greater than two meters and supersonic measurements with naturally occurring submicron particles at shorter ranges. The system has excellent wall and window flare rejection capabilities and may be used for boundary layer measurements near solid models. It is compact and rugged and has been demonstrated for supersonic measurements in high noise and vibration environments at both USAF Arnold Center and the NASA Ames Research Center. This LTA system has also been demonstrated for subsonic axial compressor measurements. In recent developments, the speed, sensitivity and reliability have been further improved in preparation for measurements up to Mach 5 at the Arnold Center Von Karman Facility in late summer 1979.

improvements to both the optical and signal conditioning systems. The data management system (DMS) has been improved under SDL private funding. Commercial copies of this even more advanced "fourth generation" system have been constructed and delivered.

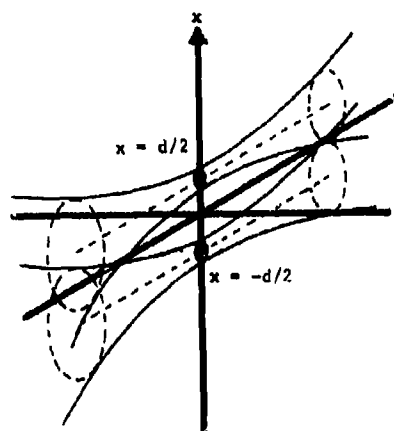


Fig. 1 - Laser Beam Geometry

1. INTRODUCTION

Laser transit anemometry (LTA) or "two-spot" techniques have received attention recently due to sensitivity, high velocity capabilities, and superior flare rejection advantages¹⁻⁷. An LTA system measures the distribution of the times of flight of scattering particles as they pass successively through two highly focused parallel laser beams as illustrated in Figures 1 and 2. The appropriateness of using pulse center estimation filters with real-time single-bit cross correlation and the need for correlation processors with 5 to 10 nano-second time resolution for supersonic flows have both been documented recently^{6,7}.

An advanced co-axial backscatter LTA system was developed and demonstrated by Spectron Development Laboratories under sponsorship by the U.S.A.F. Arnold Engineering Development Center³, NASA Ames⁶, and private funding. This system included a third generation compact and rugged optics head with a 135 mW laser, optics, spot-pair rotation, real-time graphic display of correlograms, preliminary on-line data analysis of mean speed, flow angle, turbulence intensity, and mass data transfer or storage for further off-line computer processing.

More recently, additional development funding from the U.S.A.F. Arnold Center⁸ has resulted in

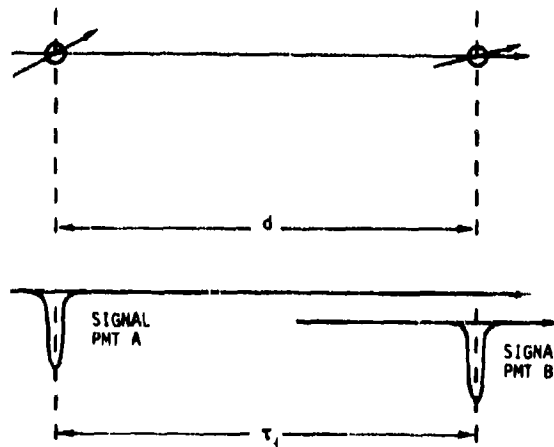


Fig. 2 - Operating Principle $V_1 = d/t_1$

CH1500-8/79/0000-0146\$00.75 © 1979 IEEE

146-ICIASF '79 RECORD

Reprinted from ICIASF RECORD, September 1979

Following sections describe various aspects of the system and our experience to date. These include the system configuration, signal conditioning electronics, the microcomputer based control and data acquisition subsystem, and display and data reduction algorithms. This is followed by a brief description of supersonic measurements and conclusions about the applicability of this technology.

2. SYSTEM OVERVIEW

Figure 3 is a photograph of the LTA optical head and the data management system (DMS). A digital cross correlation processor (not shown) and interconnection cables complete this stand-alone system, although traverse-mechanism and other interfaces are available. The optical head contains several sets of printed circuit card electronics. These subsystems include a rotator prism control card, two sets of filter discriminators, a high voltage relay circuit, and photomultiplier tube housing circuits. Figure 4 is a photograph of one of the discriminator cards.



Fig. 3 - LTA Data Management System and Optical Head

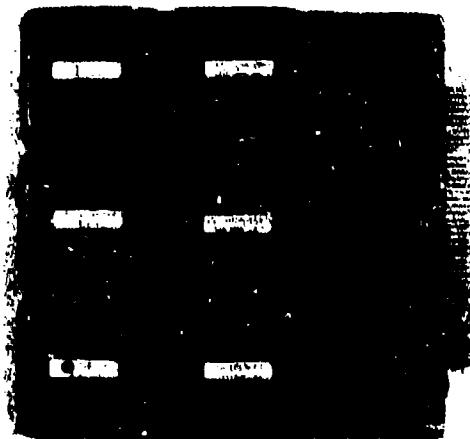


Fig. 4 - Example of Optical Head Electronics: Discriminator Card

During our LTA development, we have used a Malvern K7023 50 ns correlator to produce a single-bit cross correlation of the outputs of pulse-center estimation filters (discriminators). A faster "multiple station" correlation processor is presently under development at SDL for LTA and other applications. Figure 5 is an example cross correlogram of transit delay intervals from a 48 store correlator. The rms turbulence intensity for this example is 7%.

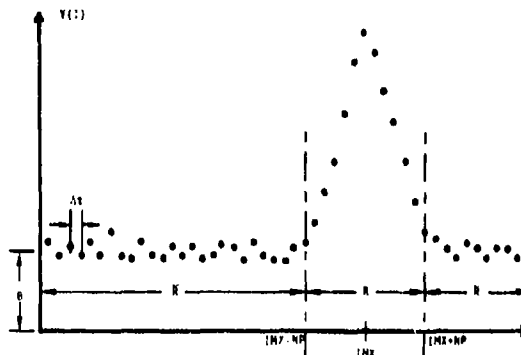


Fig. 5 - An Example Cross Correlogram with 7% RMS Turbulence Intensity

The DMS automatically rotates the two focused beams about a common center through a sequence of angles with the angular step size determined on line from the turbulence level estimated from the first data run. The correlator is started and the data transferred to the DMS in proper sequence. The operator is shown a graphic display of the correlograms, a plot of signal visibility ratio from which mean flow angle is extracted, and a printout of the estimates of mean speed, mean angle, and apparent turbulence intensity.

3. OPTICAL HEAD ELECTRONICS

Through previous experience, one of the authors (Smart) found that large electromagnetic interference fields were often present in common test environments in addition to high levels of noise and vibration. Thus, in addition to designing for mechanical rigidity, we chose to locate the analog electronics inside the optics head where short low-impedance leads and shielding could be used to maintain speed, sensitivity and good immunity to interference. Only TTL level signals are transmitted over the long signal and control cables (30 meters or more).

The photomultiplier tube circuits offered quite a challenge. We desired good single-photon response (pulses up to two volts in magnitude and less than 10 ns wide with little or no ringing and with good single photoelectron pulse height resolution) while allowing much longer classical signals. This must be accomplished in the presence of wall flare and blade flash which, for brief periods, drive the tube

output far beyond the allowed average anode current. The PMTs selected were 12 stage, 2 inch diameter EMI 9817B linear fast focused tubes with S-20 photocathode material. These tubes have high cathode maximum current limits such that the cathode is protected by the inclusion of a series 100 M Ω resistor. Good single photoelectron pulse height response and first stage gain is assured regardless of the high-voltage setting by two series 150V Zener diodes between the cathode and the first dynode.

The inputs and outputs are illustrated in Figure 6. The gain suppression does not disconnect

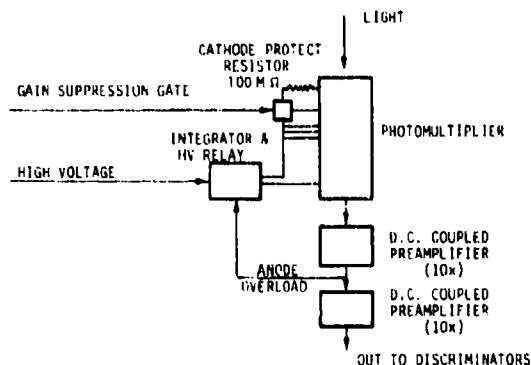


Fig. 6 - Photodetection Electronics.

the high voltage but removes the interstage gain at the first dynode thus preventing predictable transient optical overload from fatiguing the dynode electron emitters. The PMT anode load is 50 Ω . There are two direct coupled stages of preamplification which together give a gain of $\times 100$ and do not change the polarity of the output signal. These preamplifiers saturate at about -6 volts. In general, the use of such preamplifiers is not desirable, and for wind tunnel applications away from model surfaces, a 14 stage tube with one 10x preamp is a better selection. However, the applications of interest often require proximity to walls; thus, the preamplifiers are required to avoid dynode fatigue through excessive average current. Each preamplifier output drives a 50 Ω co-axial cable terminated on a discriminator board. Figure 7 is a photograph of two phototube assemblies which are partially disassembled to show the circuitry.

Between the two preamplifiers there is an integrating monitor, located physically on the high voltage relay board, which detects a condition which could, if sustained, damage the later dynodes or anode of the photomultiplier tube. This trip condition corresponds to a dc anode condition of 200 μ A for a period of 0.5s. The high voltage relay responds to the integrating monitor (actually an active low-pass filter) by disconnecting the high voltage to protect the anode and later stages of the dynode chain. Each tube has a separate sense line and a separate high voltage relay but a red overload light on both the optical head and the DMS

will come on when either tube is tripped. The red light is incorporated in a switch which resets the relays when pushed.

There is a separate discriminator card for each of the two separate photomultiplier tubes. Each discriminator card is a "mother" board with six separate plug-in "daughter" modules as illustrated in Figure 4. Each module is for a pulse width with a dynamic range of 4:1. The ranges overlap, as they increment in powers of two with range 1 being 25 ns to 100 ns, range 2 being 50 ns to 200 ns, etc. Figure 8 illustrates one of the plug-in modules functionally. The low-pass filters are designed to have

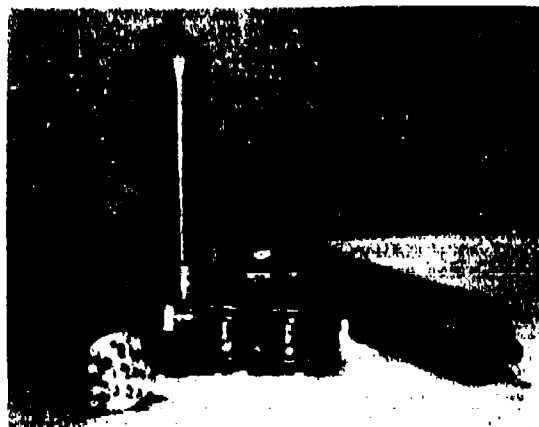


Fig. 7 - Photomultiplier Tube Assemblies

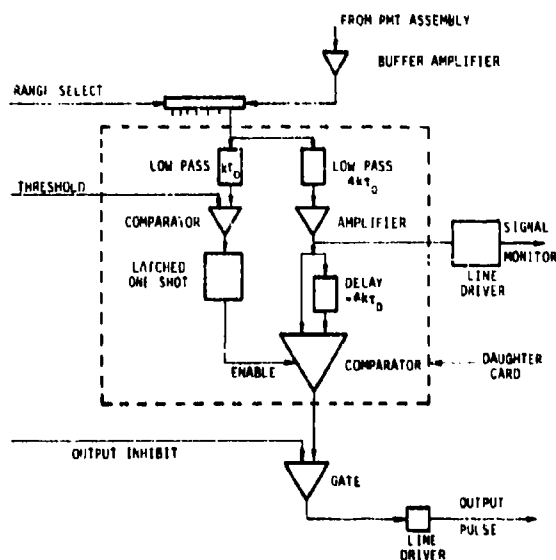


Fig. 8 - Schematic of Single Filter Discriminator Plug-in Module.

nearly symmetric, non-ringing, Gaussian impulse responses whose duration are $k\tau$ and $4k\tau$ for the detection filter and the pulse center estimation filter, respectively. The ratio selected is k , from 1 to 6. The $1/e^2$ pulse width τ for the fastest range is 25 ns for the standard units; special higher-speed plug-in modules have been developed for applications up to Mach 10.

In operation, the user electronically selects the discriminator range for which most of the spot transit durations T_j will lie within the range $k\tau < T_j < 4k\tau$. Under these conditions, the detection filter ($k\tau$) has a wider bandwidth than the classical signals to be detected, so there is no statistical biasing due to attenuation of the faster pulses. Once the detection threshold is exceeded, the pulse-center filters are enabled. Since the impulse response of these filters is longer in duration than the spot transit times, the single-photon pulses are smoothed, even when only one or a few such pulses occur in a spot transit group. The comparator thus locates the weighted average center of a photon pulse cluster.

The discriminator cards include a second level detection circuit just following the buffer amplifier which is not shown in the simple block diagram. This circuit inhibits the discriminator outputs if the signals exceed a preset level. The preset level is typically -2.5 volts to avoid very large impulses (from large scatterers or other causes). By adjusting the PMT high voltage supply, the average pulse level out of the preamplifiers is set between -0.2 and -2.0 volts.

The motor control board supplies power to the dc geared motor which drives the prism rotator such as to zero the difference between the logic word provided by the microprocessor and the analog-to-digital conversion of the signal from the potentiometer connected without backlash to the prism rotator. For incremental angle steps less than 2 degrees, 0.1 degree precision is obtained in less than 0.5s. The value of the instruction dispatch word is displayed at the microprocessor as is the word which corresponds to the angular position ultimately obtained. The prism motor may also be driven in either fast or slow mode in either direction from the manual switches on the DMS console. In this mode the readout of actual position to the DMS screen is sustained and updated many times per second.

4. DATA MANAGEMENT SYSTEM (DMS)

The DMS (see Figure 3) is normally situated remote from the optical head by up to 30 m and contains the microprocessor, keyboard, visual display unit, two mini floppy disk units, operating software and a number of manual controls. Figure 9 shows the labeled front panel layout which identifies the items shown in the photograph of Figure 1. Inside, there are low voltage power supplies and other electronic hardware to augment the microprocessor. These are 48k bytes of RAM, interfaces, and the window and delay unit (one channel of which controls the "live time" of one discriminator and the other the "blanking time" of both photomultipliers for periodic flow applications.) The

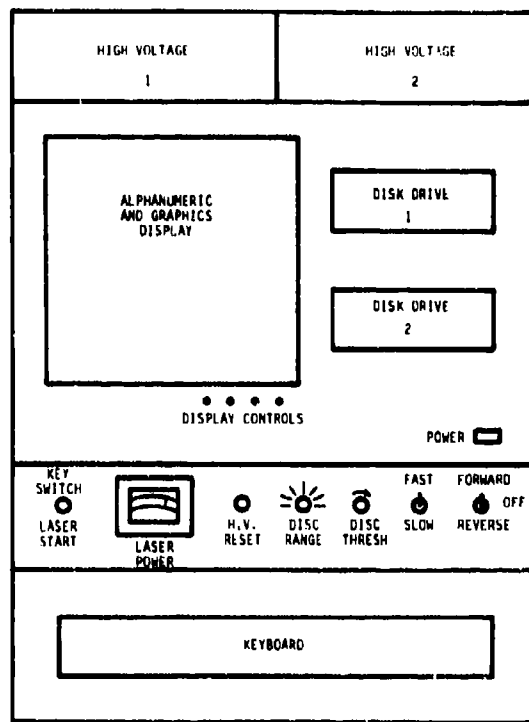


Fig. 9 - Data Management System Front Panel

parallel ports (interfaces) provided in the DMS include a buffered 8 bit duplex computer interface with four additional control lines and a 48 bit correlator interface. The correlator ports are programmable with respect to the direction of information flow. Thus, interfaces to a variety of other computers and correlators may be configured by software without hardware changes. Since all software is provided on disk rather than permanent read-only memory, the system is quite flexible.

Software as provided is read from Disk 1 on startup and Disk 2 is reserved for data storage. Either will serve both functions, if necessary. All initiation and data heading functions are entered from the keyboard in response to questions posed on the screen as illustrated in the example given in Table 1. These keyboard entries are written as initialization heading before each data record. Further details concerning the data processing algorithms are presented in Section 5 below.

The photomultipliers are each supplied from their own high voltage supply so that fine tuning on gain may be performed. The remote laser start/safe is a removable key switch with laser-ready indication. This prevents the need for access to the laser power supply except when one wishes to change power levels or the control mode. There is a laser output power meter on the control console. Manual controls which may override the computer are

Table 1 - Example of Data Entry Prior to Run

DMS PROMPT TO USER	EXAMPLE OF ENTRY
*PUT IN DATA DISKETTE?	Confirm that this is done
DATE (MONTH, DAY)	12, 25
NO. OF STORES = ?	48 (48 store correlator)
SPOT SEPAR (MM) = ?	0.27
NO. OF BLADES = ?	29
WINDOW WIDTH FOR GATE SIGNAL = ?	Width and Delay in Microseconds
DELAY FOR GATE SIGNAL = ?	
WINDOW WIDTH FOR BLANKING SIGNAL = ?	Width and Delay in Microseconds
DELAY FOR BLANKING SIGNAL = ?	
NO. OF POINTS TO USE ON EACH SIDE OF THE PEAK = ?	7 (See Section 5)
NO. OF DELTA-T'S (POWER OF 10) = ?	6
X, Y, Z = ?	10.25, 3.45, 5.00
TIME (HOUR, MINUTE) = ?	07, 43
DELTA-T (MICROSEC) = ?	0.05
DESIRED RANGE = ?	2 (Discriminator Plug-in)
THETA = [VALUE DISPLAYED WITH REAL TIME UPDATE]	Manual set then return
DESIRED THETA = ?	180.4
THETA = 180.6	
THETA = 180.4	
GO ON?	Hit Return

provided to make setting up the system easier. There is a switch which allows either manual or computer discriminator range selection. Mode switches for motor control to facilitate alignment of the spot orientation with the flow are provided. Even under manual control, the correct prism orientation is read to the screen of the DMS. The threshold control for the discriminators sets over a wide range, the level which changes the ranges the ratio of single photon events to multiphoton particle events.

5. SOFTWARE

The optical and electronic system for transit anemometry basically acquires two channels of digital events whose only information is carried at event times. To measure the distribution of event times, it is optimal to cross correlate the two channels where the delayed channel corresponds to that which a particle crosses first. This subject has been previously discussed⁷. The subject of optimum data extraction from correlograms can get very detailed. Here we will explain what we have elected to do with the system to date. Further software revisions are possible either by the user or from SDL on a new minidisk. The present software functions:

- Make a visible record of data quality so that the user may make on-line improvements to operating procedure, threshold and voltage settings,

- Give an approximate value for velocity, turbulence and angle in minimum time,
- Print these estimates on paper for brief assessment,
- Store or transmit and identify all acquired data for later processing with superior algorithms in a large computer.

Figure 1 is a schematic view of the sampling volume and shows how the velocity is resolved in the axial direction but only gives rise to a measurement of true speed if it is in the plane of the two parallel cylinders. More simply, this can be viewed as in Figure 2. Because there is no way of identifying a specific particle, we have chosen to decode the data on a statistical basis. By computing the times between all possible 'A then B' pairs such that the delay does not exceed the displayed delay time of the correlator, then it is possible to obtain a peak from those particles which crossed A and then B and a background from all others. Over short delay intervals it is permissible to assume that uncorrelated events from particles which cross only one spot or from other random events are Poisson distributed. This is not, in general, true for longer correlation times; and, indeed, provides a method of assessing turbulence scale by correlating the existence of particle concentration fluctuations⁹. Over the short time involved in a typical transit, these effects are not manifest and it is permissible to assume that the "background" is flat. Figure 5 showed a typical correlogram for about 7% turbulence and a 48 store correlator. Upon this plot are marked the various operating parameters which are used by the DMS to evaluate the flow parameters.

There are many simplifications in the following analysis. It is not to be scorned for that, as it is intended as a quick-look device and, if used correctly with proper precautions, is capable of much better than 1% accuracy in velocity, particularly for low turbulence, and no more than a few percent error on turbulence for turbulence up to about 15%. For very low turbulence more stores and/or smaller Δt correlator resolution may be required. The low turbulence limit also depends on the degree of deconvolution of the instrument broadening function; one may wish to attempt in post-detection processing. The standard algorithms are presented below.

Based on experience and "a priori" knowledge of the flow, the operator selects a number of stores NF which he expects to bound the highest turbulence conditions of the correlogram. The region R is then the set of stores located within NF stores either side of the peak IMX of the correlogram. The region \bar{R} is all the rest of the stores as shown in Figure 5. The first step in the data reduction is to compute the arithmetic average of the values accumulated in the stores of region \bar{R} . This is an estimate of the "white" level due to uncorrelated background pulses. This value is subtracted from the correlogram. Thus, if $Y(I)$ are the correlogram values, we obtain

$$(1) \quad B = \frac{1}{N\bar{R}} \sum_{\bar{R}} Y(I)$$

where Q is the total "area" under the peak (see Figure 10) which normalizes the function as a probability density function estimate; i.e.,

$$(3) \quad Q = \sum_K Y(I) - B$$

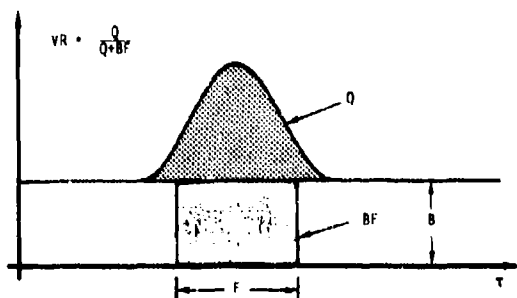


Fig. 10 - Definition of Visibility Ratio

The first order mean speed estimate (assuming that the spot pair axis is directed somewhat along the mean flow direction) is obtained from the mean delay number KBAR quite simply as

$$(4) \quad V = \frac{d}{(KBAR \cdot \Delta T)}$$

where d is the physical distance between the spots and ΔT is the correlator clock interval. This estimate of mean speed based on the inverse of the mean transit time is similar to the mean velocity component estimate obtained from burst counter processing of fringe LV data without inversion. As is well known¹¹, the use of the inverse of the mean transit time provides first-order correction of the particle rate biasing. Thus, for low turbulence flows the mean speed estimate is excellent. At higher turbulence levels, say greater than 10%, higher order data processing with the inclusion of the "pie slice" effect (accepted flow-angle at any one angle depends on particle size for a fixed threshold) and other effects may be included in a more precise model.

For simplicity the present turbulence intensity estimate, TI , is calculated as a root mean square deviation of the transit time distribution instead of the velocity distribution. This may be improved in the future. In terms of the effective width, F , of the correlogram peak we obtain

$$(5) \quad TI = F/2KBAR$$

where this somewhat unusual notation is used in the definition of the signal visibility ratio function below:

$$(6) \quad F = 2\sqrt{\sum_K (1 - KBAR)^2 \cdot \frac{Y(I) - B}{Q}}$$

The above formula for mean speed is quite insensitive to the values of NP chosen. If the data acquisition time is so short that the scatter in

the baseline is considerable as illustrated in Figure 5, then the turbulence intensity estimate becomes significantly affected by the noise on the baseline and, hence, the choice of R and \bar{R} . Under such conditions, more data should be acquired or more elaborate curve fit parameter extraction algorithms should be employed for optimum retrieval of information from the data.

The DMS uses the estimate of turbulence intensity to compute an incremental angle $\Delta\theta$ for spot-pair rotation which proceeds automatically unless another $\Delta\theta$ is chosen. The computation of $\Delta\theta$ assumes that the turbulence is isotropic to obtain a crude estimate of a "good" $\Delta\theta$. Thus, if the number of angles at which observations are to be made is N , then $\Delta\theta$ is computed as in Table 2.

Table 2 - Selection Formula for $\Delta\theta$

N	DT
3 -	$1.5 \times TI \times 180/\pi$
5 -	$1.0 \times TI \times 180/\pi$
7 -	$0.7 \times TI \times 180/\pi$

Unless $TI = 0$, in which case

$$\begin{aligned} 3 - & 1.5 \times 0.02 \times 180/\pi = 1.72 \\ 5 - & 1.0 \times 0.02 \times 180/\pi = 1.15 \\ 7 - & 0.7 \times 0.02 \times 180/\pi = 0.80 \end{aligned}$$

and TI is displayed as ≈ 0 .

During the automatic angle incrementation sequence, the signal "visibility ratio," $VR(L)$, is computed. The angle is $\theta_1 + L\Delta\theta$ where θ_1 is the initial angle selected manually or via computer. The quantity $VR(L)$ is the ratio of the area under the delay curve, Q , and the sum of this area with that portion of the background within the "width" F of the correlogram:

$$(7) \quad VR(L) = \frac{Q}{Q + BF}$$

These quantities are illustrated in Figure 10. The value of the function $VR(L)$ lies between zero and unity. The zero condition is obtained when the spot pair axis is rotated so far away from the mean flow angle that no correlated events occur and Q goes to zero.

The mean flow angle occurs in the vicinity of the peak of the plot of $VR(L)$. The present DMS software uses a 3-point parabolic fit of the peak and the value of $VR(L)$ on each side of the peak to obtain the mean flow-angle estimate as illustrated in Figure 11. The idea behind the definition of the visibility ratio function is that it removes the effects of particle rate fluctuations when the threshold is set sufficiently high for all detected pulses to be from particles. At lower thresholds and particularly when the probe volume is near a flare producing surface, many of the detected pulses are single photoelectron background pulses whose rate may be subject to angular orientation of the spots. Under such conditions, the raw data rate Q which has background subtracted out, may be

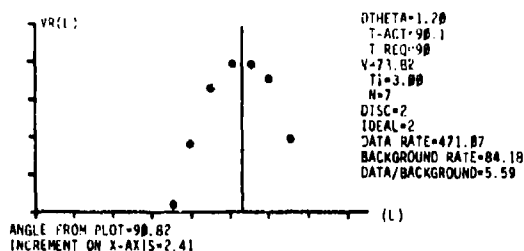


Fig. 11 - Example Screen Plot of VR(L) and Display of Reduced Data.

a better parameter to fit for mean flow angle. All of the flow estimation software is written in BASIC to allow ease of future modification. In fact, all of the operating software is provided on disk, rather than permanent memory and can easily be changed.

6. MEASUREMENTS

At the time of this writing (July 1979) additional supersonic measurements are scheduled to be conducted at the Arnold Engineering Development Center Von Karman Facility, but these will not be conducted before the submission deadline. These tests will be through windows two inches thick, without seeding, in Tunnel A at Mach numbers in the range 1.5 to 3.0. The results of these tests will be described at the Congress if they are available at that time, and will be provided later in other publications. In this section we will briefly review the supersonic measurements made with the prototype system at the Arnold Center, September 1978, and at NASA Ames, October 1978. These experiments are described in more detail in the contract reports^{5,6}.

The objective of the AEDC measurements was to demonstrate an LTA system with a digital correlator and to compare the measurements with simultaneously obtained fringe velocimeter measurements. The prototype system was transported to the Arnold Center on September 18, 1978. Demonstration measurements along the centerline of a supersonic jet with a Mach disk were made, with the LTA system; however, due to equipment difficulties experienced by the Arnold Center personnel and time and funding constraints which precluded further SDL measurements, no simultaneous measurements were accomplished.

The AEDC tests were conducted using a free jet test (unseeded) installation located in Propulsion Research Cell (R-1A-1) of the Engine Test Facility at the Arnold Engineering Development Center. Assistance was provided to SDL personnel by Mr. T. V. Giel, ETR, Mr. Virgil Gline, FWT, and the facility technicians. A 1" diameter underexpanded unheated jet with a pressure ratio of 4 was used. This jet has been tested extensively in the past with both laser velocimetry and shadowgraph techniques as reported by Barnett and Giel¹⁰ in 1977. The first and second Mach disks were located 1.73 inches and 3.39 inches downstream¹⁰. Due to other activities which had occurred since the calibrations of the

jet, a right angle bend had been installed in the jet supply pipe. It is thus possible that differences in the flow would occur with respect to the earlier measurements.

The output lens used for the jet test was a 622 mm focal length lens which resulted in a throw, or range, from the front of the instrument of 597 mm, a spot separation of 0.489 mm as calibrated prior to instrument shipping, and a spot size of approximately 20 micrometers diameter. The axial speed and apparent turbulence intensities as determined by the operator and the data management system were recorded for several locations along the center line of the jet. Figure 12 is a plot of the axial speed measured along the jet centerline.

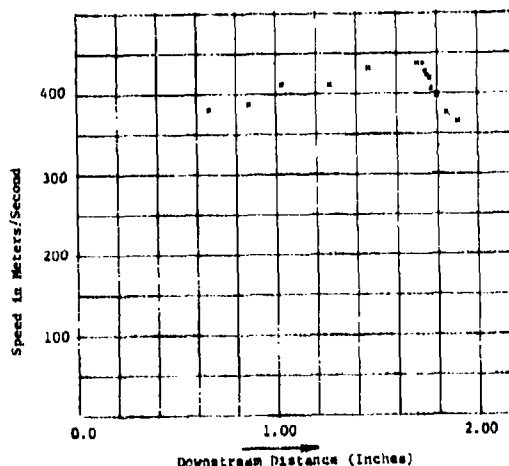


Fig. 12 - Axial Speed on Jet Centerline.

Careful study of all the AEDC data and the apparatus indicated that the selection of the collimator lens for the prototype system was inadequate to properly focus return scattered radiation on to the fiber optic light guides employed in the system. The resulting loss of scattered radiation resulted in a receiver efficiency of less than 5%. Calculations had indicated that measurements from particles down to 0.3 micrometers in diameter would be achievable. The particle lag evident in the plot of data across the Mach disk indicated that the first prototype system did not achieve this sensitivity. Contractual time and funding limitations prevented further data collection or analysis at that time.

The purpose of the NASA Ames experiment was to obtain data for design of a larger future system for the NASA Ames 11-foot transonic tunnel, if such a system appeared feasible from the tests. The test was more difficult than the AEDC test in that there was a 2-inch thick window between the LTA system and the flow field, and the larger particles impact out of a recirculating tunnel. The measurements were conducted in a piggyback test at the 6-foot transonic tunnel without seeding at Mach numbers from 0.6 to 1.6. Repeatability of the mean flow

measurements was as good as 0.15%. The tunnel was not seeded. Minor improvements in the optical system had been made to improve the optical efficiency of the receivers to nearly 10% but insufficient time had been available to replace the output collimator. Computer simulations of the signals using Mie scattering codes and measured optical parameters indicated that data was obtained from particles down to about 0.5 micrometers in diameter, but no standing shocks were available for relaxation tests in this exercise.

In December 1978, the prototype system was used to make measurements in a research axial compressor at the General Electric Co. Some of the data was obtained unseeded and some was obtained using 0.25 micrometers diameter solid seed material. For that test, which will be reported in detail at the Spring 1980 ASME Conference in New Orleans, a diffraction limited collimator lens was used with marked increase in optical efficiency and thus system sensitivity.

7. CONCLUDING REMARKS

An advanced microcomputer automated laser transit anemometer system (LTA) has been designed, constructed, and delivered. This LTA system has been demonstrated to be capable of coaxial backscatter measurements of unseeded flow near walls and surfaces and at velocities up to Mach 1.6. Further tests at speeds up to Mach 5 are planned. The prototype system has been transported to three separate real world tests with high noise and vibration environments and performed well in all cases. The successes support the design choices which include the extensive use of printed circuit electronics inside the compact optical head. The usual complaint concerning data collection time with an LTA system has been substantially overcome by microcomputer automation of the system control and the provision of on-line flow field parameter estimation and graphic operator oriented screen displays. The LTA system is more sensitive than fringe LV systems and is expected to find wide application to measurement problems requiring good sensitivity to the submicron particles which abound in most instances without seeding. A practical LTA system with unique features has been developed and demonstrated.

8. ACKNOWLEDGEMENTS

The development of the optical head electronics described in this paper was funded for the most part by the U.S.A.F. Arnold Engineering Development Center under Contracts F40600-78-C-0002 and F40600-79-C-0003. The Air Force project manager for both contracts was Marshall N. Kingery.

9. REFERENCES

1. Schodl, R., "On the Extension of the Range of Applicability of LDA by Means of the Laser-Dual-Focus (L-2-F) Technique," Proceedings of the LDA-Symposium Copenhagen, 1975.

2. Smart, A. E., "Data Retrieval in Laser Anemometry by Digital Correlation," Third International Workshop on Laser Velocimetry, Purdue University, LaFayette, Indiana, 11-13 July 1978.

3. Smart, A. E., "Laser Anemometry Close to Walls," Dynamic Flow Conference 1978, Baltimore, Maryland, 18-21 September 1978.

4. Bartlett, K. G., and She, C. Y., "Single-Particle Correlation Techniques for Remote Measurement of Wind Speed: Aerosol Condition and Measurement Rates," JOSA, **69**, 455 (March 1979).

5. Mayo, W. T., and Smart, A. E., "Comparison of Data from the Transit Time Velocimeter with Other Systems Now in Use for Velocity Measurements," AEDC-TR-79-32, May 1979 (Final Report on Contract F40600-78-C-0002).

6. Mayo, W. T., and Smart, A. E., "Feasibility Study of Transit Photon Correlation Anemometer for Ames Research Center Unitary Wind Tunnel Plan," NASA CR 152238, February 1979, (Final Report on Contract No. NAS2-10072).

7. Mayo, W. T., Jr., "Semiclassical Processing of Laser Transit Anemometer Signals," Proceedings of the 3rd International Conference on Photon Correlation Techniques in Fluid Mechanics, Churchill College, Cambridge, U. K., March 1979.

8. Final Report on AEDC Contract F40600-79-C-0003 to be published.

9. Erdmann, J. C., and Gallert, R. I., "Recurrence Rate Correlation in Scattered Light Intensity," JOSA **68**, p. 787, (June 1978).

10. Barnett, D. O., and Glal, T. V., Jr., "Laser Velocimeter Measurements in Moderately Heated Jet Flows," Arnold Engineering Development Center Report No. AEDC-TR-76-156. (April 1977).

11. McLaughlin, D. K., and Tiederman, W. G., "Biasing Correction for Individual Realization Laser Anemometer Measurements in Turbulent Flows," Phys. of Fluids, **16**, p. 2082 (December 1973).

ADDENDUM FOR

LASER TRANSIT ANEMOMETER WITH MICROCOMPUTER
AND SPECIAL DIGITAL ELECTRONICS:
MEASUREMENTS IN SUPERSONIC FLOWS

by W. T. Mayo, Jr., A. E. Smart and T. E. Hunt

Spectron Development Laboratories, Inc.
3303 Harbor Boulevard, Suite G-3
Costa Mesa, California 92626

Following equation (1), please insert:

Next, the mean delay store number KBAR is computed:

$$(2) \quad \text{KBAR} = \sum_R \frac{Y(I) - B}{Q} \cdot I$$

ADDITIONAL SLIDES SHOWN WITH PRESENTATION OF PAPER ENTITLED

LASER TRANSIT ANEMOMETER WITH MICROCOMPUTER
AND SPECIAL DIGITAL ELECTRONICS:
MEASUREMENTS IN SUPERSONIC FLOWS

by W. T. Mayo, Jr., A. E. Smart and T. E. Hunt

Spectron Development Laboratories, Inc.
3303 Harbor Boulevard, Suite G-3
Costa Mesa, California 92626

Presented at:

8th ICIASF

INTERNATIONAL CONGRESS ON INSTRUMENTATION
IN AEROSPACE SIMULATION FACILITIES

Naval Postgraduate School
Monterey, California, USA
September 24-26, 1979

Sponsored by the Aerospace & Electronic Systems Society of the
INSTITUTE OF ELECTRICAL AND ELECTRONICS ENGINEERS

SPECTRON LASER TRANSIT ANEMOMETER DEMONSTRATIONS
AT ARNOLD ENGINEERING DEVELOPMENT CENTER
SEPTEMBER 1979

- UNSEEDED FLOW
- BACKSCATTER
- 80 MW LASER POWER
- $\frac{1}{2}$ MILLIMETER RESOLUTION

TUNNEL A

- MACH NO. 4.5
- 725 m/s
- 5 s
- 0.4% VELOCITY PRECISION
- 0.1° ARC

TUNNEL B

- MACH NO. 8
- 1200 m/s
- 50 s
- 0.6% VELOCITY PRECISION

A.E.D.C. VON KARMAN FACILITY

TUNNEL A SEPTEMBER 10, 1979

DATA COLLECTION TIME	5 s
MEASURED VELOCITY	$726.1 \text{ ms}^{-1} \pm 0.43\% \text{ R.M.S.}$
CALCULATED VELOCITY	720.7 ms^{-1}
DIFFERENCE	0.77%
ANGULAR DEVIATION	$\pm 0.10^\circ \text{ ARC}$
EVENT RATE	10/s

SPECTRON LTA

A.E.D.C. VON KARMAN FACILITY

TUNNEL B SEPTEMBER 11, 1979

DATA COLLECTION TIME	50 s
MEASURED VELOCITY	$1205 \text{ MS}^{-1} \pm 0.6\% \text{ R.M.S.}$
CALCULATED VELOCITY	$1184 \text{ MS}^{-1} \pm 0.4\% \text{ R.M.S.}$
DIFFERENCE	1.77%
EVENT RATE	10/s

SPECTRON LTA

TRANSONIC COMPRESSOR
NAVAL POSTGRADUATE SCHOOL DEMONSTRATION
SEPTEMBER 21, 1979

- NATURAL PARTICLES ONLY
- UNPREPARED DIFFUSE METAL SURFACES
- 5s DATA COLLECTION
- ~150 EVENTS/MEASUREMENT
- SPEED : $135.4 \text{ ms}^{-1} \pm 0.2\%$
- ANGLE : $22.0^{\circ} \text{ ARC} \pm 0.7^{\circ} \text{ ARC}$
- TURBULENCE: $1.9 \pm 0.2\%$
- DATA RATE = 30/s
- BACKGROUND PHOTON RATE $5 \times 10^7/\text{s}$
- SUBMICRON PARTICLES
- FULL BACKSCATTER

SPECTRON LTA

LASER TRANSIT ANEMOMETER
DEMONSTRATIONS
BACKSCATTER UNSEEDED 100mW

<u>WHERE</u>	<u>SPEED</u> ms ⁻¹	<u>PARTICLES</u>	<u>DATA RATE</u> s ⁻¹
(1) A.E.D.C. 1" JET	420	LARGE	2,000
(2) N.A.S.A. AMES 6' x 6'	200 580	FOG/NATURAL	10,000/200
(3) G.E. L.S.R.C.	15 40	NATURAL/ 1/4 μm TiO ₂	100
(4) A.E.D.C. VON KARMAN			
TUNNEL A	725	CLEAN	30
TUNNEL B	1200	CLEAN	10
(5) N.P.S. (MONTEREY)	135	NATURAL	30

SPECTRON LTA

ACCOMPLISHMENTS

- ADVANCED LTA SYSTEM DEVELOPED
- OPERATES IN DIFFICULT ENVIRONMENTS
- MEASUREMENTS IN AXIAL COMPRESSOR
- UNSEEDDED BACKSCATTER UP TO MACH 8
FROM $< 0.5 \mu\text{M}$ PARTICLES

SPECTRON LTA

APPENDIX B

PAPERS DESCRIBING LTA THEORY AND SYSTEMS

A TUTORIAL: LASER TRANSIT ANEMOMETRY

A. E. Smart and W. T. Mayo, Jr., "A Tutorial: Laser Transit Anemometry,"
Proceedings from 4th International Conference on Photon Correlation Tech-
niques in Fluid Mechanics, Stanford University, Stanford, CA, 25-27 August
1980.

A TUTORIAL: LASER TRANSIT ANEMOMETRY

A. E. Smart and W. T. Mayo, Jr.
Spectron Development Laboratories, Inc.
3303 Harbor Boulevard, Suite G-3
Costa Mesa, CA 92626

1.0 INTRODUCTION

In the early part of the last decade the now conventional Fringe Laser Doppler techniques were gaining acceptance and producing useful measurements in a variety of situations. As more experience became available certain areas, for example turbomachinery research, proved to be difficult applications. After a brief period of pessimism about the fringe system great innovations were made but meanwhile other techniques were sought. Schodl [15 through 18] explored and developed an idea by Tanner [27, 28] and Thompson [29] which changed the illumination in the sampling volume from fringes to two separated spots, Figure 1. Various designations which are all synonyms which reflect the choice of the pioneering researchers include laser transit anemometry (LTA), transit velocimetry, (LTV), "two-spot," and "L2F."

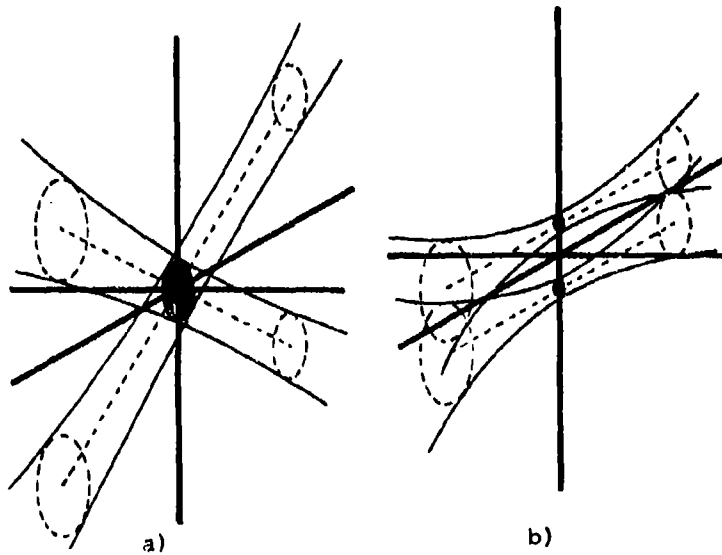


FIGURE 1. ILLUMINATED VOLUMES a) LDV, b) LTA

In generalized terms transit anemometry (LTA) may be regarded as encoding the signal differently from fringe systems (LDV) and the two systems may be regarded as Fourier Transforms of each other, Figure 2 [22]. Some significant differences emerge and it is these differences which lead to preference of one system over the other for different applications. Custom suggests more differences than are actually observed when the parameters are tailored to a specific test case but in broad terms the significant properties are summarized here. The comparisons are based upon a theoretical experiment where either fringe or transit system might be successfully used.

Details of optics are given in Section 2, information retrieval is discussed in Section 3 and in Section 4 we return to the quantification of those factors briefly discussed in this introduction. An appendix illustrates some of the geometrical properties of the LTA sampling principle.

Salient properties which are in some way special to the LTA rather than previous systems are now discussed. Increased illumination intensity is typically obtained with the LTA optical configuration and this leads to ability to observe smaller particles with similar laser power. With a typical cross sectional area reduction of the illuminating beam of 100 to 500, it is possible to restrict the sensitive volume length by a ratio of between 10 and 20. This reduces the distance from walls at which many measurements may be made with a given size of particle [14].

Because the volume is both shorter and narrower for LTA than for comparable LDV, the data rate may be less because with a given particle concentration, size distribution and flux fewer particles give rise to a detectable signal. This is partially offset by the natural tendency for increasing particle concentration with reducing particle size.

With the LTA system the signal processing by photon or event correlation has been shown to be very satisfactory [2, 10, 11, 12, 13, 20, 25, 26]. The bunching of single photons from particle transits is statistically discriminable above the background single photon rate by a filter and thresholding, resulting in separation of multiple photon events from background photon flux rates greater than 10^6 . The preference for fast digital correlation processing is the reason for the inclusion of LTA applications in this conference.

Precision can be high with LTA, particularly of mean velocity and flow angle, 0.1% and 0.1° arc are directly attainable in many situations with few special precautions. Turbulence may be measured in a different way from that available from former technologies. The measurement of speed and its distribution in a chosen direction gives access to estimates of turbulence in different directions, even to the assessment of stresses. Early systems tended to be most suitable for turbulence between 2% and 15% but this is now [14] extended down to a small fraction of one percent. The upper limit is based upon long data gathering time and as yet inadequate theory.

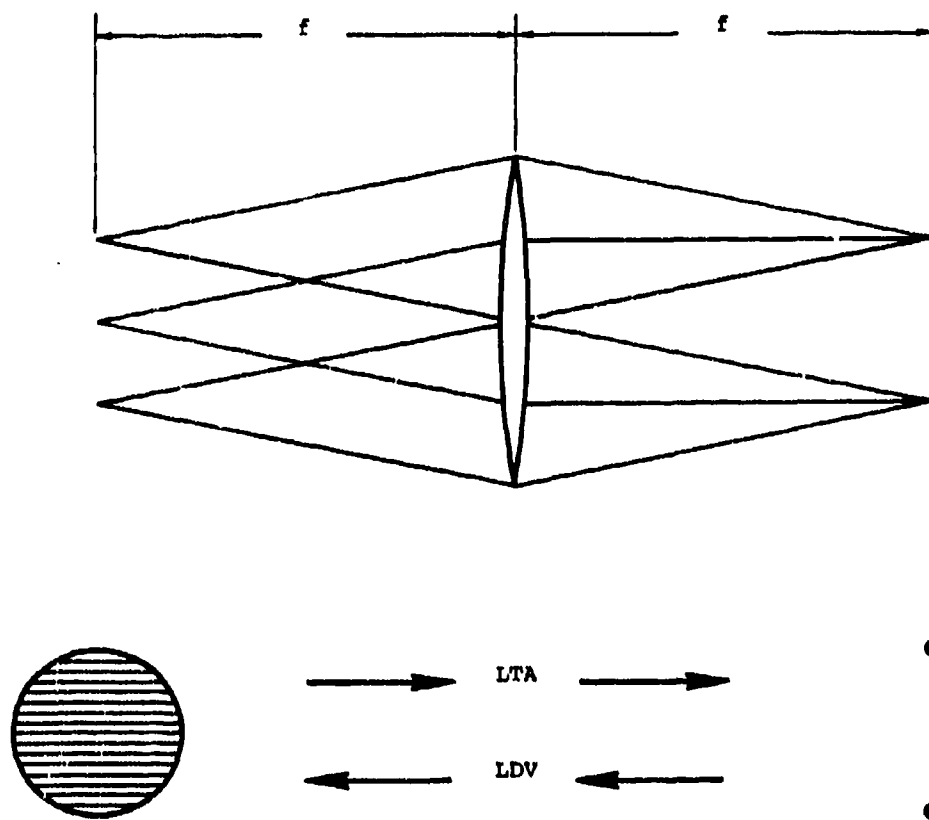


FIGURE 2. OPTICAL ENCODING SCATTERED LIGHT FOR LDV AND LTA SYSTEMS

2.0 OPTICS

The optical design of LTA systems call for more care than that formerly necessary in optical anemometry. The sampling volumes are smaller and the stray light stops capable of better rejection. The optical performance must approach theoretical limits to use the potential advantages. Figure 3, which may be referred to throughout this section has its components labelled in three ways. [A] represents essential components, [B] represents highly desirable components and [C] represents components which depend on the application.

2.1 Beamsplitting

Several types of amplitude division beamsplitter (Figure 3) are in use, the two most suitable for LTA being the Rochon and Wollaston polarizing beamsplitters. Both units produce collimated but slightly diverging beams of crossed polarization from parallel input beam but these authors see the symmetry about the axis of the diverging beams as a slight advantage of the Wollaston. Other beamsplitters are in use and offer advantages of adjustability but this can cause mechanical inconvenience or unreliability. The collimated beam from the laser is thus divided into two collimated beams which may be brought to two focal spots in the plane of a lens corrected for infinite conjugates. This lens essentially performs a Fourier transform function, the splitting face of the prism being the same optical distance behind the back principal plane of the lens as is the focus of the two spots in front of the front principal plane. In fact this distance may be slightly modified, in situations where ultimately parallel spots are essential in the test space, to yield spots which are converging at the first focus. This allows the relay lenses, whose longitudinal magnification would otherwise create diverging spots, to image the final test spots as parallel.

The imaged spots are relayed into the test space by back-to-back collimator lenses which are free from spherical aberration over the full aperture. Using this method the spot size is determined by the diffraction limited image of the Gaussian input laser beam via the magnification derived from the focal lengths of the three collimator lenses. The separation is controlled by the divergence of the splitter prism, the focal length of the focusing lens and the magnification of the two output lenses. The spot diameter to separation ratio is thus easily designed to be a chosen value but its change is not trivial.

Quantitatively if the spot separation is s , the beamsplitter divergence is β , the input laser beam diameter is D , the half width at the Gaussian waist is r focusing lens and internal and external lenses of focal lengths f_1 , f_2 , and f_3 respectively we may write

$$s = \frac{\beta f_1 f_3}{f_2} \quad (1)$$

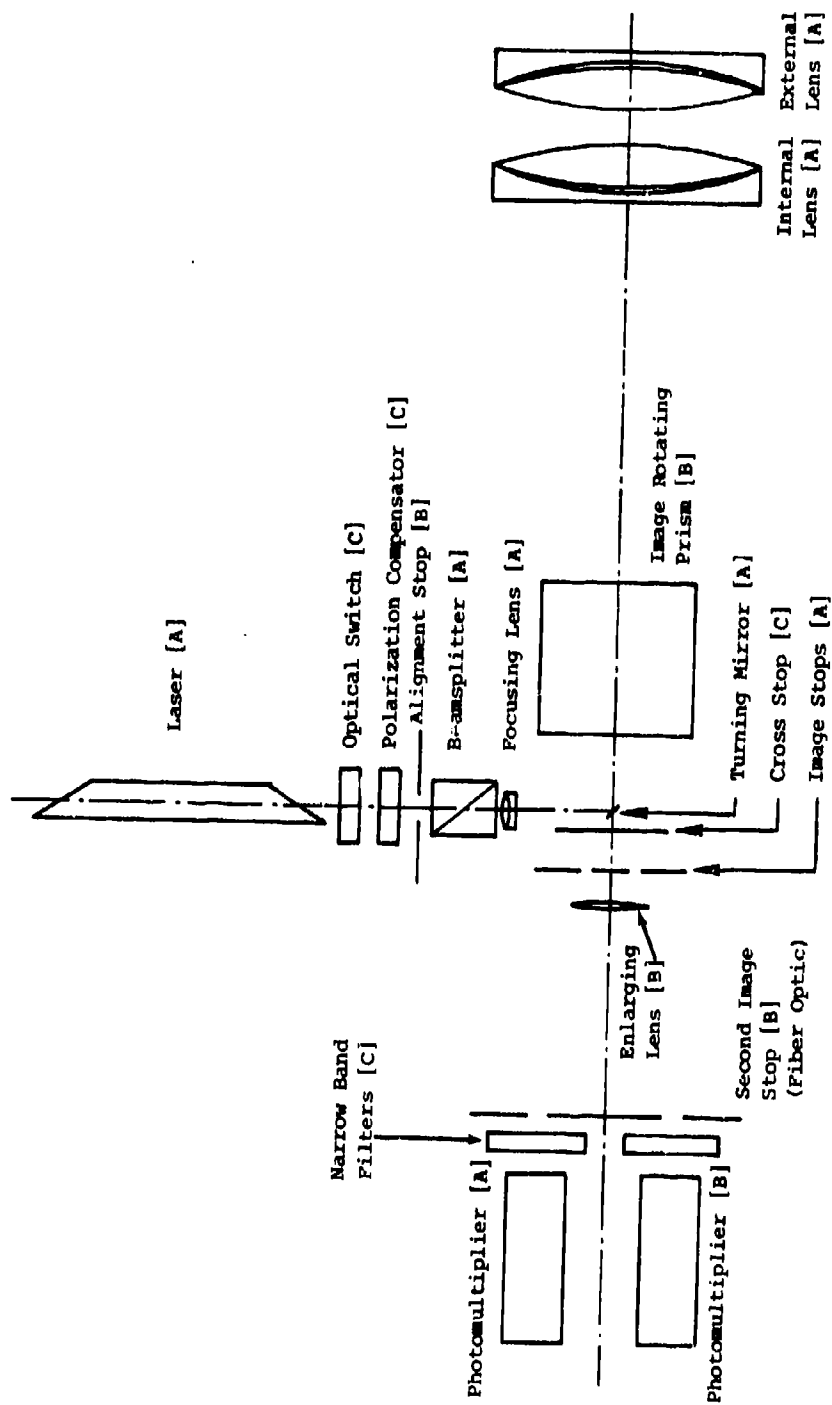


FIGURE 3. SIGNIFICANT OPTICAL COMPONENTS

$$\text{and} \quad r = \frac{2}{\pi} \frac{\lambda}{D} \frac{f_1}{f_2} \quad (2)$$

giving a spot separation to diameter ratio of

$$\frac{s}{2r} = \frac{\pi \beta D}{4\lambda} \quad (3)$$

In practice small imperfections in optical components may conspire to reduce this slightly.

2.2 Spot Rotation

In the LTA technology it is essential to rotate the orientation of the two spots and three ways of doing this have come into use: rotation of the beamsplitter and the stops separately but coupled together, use of an image rotator prior to the output lens and rotation of the whole machine.

The last method produces excellent mechanical correspondence between output and return images but is bulky and inelegant. The first two lead to a more compact design. The first has more moving parts with opportunity for less than perfect alignment. The second is efficient and rather expensive. It is usual to arrange for computer control of rotation with corrective feedback of the angular position attained which may be to a precision of 0.1° arc without great difficulty.

The important criteria associated with the ability to rotate the spots are precision/accuracy, exact placement of stops independent of angular station, preservation of beam equality, freedom from aberrations and stationarity of center of gravity of spots (rotation without displacement). With the first system described above, it is necessary to compensate the laser polarization so that the beams do not change their relative intensity with rotation. In the second case, since the Wollaston prism remains stationary, small adjustments in its angular orientation may be made to render the spots of identical intensity. Since the laser is typically plane polarized, a 45° inclination of the axis to this plane yields 50:50 partition with normal polarizations. Method three, with rotation of the laser, also is likely to cause trouble with larger lasers and is probably a simplification of the optics at the expense of mechanical difficulties and physical size.

A solution that has been used by the present authors is a modified Mirror Dove prism [23] which has an $f/4$ or better aperture. It leads to compact overall system length, introduces no aberrations into a diverging beam, is optically efficient and is insensitive to polarization. There are no surfaces normal to the optical and mechanical axis, which is good from the point of view of introduced flare, and there are no refractive elements. The input contains no critically toleranced components but is difficult to align initially.

2.3 Stops

Probably the most important design property of LTA systems is the precise specification of stops. Their function is to reject light from all sources except that scattered from moving particles in the control or sampling volume. To that end a simple pinhole overlain by the conjugate image of each sampling region would seem adequate; however, there are several potential sources of flare to be considered. Multiple reflections from within the optical system, even with well coated optics, are a source of scattered light. These may be reduced by careful consideration of all components and by 'double stopping' where the image stops are themselves reimaged on two more stops. This is effective in reducing second and higher order scatter sources, and has advantages not only in improving the rejection of flare generated from within the optical system but also from multiple scatter in any test situation and beam walk-off sources in windows. Typical rejection factors so far achieved have been up to twelve orders of magnitude defined as photon rate from input laser to detected single photon rate from P.M.T. It is not necessary to do better than this for turbomachinery applications where the internal flare is dominated by the scatter from walls. (One always desires to measure closer to walls until the flare mechanism overrides the useful data.) It is very useful to improve this figure for wind tunnel measurements where there is no significant flare generated near the test space, although window flare may still limit the usefulness of the so called improvement.

In addition to the field stops discussed so far, two other types of stops are necessary to the system. An aperture stop is automatically provided by the outer edge of the final lens and by the edge of the turning mirror which separates outgoing from incoming light. It is necessary to extend the stopped area of the turning mirror to prevent diffracted flare from its edges. This is conveniently done by two more stops, one of which restricts the input beam to an area slightly smaller than the turning mirror and one of which occludes an area slightly larger than the turning mirror from behind. These latter stops are not purely aperture functions.

Yet another stop is essential to improve wall proximity. Flare may be seen by one photomultiplier which has arisen from light in the other channel [26, 27]. This may be prevented by stopping part of the received area. There is a reduction in optical efficiency of the machine and this stop is only necessary when wall proximity is important. This is executed as an extension to the stop immediately adjacent to the turning mirror. Some wall proximity tests are documented in Reference 14.

2.4 Aberrations

The LTA principle relies heavily on having very small spots and well defined images. It is necessary to approach diffraction limited performance as closely as possible and in this respect LTA systems are more difficult to design and build than equivalent LDV systems. Because this system has a small field only spherical aberration is of consequence among the first order Seidel sums. It is, therefore, of extreme importance

to obtain lenses whose design conjugates conform to the overall system. Infinite conjugate design is needed for the three essential lenses. Chromatic correction is not needed unless the system is to be used with a fluorescent seed medium; however, fluorescent particles tend to be of the order of 1 μ m diameter or larger to scatter a significant amount of wavelength shifted light and will not be small enough for many applications. The peculiar advantages of LTA may not be so well taken if it is necessary to add such large particles to the test flow.

Projected spot quality and receiver efficiency are both impaired by normal and more by oblique incidence through a thick window. This effect is studied and quantified in Reference 26, but typically up to 2" thick windows with less than 10° incidence do not cause serious deterioration with f/4 systems. If windows up to 4" thick are essential, near normal incidence is desirable. Curved windows are not advised unless they are quite thin, or of large radius of curvature as they, like inclined plane windows, may introduce unacceptable tangential or sagittal astigmatism.

2.5 Mechanical

In a system which relies upon optical precision, mechanical properties are at least as important. Small size leading to rigidity, and low weight leading to ease of handling and traversing are important. Retention of alignment in bad thermal and vibration environments is an essential feature of optical anemometers in many applications. It is both more critical and more difficult to achieve with LTA systems than with other configurations because of the relatively tighter tolerances.

2.6 Photomultipliers

The requirements for photodetectors [Figure 3] are complex in that it is desirable to have single photon counting resolution with low time and amplitude fluctuation. The detector should not be damaged by, nor be subject to a significant recovery time after, overload. The details of this are the subject of paper No. 10 in this volume. It has been convenient to make the stops to be the ends of single fiber optics whose flexibility makes small adjustments both easy and precise without moving the comparatively bulky photomultiplier tube assemblies.

3.0 INFORMATION RETRIEVAL

The optical configuration of the sampling volume for an LTA system is quite different from its counterpart in LDV. While it is obvious that an LTA system measures transit time it is not so obvious that this is also what is measured, more indirectly, with an LDV system. Many ways of regarding the LDV fringe signal have been discussed, with models of varying completeness, but a time measurement, in one or other guise, has always been available. The significant differences are in the precision and interpretation of this time, and in the form of the measurement.

Again trivially the LDV measures the velocity component at right angles to the fringes and has a precision controlled by the total amount of light and more deviously, the number of fringes. This is for a perfect

(optimum) signal processing technique. The issue of matched filtering based on 'a priori' data is thorny and much argued but applies also to LTA in a much simpler way. The precision here may be enhanced by moving the spots further apart but this, for a given level of turbulence, restricts the number of events, and because of this reduction in statistical numbers may not lead to a final improvement in overall accuracy.

Suffice it to note that the types of velocity measurement are quite different in LDV and LTA and each may have the more appropriate output for a specific application.

3.1 Time Detection for LTA

The detection of the best possible estimate for the time when the particle crossed the peak (nearest point to the center of the illuminated region) is derived by filtering the signal with a Gaussian filter whose roll off is well shaped and sufficiently close to the estimated velocity (within a factor of two or better) to induce minimal distortion into the assessment of peak time. Such discrimination is described elsewhere ([12], and paper 10 of this volume). The peak disparity is a function of how many photons are received and detected. For one photon or less the spread on the time is the same fraction as the spatial spread on the spot (both referred to the time or space separation between spots). As the photon numbers increase this improves dramatically as the filter has an optimum tendency to take the 'center of gravity' of the photon burst so long as the photodetections occur within a period short compared with the inverse filter bandwidth.

For a few photons per transit, typical discriminator jitter is in the region of 1 ns to 2 ns for a total transit time of one spot of 15 ns and is proportionally greater for longer transit times. This mechanism has a similarly good performance whether the number of photons is just three or four or corresponds to the quasi-classical continuum of photons resulting in a pulse of widely variable height [11]. To achieve the best overall performance of such a discriminator, it is desirable to separate the event detection filter from the pulse center estimation filter by about a factor of four. This allows a smaller bandwidth on the event detection filter without compromising center finding sensitivity and precision with a large dynamic range of spot transit times [13].

Discriminators such as outlined need only produce a clean pulse at a fixed time after the estimated peak. Any delay is not important so long as it is the same for the complete detector/discriminator units for each spot. A good way to confirm this is to make a velocity measurement from spot A→B (say) and then rotate the spots and measure from B→A. Now the two channels may be checked out 'in toto' or at various subsections by exchanging connections at different points in the system.

3.2 Instrumental Broadening

There is a group of parameters which may affect the observations and it is useful to summarize these and consider (without proof here)

the consequences on a qualitative basis. Considering a possible trajectory across the region illuminated by the two spots there are several ways the assumed geometry, Figure 4 and 5 is not satisfied by the real world. The parameters may be summarized.

- 1) Particles miss the center of the first illuminated region in either of two directions, along or normal to the optical axis by distances $b_{//}$ and b_{\perp} .
- 2) Particles may not move at right angles to the optical axis by an angular deviation ϕ nor in the common plane of the axis of the two spots by an analogous angular deviation θ .
- 3) Particles may be of different sizes (radius = a).

Within limits defined by the spot diameter to separation ratio and the increase in this ratio with progression along the optical axis in either direction, the values of the above parameters may take a wide range of values. For isotropic particle loading, the positional coordinates under 1) will be uniformly and equally probable. For the angular parameters under 2) it is necessary to anticipate the turbulence distribution in velocity space since this is convolved with the geometrical transfer function of the whole illuminated space. The consequences under 3) are determined by the particle size distribution which is most often not known.

The detailed examination of these factors show that in any real flow situation the mean transit time is obtained from all those particles which fall within the boundary conditions defined by the above variables. The interrelationships are complex.

If the signals are such that only one photon arrives from the experimental configuration at one time then the broadening may simply be described as the product of the sensitivity quadric (the illumination intensity times the receiver aperture function) and the particle path as a sampling function. This arises because the probability of scattering (and hence receiving and detecting) a single photon on a statistical basis is predicted by the classical continuum descriptors. The instrumental broadening is thus described by the defined illumination/reception function and the integrated probability of finding particles with each of the five parameter restrictions just described. If there is some method of looking at a large number of photons, say enough to approximate the classical estimation under all conditions, then it is possible to use the same peak time detection to estimate the center of the classical pulse. The positions in the x direction of these centers do not change with changes in b_{\perp} , $b_{//}$ or a . Hence, there is no intrinsic error nor broadening. With respect to ϕ , any variation will be simply resolved into the measurement direction. For most commonly used configurations this is true provided that $\phi < 70^\circ$. This is in accord with the transit system resolving velocity components in the plane of the two spots into a direction parallel to their common normal.

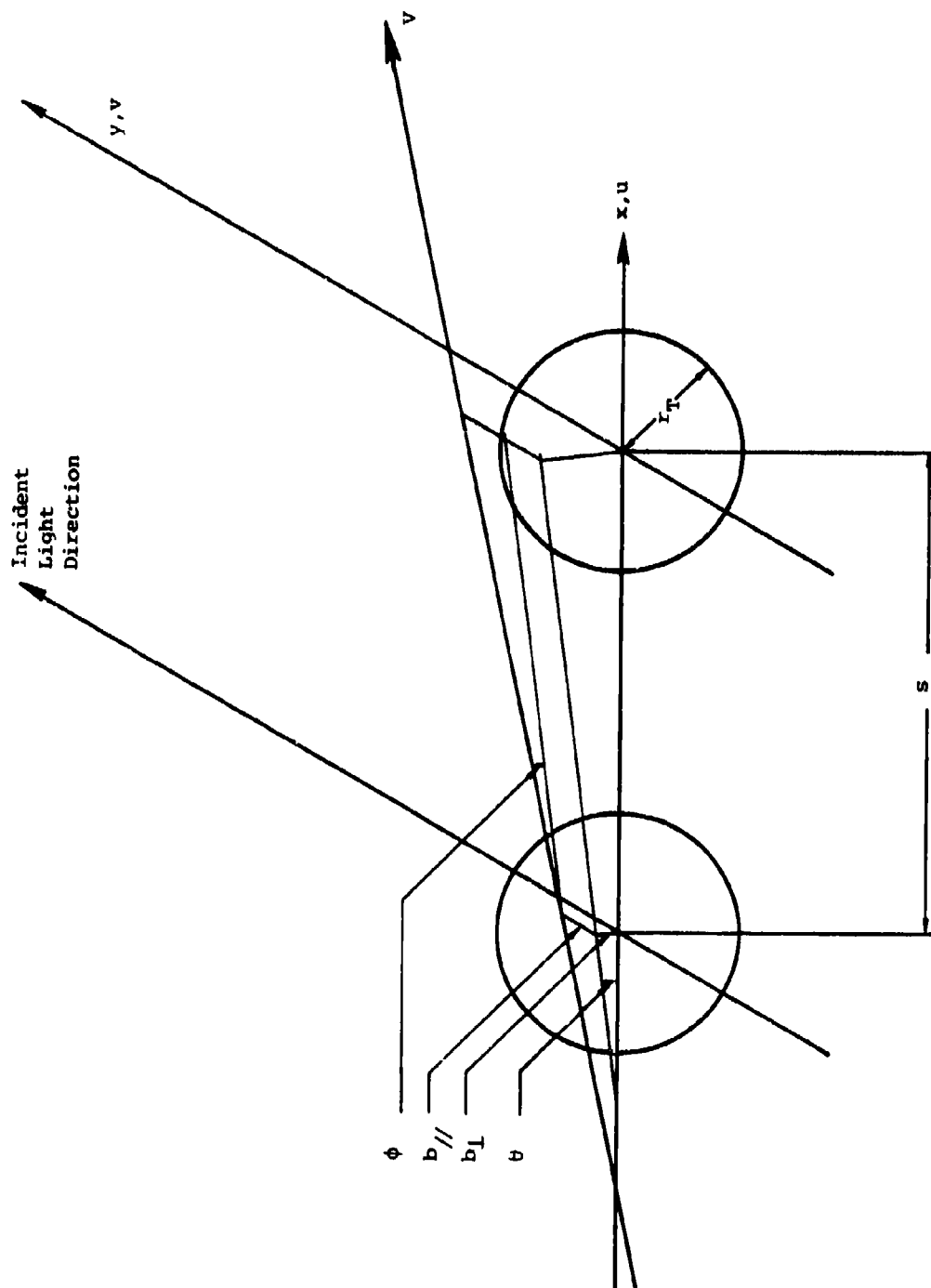


FIGURE 4. TRANSIT SYSTEM GEOMETRY

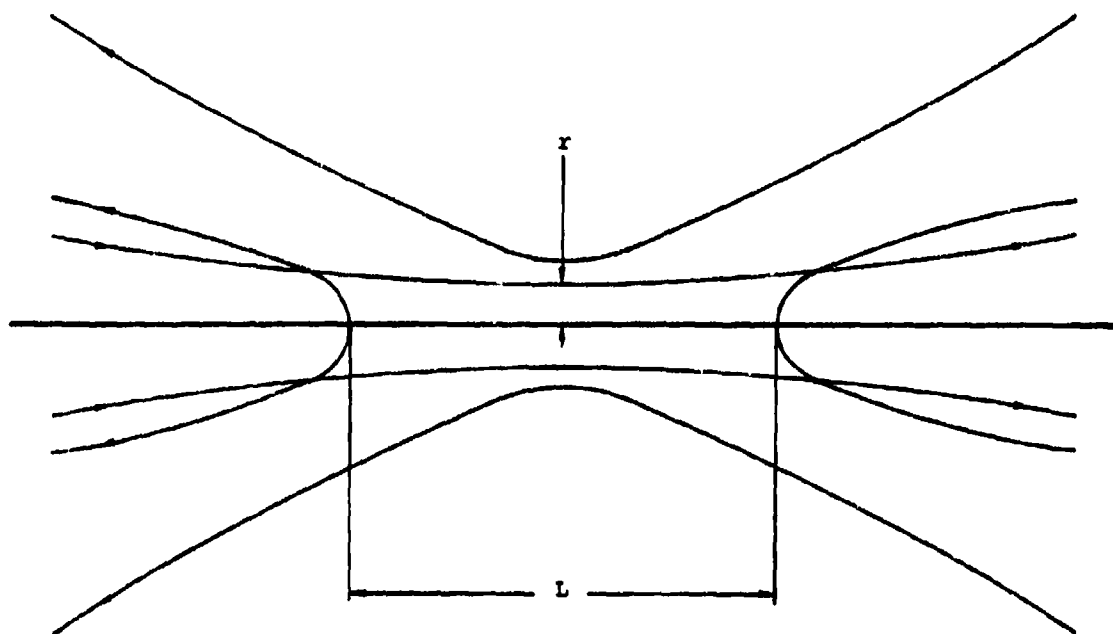


FIGURE 5. ILLUMINATION AND RECEIVING VOLUME

The final parameter θ has complicated functional properties. If the spot diameter to separation ratio is small, say a few percent, then to first order this is not significant but for high precision it should be considered, particularly in turbulent flow situations where measurements are made with the spots at different rotations compared with the mean flow, i.e., various discrete values of θ . A complete analysis of the effects of these five parameters is not within the scope of this tutorial but a brief examination of the effects and properties of a typical system is presented in the Appendix.

The spot transit broadening may be removed by peak detection in the direction of the mean velocity [14]. Where measurements of turbulence are to be made, it is apparent that the broadening at right angles to the mean flow may be more difficult to remove. The success of its post observation deconvolution will depend on the spot separation to diameter ratio and the level of turbulence of interest. For mean velocity and longitudinal turbulence measurement the θ broadening is not of primary concern.

With the availability of increased computing power it may be desirable to look at all the data from a variety of angles and to reconstruct the event distribution in real space and averaged over time. The non-linear transformation into velocity space may be performed without too much theoretical objection although the old controversy of the particle vs. fluid velocity field occurs once more. It is now in a slightly different guise because of the topics mentioned earlier in this section and we have every confidence that papers in this conference will illuminate the subject further.

If an array of data points is available in velocity space then the properties of the flow/particles may be quantified. Two provisions are that each angle should be measured over a time which is statistically stationary to some prescribed variance of the flow, and that it should comprise sufficient particle samples to maintain a chosen and accepted maximum variance at the limiting area of interest of the final velocity-space distribution.

Because there is no way that event counts far from the mean values can satisfy the criteria postulated, it may be good either to fit a flow model with 'a priori' reality conditions or to truncate the data field at given distance from the areas of maximum interest. Failure to do this must lead to catastrophic breakdown of any computing algorithm, analogous to attempting super-resolution in a space where the normalizing eigenvalues are already hidden beneath the statistical noise level. This means that with a given number of observed events only certain questions may be asked of the data.

4.0 QUANTITATIVE PROPERTIES

It is instructive to quantify the general remarks of the introduction. Many approximations will be made to show trends with which more specific parametric analyses may be made by the exacting user.

4.1 Illumination Intensity

Referring to the illumination intensity, the overall profile is Gaussian at right angles to the Poynting vector. For a fringe system this is oversimplified as this region is illuminated by two nearly plane wavefronts inclined at a slight angle which specifies the 'fringe' spacing. For comparisons this model is adequate. The volume size need not 'per se' be controlled by the mechanism of LDV vs. LTA but in practice the volume for LTA in high speed applications is much smaller than that for LDV. This constraint is applied because the LDV area must typically contain several fringes and, depending upon the application, these must be widely enough spaced not to exceed the frequency handling capability of the signal processor for a typical high speed flow. Related limitations do exist for LTA but the spots may be made the size of a typical single fringe width and the resolution is typically much better. If the velocity is low enough and a large angular aperture is available, a fringe system may show axial light rejection comparable with the LTA, because the signal processing frequency constraint is eased and very small probe volumes become tolerable. In such applications as automotive reciprocating engines with high turbulence and low velocities, no immediate advantages are seen from the LTA system properties. Illuminated spots may be 10 μm to 20 μm with sufficient, closely spaced fringes to enable excellent experiments to be performed in high swirl, high turbulence, non-stationary environments.

In environments where velocities are high and the physical dimensions of the test assembly are not proportionally increased, the high frequencies demanded by the fringe system are not so easily managed, in turbomachinery for example. Here there are advantages in using smaller particles which will more readily follow flows and may naturally (or artificially) be present in larger quantities. We will handle the smaller size first. The photon flux F_1 through the sampling volume is:

$$F_1 = \frac{P}{h\nu\pi r^2} \text{ photons/s/ unit area.} \quad (4)$$

Where P is the laser power, r is the radius and $h\nu$ is the energy per optical photon.

The photon flux scattered by a particle of radius a during its transit of the peak is $\pi a^2 F_1 q(a)$, where q is the scattering efficiency. Hence the total number of photons scattered during the transit, G_s , will be the flux multiplied by the transit time, $2r/V$, hence

$$G_s = \frac{2a^2 P q}{h\nu r V} \quad (5)$$

This is necessarily approximate because no allowance is made for which part of the illuminated region is intercepted by the particle, nor the profile function, nor the collection and detection efficiency for scattered photons. It is assumed that these are at least closely comparable for LDV and LTA systems and will, thus, not have significance in their comparison.

For a particle of radius a , therefore, the number of photons scattered during a transit of an LTA volume compared with an LDV volume is $2r_D/r_T$ (where r_D and r_T are the beam waist radii for LDV and LTA respectively) assuming that the same laser power as in the LDV volume is equally divided between the two LTA spots.

The peak photon rate for the two systems, because of the different transit times varies as $2(r_D/r_T)^2$. Thus, both photon number and peak rate are increasing from LDV to LTA if $r_D > r_T$, as is the usual case. If a given number of photons or a given rate excess over background is the criterion of signal detectability then the same success will be met by smaller particles in LTA than LDV. As an aside, we note that the quality of optics necessary for typical LTA systems is significantly higher than that for LDV which operates successfully far away from diffraction limited conditions, except in situations where the flows are very slow, and high spatial resolution is demanded.

The comparative ratios here and throughout this section are summarized in Table 1.

TABLE 1
RATIOS OF LTA VS. LDV FOR VARIOUS PROPERTIES
OF EQUIVALENT SYSTEMS

	<u>Ratio LTA/LDV</u>
Number of photons scattered in transit	$\frac{2r_D}{r_T}$
Peak photon rate detected	$2 \left(\frac{r_D}{r_T} \right)^2$
Sample Volume length	$\frac{r_T}{r_D}$
Data rate for monodispersion	$\left(\frac{r_T}{r_D} \right)^2$
Data rate for $n(a) \propto a^{-4}$ (a_D, a_T = minimum detectable radius)	$\left(\frac{r_T}{r_D} \right)^2 \cdot \left(\frac{a_D}{a_T} \right)^3$
Data rate for $N(a)$ (with allowance for $q(a)$ and retrieval efficiency)	$\left(\frac{k}{2} \right)^{3/4} \cdot \left(\frac{r_T}{r_D} \right)^{5/4}$

Typical ratio of probe volume radii for high speed flow r_D/r_T is 10 to 20.

4.2 Sampling Volume Length

The sampling volume for each system may not be directly compared on the basis of instrument function but it is possible to compare one spot of the LTA with the sampling volume of the LDV for considerations of axial sensitivity. This parameter is not quantifiable with any great precision but on the basis of perfect optics it is possible to assume that axial acceptance length is approximately proportional to r . For proximity to walls, all other things being equal, the smaller is r the smaller is L and closer to walls may data be obtained. If this were the only factor involved, the ratio of wall distance for LTA over LDV would be r_T/r_D . However, wall proximity includes rejection of background flare as well as probe volume length, and this is even more strongly influenced by the radius r and the field stop.

4.3 Data Rate

Data rate may be quantified only with some reservations. In a cloud of monodisperse particles, whose size is sufficient to give good measurements with either system, the data rate is proportional to the swept volume. This is the cross sectional area normal to the flow multiplied by the velocity, i.e., $2LrNV$, where N is the number of particles per unit volume, each of which is of radius a . The data rate ratio for LTA to LDV is therefore $(r_T/r_D)^2$, again because $L \propto r$.

In practice, natural aerosol distributions exhibit a number density distribution approximately proportional to the inverse fourth power of radius, of the form of Figure 6. The observation that LTA will see smaller particles than LDV for comparable laser power and other suitable conditions means that more events will be observed. Supposing that each system will see up to and including the maximum size present, of which there is a negligible number, those particles which are above a given size a will be given by

$$N_T(a) \propto \int_a^{\infty} a^{-4} da \quad (6)$$

$$N_T(a) \propto a^{-3} \quad (7)$$

The ratio of data rate for LTA to LDV is now modified to $(r_T/r_D)^2 \times (a_D/a_T)^3$ where a_D and a_T are the smallest particles which may be observed consistently by the LDV and LTA systems here postulated.

Once more there is a modification to this because as the particles are smaller so also their scatter cross section (scattering efficiency) reduces still faster ($q(a)$ on Figure 6). If a given number of photons is necessary for detection, we will assume that K more photons are required for LTA than LDV (Note that $K < 1$) then

$$K \frac{(a_T)^2 q(a_T)}{r_T} = \frac{2(a_D)^2 q(a_D)}{r_D} \quad (8)$$

Now in the range of interest $0.1 \mu m$ to $1 \mu m$ the value of $q(a) \propto a^2$.

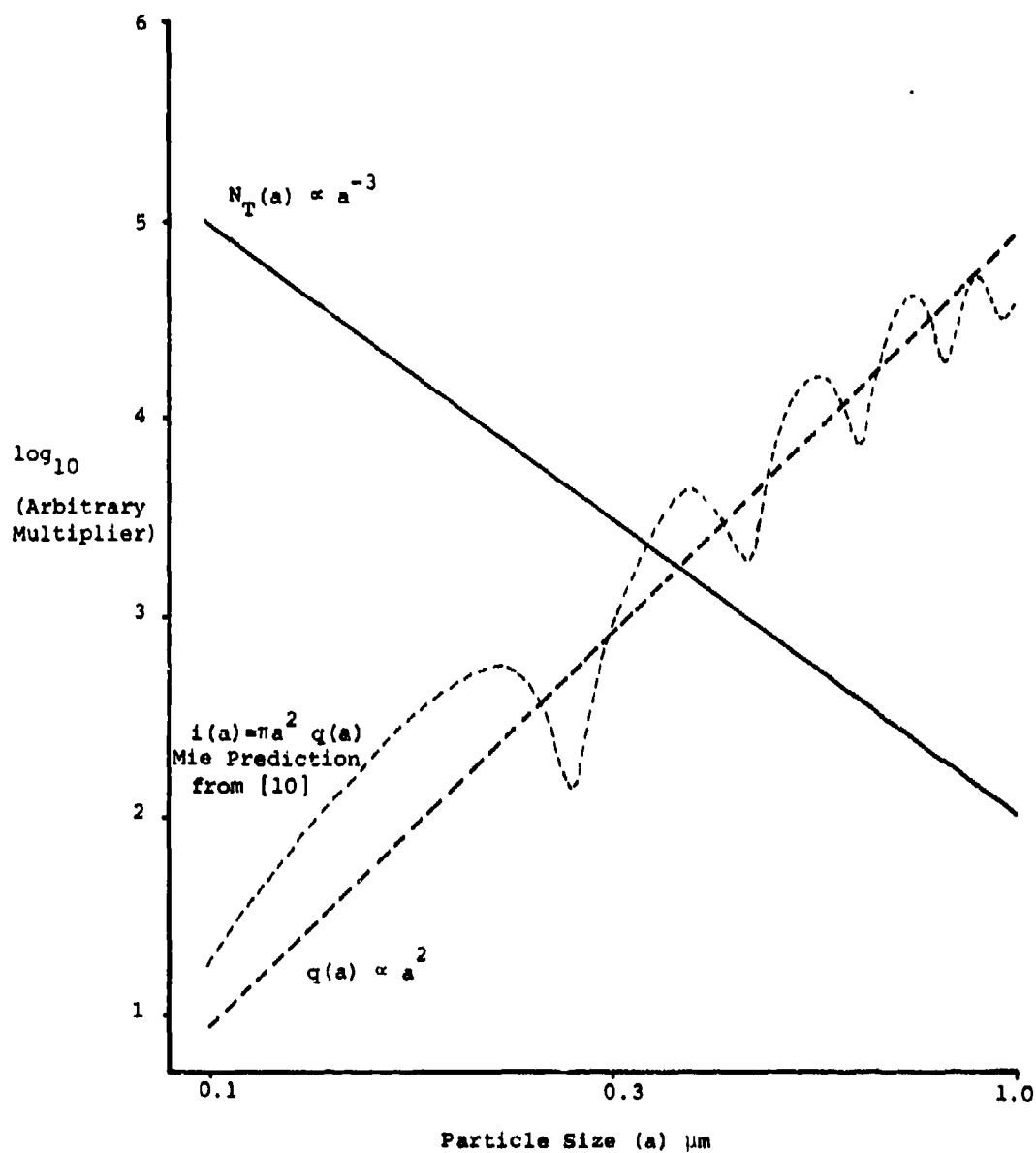


FIGURE 6. DEPENDENCE OF SCATTERING EFFICIENCY AND CUMULATIVE
 NUMBER OF PARTICLES OF RADIUS GREATER THAN a ON
 PARTICLE RADIUS, a

Hence, the limiting particle sizes for each system are approximately related as

$$\left(\frac{a_T}{a_D}\right)^4 = \frac{2 r_T}{K r_D} \quad (9)$$

which defines the limiting ratio of minimum usable particle sizes as

$$\frac{a_T}{a_D} = \left(\frac{2 r_T}{K r_D}\right)^{1/4} \quad (10)$$

and hence the equivalent value of data rate ratio becomes

$$\left(\frac{K}{2}\right)^{3/4} \left(\frac{r_T}{r_D}\right)^{5/4} \quad (11)$$

This is only true if the velocity direction produces no angular excursions outside the range of acceptability of the two spots (low turbulence). The ratio reduces rapidly when turbulence increases such that only a small number of particles produce events on both channels in any one orientation. The above ratio tends, therefore, to be a 'best' achievable with natural particulates.

4.4 Detection

Detection is another complex area. In principle, the detection of a transit event is easier than the assessment of frequency within a longer pulse, but as each system approaches the regime of quantum realization then other factors come into play. A typical spectrum of a classical fringe crossing with added noise looks like Figure 7(a). The component near zero (the intensity fluctuation spectrum) is usually rejected by a band pass filter, represented by the dotted window. In an ideal fringe processor this window is a tracked envelope the same width as the spectrum of a single transit and infinitely agile. This is seldom achievable. In the transit system of Figure 7(b), the 'matched' filtering is now only a low pass function which extends slightly beyond $1/\tau_T$ to cover fluctuations in transit time. In principle this need only include the equivalent low passed intensity fluctuation of Figure 7(a) (because the single spot transit has no modulation) but in practice single spots are typically of the order of size of a single fringe and hence cover almost the same range in frequency space except for the low cut. Certainly its noise acceptance is comparable and, hence, appears to have no immediate advantage.

There is an advantage, however, and this may best be seen in the time domain. Although this may not be seen from Figure 7, it is clear from Figure 8 that the non-linear thresholding offers an immediate mechanism for rejection of 'noise' while observing 'events' where the difference is defined as transient photon rate. The explanation of this principle was presented in reference 13.

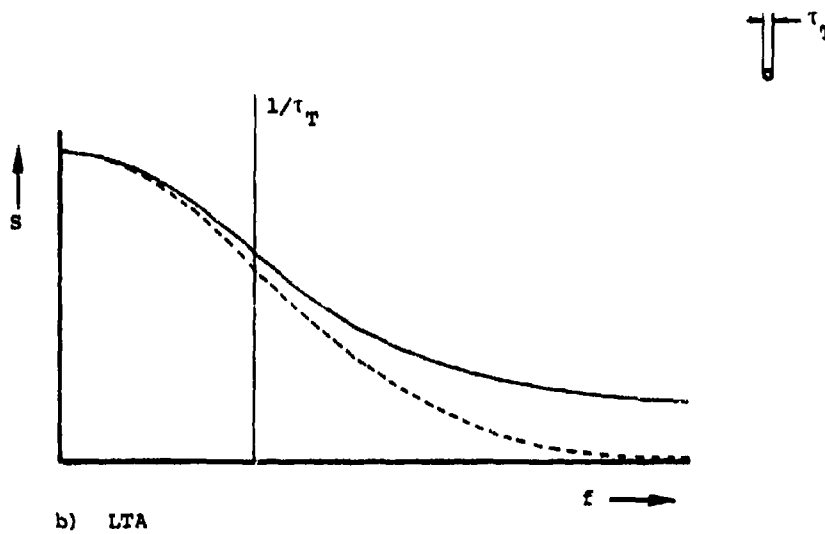
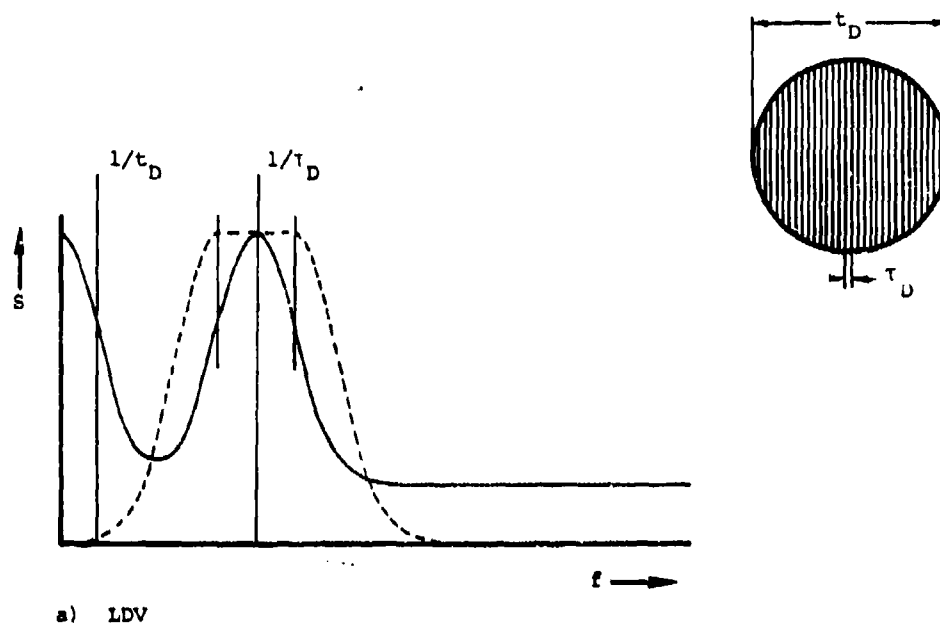


FIGURE 7. SPECTRAL DISTRIBUTION OF LDV AND LTA SIGNALS

In an experiment without additional background light where only light scattered by isolated particles is detected it has been shown that 30 to 60 photons are necessary for 1% velocity resolution in a fringe system [4]. This becomes 2 to 4 per spot for a transit system. Indeed, it may be only 1 per spot if the spots are far enough apart and there are no other photon sources. The chosen properties of the filter for the fringe system are not so necessary for the transit system because any error which may accrue from imperfections of the filter will be the same for both spots and not incur any first order error.

The idea of using an appropriate low pass filter is very efficacious in noise rejection because of the possibility of analog thresholding to decide whether an event has occurred [See Figure 8]. A single photon (noise) ideally will not rise to this threshold when convolved with a Gaussian analog filter but two or more photons occurring within the inverse filter bandwidth will cross this level [Figure 8b]. In any real transit experiment the peak photon rate is almost always too high for quantum resolution and the analog filtering represents an excellent method of discriminating 'events' from 'no events' where an event is now associated with a group of photons from a single particle. A separate filter which then makes an estimate of time of occurrence of the highest instantaneous photon flux [Figure 8c] may generate a digital signal [Figure 8d] to be correlated with a similar system which views another spot. The actual fixed delay manifest between Figure 8c and 8d is not shown.

In practice most transit systems rely on having 2 or 3 or more photons scattered from a particle before that crossing is deemed a successful event. This is a property of where the systems are used and mostly their advantages are great when operating close to walls or other flare sources. In these situations there is a background rate of detected photons which are almost always individually realized in a system of sufficient speed to look at transits with high precision. We will quote an example.

At 400 ms^{-1} crossing a $10 \text{ }\mu\text{m}$ diameter spot takes 25 ns. We would look at the signal with a low pass filter whose Gaussian shape and cut-off point will yield an analog pulse two to three times greater for three photons during the transit than for one at any other time. In principle, a background rate where no more than two photons occur in 25 ns will yield no events. This is not true in practice because of the Poisson nature of arrivals, the pulse height variations of the photomultiplier [Paper No. 10 in this volume], and other factors but typically three photon events may be discriminated in the presence of background of up to 10^7 photons/s of 'noise'. This property also removes any need for low noise photomultipliers but does demand a photon counting tube with pulse height stability. Again with some considerations the speed of the photomultiplier and detection filter circuits control the speeds measurable by a given transit system. Basically the circuitry must be fast enough to accommodate signals whose speed depends on velocity and optical geometrical specifications. The authors have measured Mach 8 (1200 ms^{-1}) with $12 \text{ }\mu\text{m}$ spots to better than 2% using 15 ns filters [25].

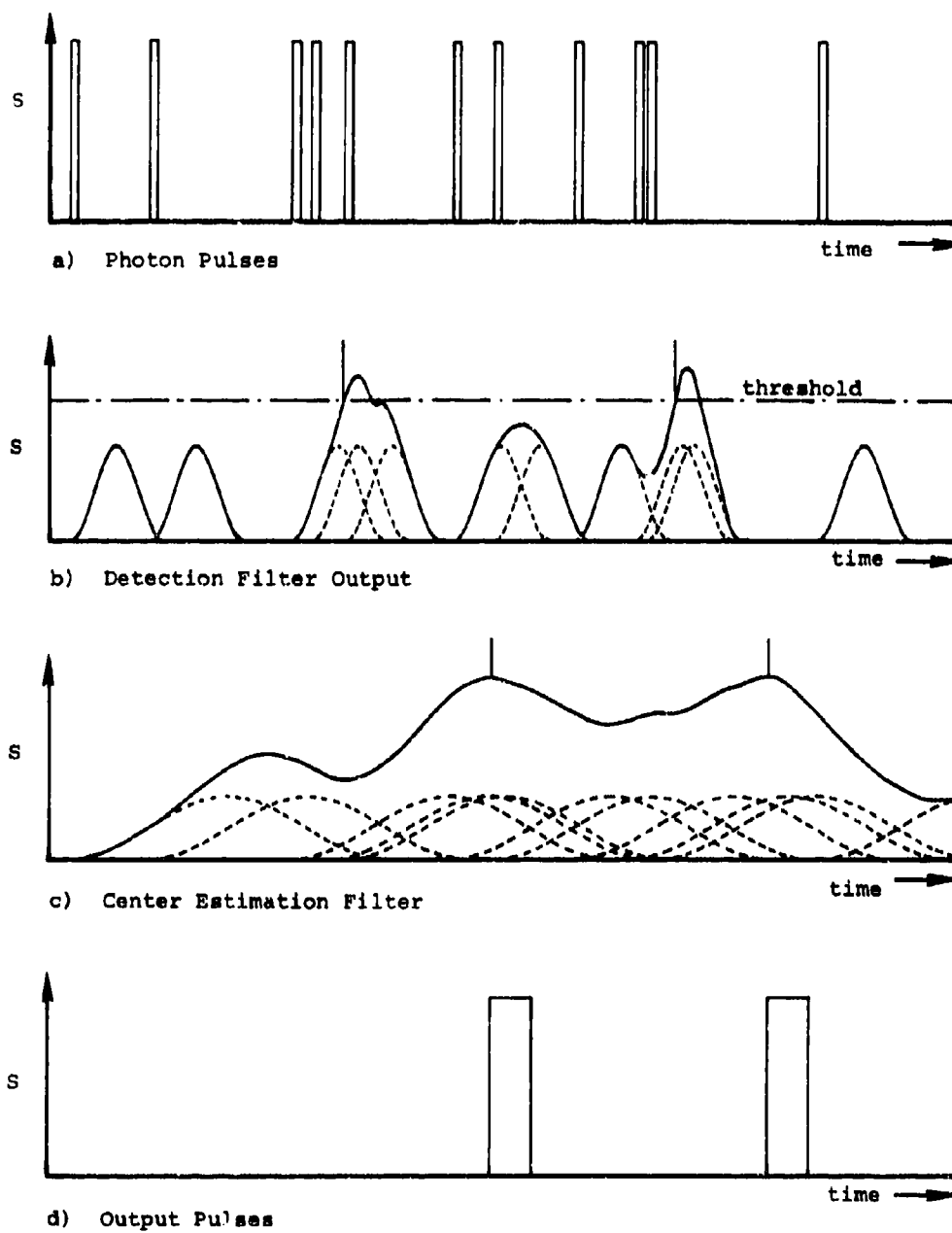


FIGURE 8. DISCRIMINATOR OPERATION

Where there may be no significant flare sources, as in wind tunnels away from models, the threshold may be lowered to include every photon but this then increases the 'instrumental broadening' to a fractional level corresponding to the spot diameter to separation ratio. This broadening is progressively reduced as the number of detected photons/transit increases.

4.5 Data Processing

Several methods of measuring event times are in use, the two most significant, since it is intervals which contain the required information, are direct timing and correlation. In sparse particle situations, where the transit time from one spot to the other is short compared with the mean interval between particles, there appears at first to be no significant advantage of one method over the other. Where particles may occur more frequently, the efficiency of timing falls rapidly compared with correlation. In all cases it is shown very much more satisfactory to use two photomultipliers. With one PMT, timing can only stop on the next consecutive event, and this yields a sloping background which must be compensated and is difficult to model theoretically. Auto-correlation yields a flat and subtractable background but this is four times as great as if two P.M.T.s and cross-correlation are used. With two P.M.T.s and timing the 'start' may be on one event on one channel and the 'stop' may be on the next event in the other channel. A more satisfactory scheme is to display each of all 'stops' on the second channel which occur during the display time window after an initiating event on the first channel. The latter method may be less efficient again, but at least produces a subtractable background. These authors have found in practice that the cross-correlation principle is capable of much more satisfactory background removal and, of much more significance, of operation with a lower threshold of particle transit event detection.

This last point may be explained further. The typical setting of the threshold which detects 'real events' and rejects 'noise events', (particle transits and background noise fluctuation peaks which look the same) is determined by the need to obtain an 'event peak' above a 'noise background'. In any case where a wall is approached, the operating threshold is always adjusted to boost the event rate, until the noise becomes detrimentally intrusive. This simulates a high event rate and favors cross-correlation: specifically this may be seen as the capability of the method of correlation detection to look at smaller particles, of which there are usually many more, than with timing where the presence of background, or spurious events is less easy to quantify and correct.

With either detection system for constructing a distribution function for event interval times the precision of the final estimates of mean velocity, turbulence and other parameters, such as flow direction and shear stresses, from measurement at several angles, is determined by the total number of correlated events in the signal peak and its separation from the background noise. If the background has a statistically flat probability then the variance of any assigned 'bin' away from the signal peak is equal to the square root of the mean occupation number of

the background. This must be considered when using the occupation numbers in the signal peak after subtraction of the mean background computed over many 'bins'. Schodl [18] has suggested a scheme for improving estimates of mean properties where several angles are measured. Whereas a fully resolved velocity probability distribution is necessary for shear stresses the accumulation of separate ensemble averages in time and angle means that average properties only may be obtained to precision equivalent to the former unaveraged measurements with only one tenth of the data. This shortens the equivalent observation time, and is a much more efficient way of using the data. The method is directly applicable, however the distributions are obtained, by timing or by correlation. Depending on the way that correlation is calculated the distinction between limiting and correlation become a little smeared.

4.6 Precision

Precision is not such a contentious subject as accuracy, but any fringe vs. transit discussion is open to argument on either topic. It has been our experience that LTA systems are potentially superior in both areas but that, as always, there is a price. The first and most obvious price is the need to rotate the spots in time and thus to lose time resolution and to presume statistical stationarity of the flow. Much has yet to be said. So far, less creative problem solving has been addressed to the LTA to extend its powers in the way that has been done over many years with LDV.

The only real calibrations for LTA are laser wavelength and spot spacing. The former is known adequately and the spot spacing may be measured to better than 0.1% with nothing more elaborate than a polarizing filter and a tape rule. Calibration for LDV is more difficult. As an aside, in areas where the beams are projected through a turbulent region the fringe contrast deteriorates very rapidly and a small change in spacing may occur. In the LTA the spots may broaden but are unlikely to incur systematic error because the illuminating beams essentially travel through the same paths in the fluid until they begin to separate close to the sampling volume.

Precision of mean velocity may be made arbitrarily high by moving the spots further apart and by taking a longer time average. In the case of extremely low turbulence this is especially effective. If the experiment time is shortened, fewer particles will cross both spots and give rise to correlated data. From direct statistical considerations and the finite bin width of correlators, precision is impaired when only a few events are available.

High angular precision, which for LDV requires crossed fringes and has time resolved properties, is achieved by spot rotation. This is easily achieved to 0.2° arc for low turbulence flow and flow direction has been measured by observing event number statistics as the angle is scanned either side of the direction corresponding to the highest correlated event rate. A peak fit will yield the mode direction. Because of the finite spot

diameter to separation ratio, this angular probability curve appears convolved with the instrument broadening function associated with the direction window width within which trajectories may still be correlated. This instrumental broadening is of the same order as the longitudinal effects before reduction, due to peak time detection and other correlator defined algorithms.

Using all the correlated data at a range of angles the statistical properties of the flow field may be accumulated in time and inverted into velocity space to fit known or hypothetical functions for access to higher moments of velocity and stresses. There is, so far, little work on this as the instrument functions based on optical, geometrical and signal retrieval phenomenology become very complex once the basic simple formalism is extended. For all practical purposes of mean flow velocity and angle these sophistries are of no importance for low turbulence. In that mode also the turbulence may be well measured up to (say) ten percent. Above this level and referring to higher moments or cross statistics the modelling is as yet in its infancy. There are some suggestions of systematic disparities from the simple intuitive model at increasing turbulence levels and we look forward with interest to new work in this area.

4.7 Turbulence

Turbulence has been touched on briefly in the previous section and at various periods LTA has been regarded as suitable or not suitable for very high or very low turbulence. Currently it seems unwise without exhaustive justification to believe LTA data above 15% turbulence. It is certainly possible, and fairly practical, to acquire data at levels much greater than this and while the data is not in question its interpretation most assuredly is. To use the simple models at 30% turbulence is most unwise.

Below 15% down to about 2% LTA with cross-correlation seems at least as good as other optical anemometry techniques and depending upon the application may be much better. Earlier work with correlators suggested that the finite bin width was no impairment to ultimate velocity precision provided enough events were observed to satisfy the requirements of conventional statistical estimators. This means that even though the correlator time bins were quite large compared with the time resolution required the event assignment to these bins is very precise and if enough events occur in each bin then interpolation may be made to a high resolution which is a function of bin width.

Recently [14] it has been shown that there is a first order inversion algorithm for subtracting the equivalent mean square turbulence apparent from "bin width" effects to yield the 'true turbulence'. The magnitude of the effect depends on the position of the velocity peak with respect to the time boundaries of correlator bins. Using the presently implemented scheme turbulence levels below 0.5% may be measured with repeatability and close correspondence with hot wires.

The inversion to velocity of what are really time of flight measurements is well understood in its simplest form. The measurement of mean transit time may be simply divided into the spot separation to yield velocity. Two 'errors' [9] which compensate to first order are involved in this. With increasing turbulence this compensation deteriorates and more rigorous algorithms must be sought. There are effects of "particle bias" [8] coming from the lack of well defined correspondence between the particles and the fluid velocity field but these are probably insignificant below 5% turbulence.

5.0 CONCLUSIONS

This tutorial is a brief introduction to LTA principle, and shows that it is a significant alternative to the widely accepted LDV technology. The two areas most clearly identified to date are turbomachinery and wind tunnels where it may have important advantages. Table 2 is a brief resume of the areas and properties where LTA and single and two channel LDV may be compared. It is based on opinion and experience to date, and while any item may be the object of an interesting discussion the broad conclusions reflect opinion trends.

There is a great deal of work to be done on the interpretation of the data derivable from LTA instruments and this conference will help to fill some present gaps in understanding.

TABLE 2

Comparison of LTA with one and two channel LDV systems on a 'figure of merit' basis.

Experiment Property (All Others Being Equal)	<u>Rank Order of System Superiority</u>		
	LTA	LDV Single Channel	LDV Two Channel
High Speed	1	2=	2=
Precision/Accuracy	1	3	2
Angular Resolution	1	3	2
Low Turbulence	1	3	2
Small Particles	1	2=	2=
High Turbulence	3	2	1
Data Rate	3	1	2
Close to Walls	1	2	3
Cost	2=	1	2=
Ease of Use	1=	1=	2
Available Information			
Time Resolved Data	2	1=	1=
Shear Stresses	1=	2	1=
Spatial Resolution	1	2=	2=

NOMENCLATURE

a	- Particle radius
b_{\perp}	- 'Impact parameter' normal to optical axis (y) [See Figure 4]
$b_{//}$	- 'Impact parameter' parallel to optical axis (y) [See Figure 4]
c	- A proportionality constant $= \left(\frac{2\lambda}{\pi r^2} \right)^2$
f_1, f_2, f_3	- Focal lengths of focusing lens, internal collimator and external transceiver lenses respectively
h	- Planck's constant
$\sigma(a)$	- Scatter cross section allowing for the efficiency
$n(a)$	- Number density of particles of size a per unit volume
$p(\)$	- Probability distribution function (different according to parameter)
$q(a)$	- Particle scattering efficiency for size a
r	- Beam $1/e^2$ radius at Gaussian waist (sampling volume)
s	- Spot separation
t	- Transit time of a fringe volume or between spots
u, v, w	- Velocity components
x, y, z	- Cartesian coordinates
D	- Diameter of input laser beam at beamsplitter face
F	- Photon flux density
F_1	- Photon flux through sampling volume
G_v	- Photons scattered during a single transit
I	- Illumination intensity
K	- Ratio of number of photons needed for an LTA detection compared with LDV
L	- Sampling volume length
$N_T(a)$	- Cumulative number of particles above a given size a

P	- Laser power
S	- Scattered signal level at various places
T _a	- Transit time
V	- Velocity
β	- Divergence angle of beamsplitter prism
ε	- Ratio of sampling volume length to diameter of spot
λ	- Optical wavelength
ν	- Optical frequency
θ	- Incident angle to common plane of spots
φ	- Incident angle in common plane of spots
τ	- Transit time of a spot or fringe
< >	- Ensemble Average

Subscripts

T	- LTA
D	- LDV

References

- [1] Barnett, D. O. and Giel, T. V., Jr., "Laser Velocimeter Measurements in Moderately Heated Jet Flows," Arnold Engineering Development Center Report No. AEDC-TR-76-156. (April 1977)
- [2] Bartlett, K. G. and She, C. Y., "Single Particle Correlated Time-of-Flight Velocimeter for Remote Wind Speed Measurement," Optics Letters, Volume 1, pp. 175-177. (November 1977)
- [3] Bartlett, K. G. and She, C. Y., "Single-Particle Correlation Techniques for Remote Measurement of Wind Speed: Aerosol Condition and Measurement Rates," JOSA, 69, 455. (March 1979)
- [4] Cummins, H. Z. and Pike, E. R., "Photon Correlation Spectroscopy and Velocimetry," NATO Advanced Study Series B23, Plenum. (1977)
- [5] Eckardt, D., "Detailed Flow Investigations Within a High Speed Centrifugal Compressor Impeller," ASME 76-FE-13. (1976)
- [6] Erdmann, J. C. and Gellert, R. I., "Recurrence Rate Correlation in Scattered Light Intensity," JOSA 68, p. 787. (June 1978)
- [7] Lading, L., "The Time-of-Flight Laser Anemometer," AGARD CP193, Paper 23.
- [8] Maxwell, B. R., "Particle Flow in Turbomachinery with Application to Laser Doppler Velocimetry," AIAA Journal Vol. 12, No. 10, pp. 1297-1298. (October 1974)
- [9] McLaughlin, D. K. and Tiederman, W. G., "Biasing Correction for Individual Realization Laser Anemometer Measurements in Turbulent Flows," Phys. of Fluids, 16, p. 2082. (December 1973)
- [10] Mayo, W. T., Jr. and Smart, A. E., "Feasibility Study of Transit Photon Correlation Anemometer for Ames Research Center Unitary Wind Tunnel Plan," NASA CR 152238, (Final Report on Contract No. NAS2-10072). (February 1979)
- [11] Mayo, W. T., Jr. and Smart, A. E., "Comparison of Data from the Transit Time Velocimeter with Other Systems Now in Use for Velocity Measurements," AEDC-TR-79-32, (Final Report on Contract F40500-78-C-0002). (May 1979)
- [12] Mayo, W. T., Jr., Smart, A. E. and Hunt, T. E., "Laser Transit Anemometer with Microcomputer and Special Digital Electronics: Measurements in Supersonic Flows," 8th ICIASF, held at Naval Postgraduate School, Monterey, CA. (September 24-26, 1979)
- [13] Mayo, W. T., Jr., "Semiclassical Processing of Laser Transit Anemometer Signals," Optica Acta, Vol. 27, No. 1, pp. 53-66. (1980)

- [14] Mayo, W. T., Jr. and Smart A. E., "Limitations of LTA Technology at Mach 8: Theory and Practice," to be held at the German-French Research Institute, ISL, Symposium on Long Range and Short Range Optical Velocity Measurements. (15-18 September 1980) (To be published).
- [15] Schodl, R., "A Laser Dual Beam Method for Flow Measurement in Turbomachines," ASME Paper No. 74-GT-157. (1974)
- [16] Schodl, R., "On the Extension of the Range of Applicability of LDA by Means of the Laser-Dual-Focus (L-2-F) Technique," Proceedings of the LDA-Symposium Copenhagen, DISA, (1975)
- [17] Schodl, R., "Laser-Two-Focus Velocimetry (L2F) for use in Aero Engines," Lecture No. 4 in AGARD LS-90. (August 1977)
- [18] Schodl, R., "A Laser-Two-Focus Velocimeter for Automatic Flow Vector Measurements in the Rotating Components of Turbomachines," Measurement Methods in Rotating Components of Turbomachinery, ASME, 345 E. 47 St., New York, NY 10016. (March 1980)
- [19] She, C. Y. and Fairbank, W. M., Jr., Billman, K. W., "Measuring the Velocity of Individual Atoms in Real Time," Optics Letters, Vol. 2 No. 2, pp. 30-32. (1978)
- [20] Smart, A. E., "Measurement of Velocity Fields within Rotating Blades with a Photon Correlator," Proc. Conf. on Photon Correlation Techniques and Fluid Mechanics, Cambridge, England. (April 1977)
- [21] Smart, A. E., "Special Problems of Laser Anemometry in Difficult Applications," AGARD Lecture Series No. 90. (August 25-26, 1977)
- [22] Smart, A. E., "Data Retrieval in Laser Anemometry by Digital Correlation," Laser Velocimetry and Particle Sizing, ed. H. D. Thompson and W. H. Stevenson, Hemisphere Publishing Corp. (1979) [presented at the Third International Workshop on Laser Velocimetry (LV-III), Purdue University 11-13 July, 1978].
- [23] Smart, A. E., "A Compact Wide Aperture Image Rotator Without Aberrations," submitted to J. Phys. E. (April 1979).
- [24] Smart, A. E. and Mayo, W. T., Jr., "Applications of Laser Anemometry to High Reynolds Number Flows," Photon Correlation Techniques in Fluid Mechanics - Proceedings from the Second International Conference, Physica Scripta 19, Stockholm, Sweden. pp. 426-440. (1979)
- [25] Smart, A. E., and Mayo, W. T., Jr., "Experimental and Analytical Development of the Application of a Transit Laser Velocimeter," Reported under AEDC Contract F40600-79-C-0003, in press.

- [26] Smart, A. E., Wisler, D. C. and Mayo, W. T., Jr., "Optical Advances in Laser Transit Anemometry," published by ASME 1980, Measurement Methods in Rotating Components of Turbomachinery, presented at Joint Fluids Engineering Gas Turbine Conference and Products Show, New Orleans, Louisiana, pp. 149-156. (March 10-13, 1980)
- [27] Tanner, L. H., Journal of Scientific Instruments, Vol. 4, 1967, pp. 725-730
- [28] Tanner, L. H., "A Particle Timing Laser Velocity Meter," Optics and Laser Technology, pp. 108-110. (June 1973)
- [29] Thompson, D. M., "A Tracer Particle Fluid Velocity Meter Incorporating a Laser," J. Sci. Inst. (J. Phys. E.) Ser. 2, Vol. 1, pp. 929-932. (1968)

APPENDIX

GEOMETRICAL PROPERTIES

We use the defined notation and that on Figures 4 and 5 in the text and the classical modelling of smooth light intensity receivable from all points on the trajectory. This is proportional to the product of the illumination and receiver geometries and it is convenient to express the measured transit time from peak detection methods of a single particle of radius a as

$$T_a = \frac{s}{|V|} \frac{\cos \theta}{\cos \phi} \quad (1)$$

where s is the spot separation and $v^2 = u^2 + v^2 + w^2$, ϕ and θ are defined on Figure 4. Since it is only possible to make assertions about the known direction u , as that is the only measurement available (the spot orientation takes the coordinate system with it for this analysis) the value of transit time becomes

$$T_a = \frac{s}{u} \cos^2 \theta \quad (2)$$

If the flow were perfectly aligned with x , u would be what was measured. If it is not then what we really measure is a component of V according to the sampling and geometrical principles of the LTA. This appendix discusses the disparity.

In any real experiment the value of T_a must be accumulated over many particles, a statistically representative sample. Hence, the mean value of T_a is obtained by integrating over the boundaries of b_{\perp} , $b_{//}$, ϕ , θ and a . We will postulate functions $p(\)$ (which will be different for each parameter in parenthesis) and state the integral

$$\langle T_a \rangle = \int_{b_{\perp}} \int_{b_{//}} \int_{\phi} \int_{\theta} \int_a \frac{s}{u} \cos^2 \theta p(b_{\perp}) p(b_{//}) p(\phi) p(\theta) p(a) db_{\perp} db_{//} d\phi d\theta da \quad (3)$$

For isotropic particle loading $p(b_{\perp}) = p(b_{//}) = 1$ and may be omitted.

The above integral is not simple nor separable because the boundary conditions are not mutually independent. Some idea of this is available by looking in detail at the definitions of sampling volume.

The illuminated volume is Gaussian in radial coordinates from the optical axis and falls off approximately hyperbolically with axial

distance. This may be represented as

$$I(x, y, z) \propto \sqrt{\frac{2}{\pi}} \frac{P}{r \sqrt{(1 + cy^2)}} e^{-\left(\frac{2(x^2 + z^2)}{r^2(1 + cy^2)}\right)} \quad (4)$$

for each spot where $c = \left(\frac{2\lambda}{\pi r^2}\right)^2$

The fixed dependence upon z is determined by the definition of diffraction limited spots. The receiving aperture is not so easy to define but from Figure 5 it may be approximated as a hollow cone whose inner and outer bounds are roughly paraboloidal and hyperboloidal. The ratio of axial length to spot diameter is a function of the design of the receiving aperture and it shall be designated ϵ . For a practical system ϵ might be ~50. Because of this ϵ is not significant to modify expression (4) unless the flow is very badly misaligned or excessively turbulent neither of which conditions is under discussion here.

Expression (4) must be extended to include the second spot under the transform $x \rightarrow x-s$

$$I(x, y, z) [2] = I(x, y, z) + I(x-s, y, z) \quad (5)$$

If a particle goes through these spots it will give rise to a signal which has dependence upon b_{\perp} , b_{\parallel} , ϕ , θ , a , u , v , and w and with sufficient devotion the express dependence may be written down.

With some tedious algebra and much patience it is possible to show certain features.

- a) The variation of b_{\parallel} is not significant if peak detection is used and results in a broadening corresponding to the increase in spot diameter with s if quantum resolved signals are processed.
- b) The variation of b_{\perp} is interactive with θ and will result in some events being missed in peak detection if b_{\perp} and θ both vary, as it is almost certain they will. The consequence is complex and discussed further under d). In quantum detection no events are missed and the thresholding effect resulting in a sharp boundary is transformed into a steady Gaussian roll-off.
- c) Variation of ϕ has no error effects so long as $\phi < \sim 70^\circ$. The velocity component in the zx plane is resolved into the x direction. No broadening occurs for peak time detection but significant spread may be apparent for quantum resolution. This spread will increase with increasing $|\phi|$.

- d) The consequences of θ variation really get complicated because the usual mode of machine operation is to rotate the spot in the direction θ to make measurements. The boundary on θ is dependent upon b_{\perp} and a and for the first time a systematic error in T_a may occur. b_{\perp} is less significant of itself but it could increase the uncertainty of boundaries in θ and a domains. For peak detection the boundary condition on a defines a spot maximum radius of intersection beyond which no event will be detected. This is a smooth roll-off with quantum resolution but is still an attenuation. For a constant photon flux there is also a reduction in photon rate with increase in total speed, $|v|$, yielding a velocity bias effect which is a boundary definition rather than a ubiquitous scaling parameter, although it may later cause this effect because there are two spots. It is further apparent that any increase in $|\theta|$ in either direction from zero has an effect of modifying the measured transit time in the same direction. This yields a systematic erroneous decrease in apparent transit time average if there is a wide spread of θ and an error of similar sign but different size if the θ variations are not symmetric about the spot to spot direction. This effect can not easily be quantified (which means I haven't done it) but the effect may be minimized by reducing the spot diameter to separation ratio. For all practical application for low turbulence this error seems vanishingly small.
- e) Effects with variation of a do not yield systematic errors. If an exclusion limit is placed upon the maximum particle size then particles above this size may only contribute if b_{\perp} , b_{\parallel} , ϕ , θ or combinations are increased accordingly. The spread will increase and there will be a bias against those particles which went through the center of one or both spots. Smaller particles will have a smaller range of the above parameters and will contribute less to broadening. The boundary of particles too small is a roll-off without error.
- f) The effect of changes in u is to change the equivalent signal level by the velocity inverse and can be inverted from average time measurements by a simple algorithm (s/T_a for single event, $s/\langle T_a \rangle$ to first order only for stationary averages in low turbulence). For peak detection there is no systematic error and no broadening if the discriminators are perfect. This, naturally, is only so for measurement of the velocity properties of the particle field and the usual corrections are necessary for the transformation to fluid field, together with the usual

In summary, the various geometrical boundaries are reviewed and none is found to yield systematic error except the θ variation which has a tendency to bias the measurements of transit time to lower values, leading to falsely high estimates of mean velocity. The magnitude of this effect is very small. For spot separation to diameter ratio of 25:1 it typically might be of the order of 1 part in 10^4 or less for turbulence sufficiently high to offer transits over all possible θ values and could possibly increase to 3 parts in 10^4 for turbulence of less than 0.2% misaligned with the sensitive direction by up to 1° (but thought to be correctly aligned). Any angular search would show the disparity immediately as it becomes most highly sensitive at low turbulence.

The systematic errors of the transit geometry are, therefore, shown to be almost insignificantly small. Any residual error associated with the relation of the particle to fluid flow field must be considered separately. We show our final Figure A1 which is the relationship of the boundary contours in b_{\perp} and θ for varying values of the parameter a . This is no more than the flat perspective projection of a three dimensional section of the θ -space of coordinates b_{\perp} , $b_{//}$, ϕ , θ , a , u , v , w . The salient features are briefly as follows.

The coordinate boundaries of $b_{//}$ and ϕ , together with v do not change significantly the topographical form of this plot nor indeed do they produce any non-linearities which would render it less representative. It is technically degenerate under w as no measurement may be made if there is only a significant w component (not accommodated under θ). The v component is similar in its consequences to θ , but with a scaling factor which would not show on this plot. The effect of the magnitude of u is to scale the diagram and also to distort the a coordinate - because faster particles scatter less photons.

The remaining three parameters are plotted as boundary values. Inside the shape data are obtained. Outside they are not. The edges should really be represented as fuzzy. The θ axis is shown approximately quantitatively with an axis interval of 0.5° arc for a 25:1 ratio system. The quantitative marks on b_{\perp} are in integral multiples of r_T the sensitive volume minimum radius to $1/a^2$. The a axis is not typically quantified but scales with each size of particle and with inverse of speed of that particle. The quarter space thus plotted shows simply that values of b_{\perp} , θ , greater than certain values do not contribute to the transit time measurements and that values of a below a certain size (or for a fixed size, above a certain speed) may not contribute. If there is a method of excluding particles that are above that given size, then the represented volume develops a hollow exclusion core, otherwise the center regime also contributes. (Leading to possible slippage errors from large particles if they are present.) This figure must be convolved with the probabilities of finding any of the parameters within the ranges of interest and may not be shown here. It would correspond to a distortion only. For example, a monodispersion of a at a fixed velocity would be a slice parallel to the b_{\perp} , θ plane. A further restriction of angle θ would reduce this plane to a horizontal band.

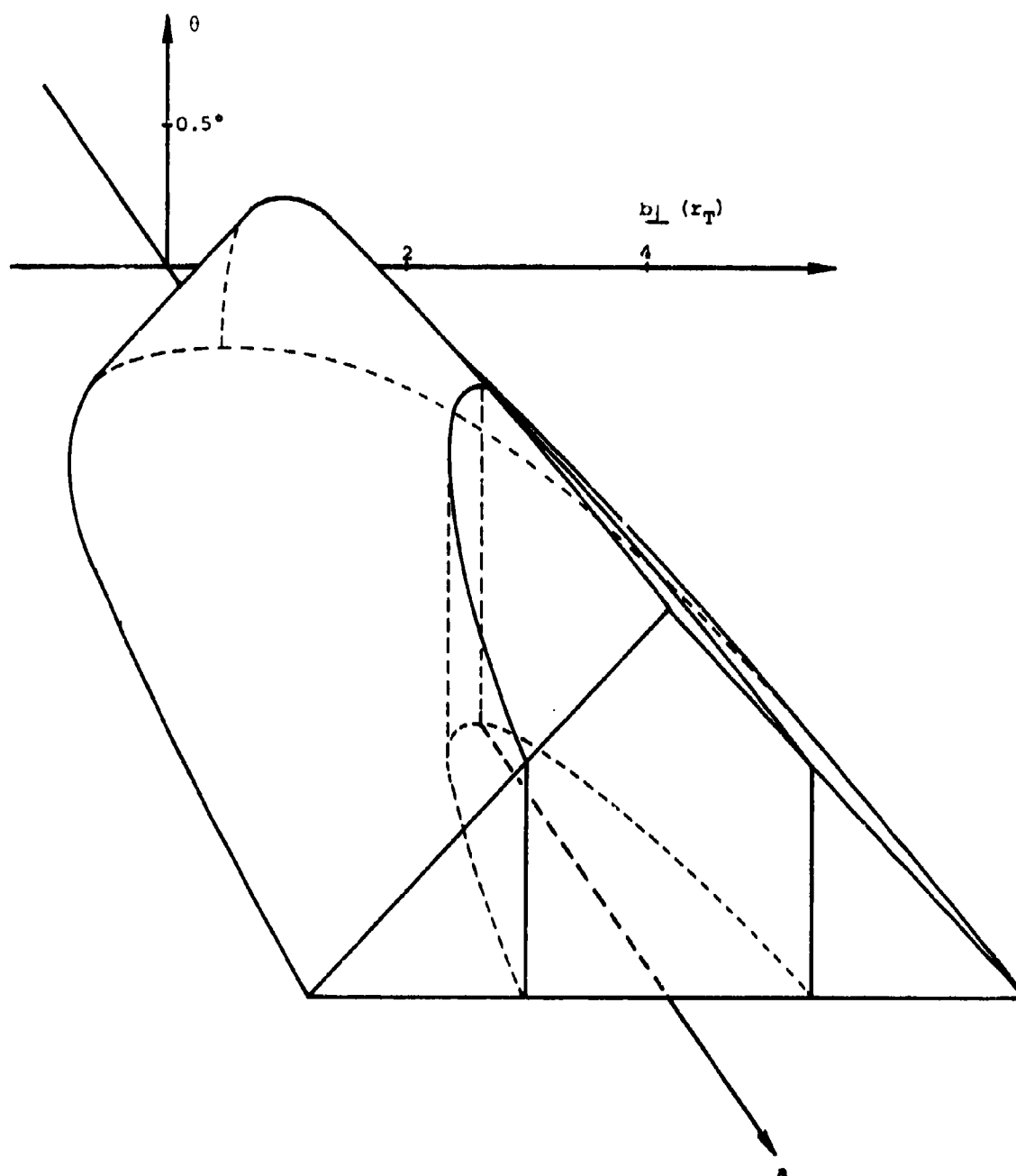


FIGURE A1. BOUNDARIES OF ACCEPTABLE PARAMETER VALUES FOR A MEASUREMENT
(SEE TEXT FOR EXPLANATION)